UNIVERSITAT DE BARCELONA

Deciphering the context of cancer cell dependency on p38a MAPK

Nevenka Radic

UNIVERSITAT DE BARCELONA
FACULTAD DE MEDICINA
PROGRAMA DE DOCTORADO EN BIOMEDICINA

Deciphering the context of cancer cell dependency on p38α MAPK

Memoria presentada por Nevenka Radic para optar al título de doctor por la Universitat de Barcelona
Esta tesis ha sido realizada en el Instituto de Investigación Biomédica de Barcelona
(IRB Barcelona)

Dr. Angel Rodríguez Nebreda
(Director de la tesis)

Dra. Isabel Fabregat Romero
(Tutora de la tesis)

Nevenka Radic
(Doctoranda)

Barcelona, 2023

Mojoj породици

"...But in the end, do not past and present confront us with similar phenomena and with the same problems: to be a man, to have been born without knowing it or wanting it, to be thrown into the ocean of existence, to be obliged to swim, to exist; to have an identity; to resist the pressure and shocks from the outside and the unforeseen and unforeseeable acts – one's own and those of others – which so often exceed one's capacities? And what is more, to endure one's own thoughts about all this: in a word, to be human."

Excerpt from the speech of Ivo Andrić
Stockholm, December 10, 1961

Acknowledgements

Finishing a PhD feels almost as weird as starting one. I am still clueless, but I can better identify what exactly I am clueless about. And I have a long list of people who have helped me throughout these years to reach where I am now.

First of all, I am sincerely grateful to Dr Angel R. Nebreda for giving me the opportunity to spend the last couple of years working on an exciting project. I am grateful for all the support and guidance throughout my many failures, for the immense patience and understanding. And most importantly, for his contagious enthusiasm throughout all the discussions, for being willing to listen to every idea and for always having useful advice. I have been truly fortunate to work with the best PI a student could wish for.

I would also like to extend my gratitude to the Thesis Advisory committee members, Dr Travis Stracker, Dr Isabel Fabregat Romero and Dr Manuel Serrano for all their advice and feedback which has been invaluable throughout these years.

I have been very fortunate to be part of the Nebreda group and none of the work I have done would have been possible without these amazing people. This is especially true for Begoña, since I literally would not have done anything without her. I thank Bego for always having a minute for me (even though the minute I needed was never only one), for listening to all of my crazy ideas, for all she has taught me, for being my common sense and helping me stay on track without losing my mind. And of course for all the board games, vermuts and important Spanish phrases she has brought to my life. Above all, for doing all this despite me continuously messing up her last name and recommending the movies she hates. I have been very lucky to annoy her these last couple of years. Another thank you goes to Monica, for her patience and help, for all the oligos ordered over the years (sorry), for always knowing what to do and for her love for science that leaves no one

indifferent. I am also extremely grateful to Eli for all she has taught me, for all the help and all the fun, he tingut la gran sort de conèixer-te! I have been also very lucky to share this journey with Yuzhen and Clara. To Yuzhen, who has been an incredible friend and has went through all of this with me, for all the discussions and all the analysis we have done together. To Clara, I am thankful for having met one of the most talented humans I have known, a fierce fighter for everything she believes in, it has been lovely sharing the bench with her. I am also grateful to Nerea for embarking on this project, for all the help and for enduring me over the last two years. To Anna, Diana, Jordi and Melisa for all the comments, advice and discussion, it has been wonderful working alongside them. I am also very grateful to former lab members, Konstantin for substantial help in my first years, to Nuria, Laura and Lorena for all the times shared and Melissa, the first student I have had a chance to work with, who has helped me out with parts of this project and set the bar for other students extremely high.

I am also grateful to all of the people who have been instrumental during the development of this project. To Adrià Caballe from the IRB Biostatistics facility, for performing the analysis and all the useful discussion and advice from his side that have been vital. To Nikolaos Giakoumakis and Anna Llado from Advanced Digital Microscopy facility, for all the help and time spent helping us optimise everything and get the most out of the samples. I am also very grateful to the incredible people at CCiTUB cytometry facility, Jaume, Ricardo, Sonia and everyone for all the patience and kindness over the years. To Amaya Amador from CCitUB genomics facility, for all the work, all the explanations and immense patience.

I would also like to thank the people who have been key in my decision to pursue a PhD. Dr Aleksandra Nikolic, for her guidance and support, for her commitment to us lost biology students, I am just one of many who have been fortunate to be inspired by her. Dr Faso, for being an incredible supervisor, I am grateful for all she has taught me and for pushing me to do better than I thought I could. Dr Durand, for his immense help and support.

None of my time here would have been the same without those I dedicate this paragraph to. This is to Petra, for being my favourite human, for all the adventures, for sharing the best and the worst of these years. To Cris for all the time spent together and for being the best friend I could have wished for. To Michael, for his futile efforts to teach us proper English, to David for everything and to Fabian for being there even when late. To Peđa, my partner in crime for getting stuck in the lab until late, an incredible friend (and a trusted pharmacist). To Valentina for being an epic human I have shared amazing moments with. To Jura, Jelena and Saška, thank you for everything. I am so happy to have met you all, you have made these years incredible. Finally, to Đole, for motivating me when I needed it the most (probably without even realising it) and to Ina, for always being there and helping me stay sane despite all the kilometres between us.

Most of all, I am grateful to my family. This thesis is dedicated to Ranka, Mihajlo, Ružica and Aleksandar, who have stood by me and given me unconditional support at every step. Everything I have ever achieved, I owe to them.

Last but not least, thank you, the person on the other side of these pages, for reading this work and embarking on this journey with me. I hope you will enjoy it at least a fraction of how much I have enjoyed writing it.

Contents

Acknowledgements **3**

Abbreviations **11**

Summary **17**

Resumen **19**

Introduction **21**

The complexity of cancer phenotypes 23

Exploiting cancer cell vulnerabilities 27

Oncogene addiction 28

Synthetic lethality 29

Mapping cancer cell dependencies 31

Non-oncogene addiction 36

The p38 MAPK signalling pathway 39

Activation of the p38 MAPK pathway 41

Regulation and termination of p38 MAPK signalling 43

Versatility of p38 functions 44

Context dependent role of p38α in cancer cells 49

Objectives **53**

Materials & Methods **57**

Materials 59

General buffers and solutions 59

Commercial reagents and kits 60

Cell culture *60*

Commercial kits *61*

Cellular and molecular biology *61*

Methods 63

Cell culture 63
Cell lines *63*
Cell counting *63*
Cryopreservation of mammalian cells *63*
Mycoplasma detection *64*
Cell treatments *64*
Calcium chloride transfection of HEK293T cells *65*
PEI transfection of HEK293T cells *66*
Lentivirus production *66*
Generation of the BBL358-Cas9 cell line *66*
Cas9 activity assay in BBL358-Cas9 cells *67*
Generation of mammalian knock-out cells using CRISPR/Cas9 ..... *67*
Cell viability assays 70
Colony formation assay *70*
EdU labelling assay *70*
Metabolic viability assays *71*
Cell death assay *72*
Bright-field microscopy *72*
Competitive proliferation assay *72*
Molecular biology 73
Protein detection by western blotting *73*
qRT-PCR analysis of gene expression *75*
Genome-wide CRISPR/Cas9 screen 77
Screen conditions *77*
sgRNA amplification and sequencing *78*
CRISPR screen data analysis *80*
DepMap data analysis 82

Statistical analysis 82

Results 83

Genome-wide CRISPR/Cas9 screen 85

CRISPR/Cas9 screen data analysis 90

Validation of the CRISPR/Cas9 screen hits 97

Depleting Zcchc14 increases viability of p38α KO cells 98

Inhibiting p38α potentiates the effect of mTOR inhibition 102

p38α KO cells are sensitized to mitochondrial translation inhibition ... 106

Role of other p38 MAPK pathway components 109

Downregulation of p38δ rescues the effect of p38α deletion 110

Inhibiting p38α potentiates the effect of a TAK1 inhibitor 114

Investigating hits predicted to synergize with the p38α KO 115

Targeting the top 10 depleted hits 115

Substantial enrichment of sgRNAs targeting *Trp53* 116

Analysis of samples at earlier time point avoids the p53 bias 118

Exploring p38α dependency by mining the public datasets 124

Identifying cancer cell lines dependent on p38α 124

Discussion 131

Conclusions 141

Appendix 145

References 157

Abbreviations

4-OHT	4-hydroxitamoxifen

A

a.u.	Arbitrary Units
ALK	Anaplastic Lymphoma Kinase
AP-1	Activator Protein 1
APS	Ammonium Persulfate
ASK1	Apoptosis Signal-regulating Kinase 1
ATF2	Activating Transcription Factor 2
ATM	Ataxia Telangiectasia Mutated
ATP	Adenosine Triphosphate
ATR	ATM And Rad3-Related

B, C

BRCA1	Breast Cancer 1
BSA	Bovine Serum Albumin
CCLE	The Cancer Cell Line Encyclopedia
CDK	Cyclin-Dependent Kinase
cDNA	Complementary DNA
CRISPR	Clustered Regularly Interspaced Short Palindromic Repeat DNA Sequences
CtIP	CtBP-Interacting Protein

D

DAPI	4, 6-Diamidino-2-Phenylindole
DDR	DNA Damage Repair
Dep	Dependent
DepMap	Dependency Map

DEPTOR	DEP Domain-Containing mTOR-Interacting Protein
DMEM	Dulbecco's Modified Eagle Medium
DMSO	Dimethyl Sulfoxide
DNA	Deoxyribonucleic Acid
DNAse	Deoxyribonuclease
DTT	Dithiothreitol
DUSP	Dual Specificity Phosphatase

E, F, G

EDTA	Ethylenediamine Tetra-Acetic Acid
EGFP	Enhanced Green Fluorescent Protein
EGFR	Epidermal Growth Factor Receptor
ER	Estrogen Receptor
ERK	Extracellular Signal-Regulated Kinase
FACS	Fluorescence-Activated Cell Sorting
FBS	Fetal Bovine Serum
FDA	Food And Drug Administration
GOF	Gain Of Function
GPCR	G Protein-Coupled Receptor

H, J, K

HER2	Human Epidermal Growth Factor Receptor 2 (*Erbb2*)
HSF1	Heat-Shock Factor 1
JNK	C-JUN NH2-Terminal Kinase
KO	Knockout

L, M, N

log_2FC	Log_2 (Fold Change)
LOF	Loss Of Function
LPS	Lipopolysaccharide

LY	LY-2228820, p38 inhibitor
MAPK	Mitogen-Activated Protein Kinase
MEFs	Mouse Embryonic Fibroblasts
MK2	MAPK-Activated Protein Kinase 2
MKK/MAP2K	Mitogen-Activated Protein Kinase Kinase
MKKK/MAP3K	Mitogen-Activated Protein Kinase Kinase Kinase
mRNA	Messenger RNA
MSK1	Mitogen And Stress-Activated Protein Kinase 1
mTOR	Mammalian Target Of Rapamycin
MTT	3-(4,5-Dimethylthiazol-2-Yl)-2,5-Diphenyltetrazolium Bromide
NonDep	Non-Dependent

P, Q

PAGE	Polyacrylamide Gel Electrophoresis
PAM	Protospacer Adjacent Motif
PARP1	Poly [ADP-Ribose] Polymerase 1
PARPi	PARP Inhibitor
PBS	Phosphate Buffer Solution
PH	PH-797804, p38 inhibitor
PI	Propidium Iodide
PyMT	Polyoma Middle T
qRT-PCR	Quantitative Real Time Polymerase Chain Reaction

R

RAPTOR	Regulatory-Associated Protein Of mTOR
RB	Retinoblastoma Protein
RICTOR	Rapamycin-Insensitive Companion Of mTOR
RIPA	Radioimmunoprecipitation Assay
RNA	Ribonucleic Acid
RNAi	RNA Interference
RNase	Ribonuclease

ROS	Reactive Oxygen Species
RT	Room Temperature
RTG	Realtime-Glo Assay

S

SAPK	Stress-Activated Protein Kinase
SD	Standard Deviation
SDS	Sodium Dodecyl Sulfate
sgRNA	Single Guide RNA
shRNA	Short Hairpin RNA
siRNA	Small Interfering RNA

T, U, W

TAB1	TAK1 Binding Protein 1
TAK1	TGF-beta-Activated Kinase 1
TBS	Tris-Buffered Saline
TCGA	The Cancer Genome Atlas
TEMED	N,N,N′,N′-Tetramethylethylenediamine
TGF-β1	Transforming Growth Factor Beta 1
TNFα	Tumor Necrosis Factor alpha
TP53	Tumor Protein P53
UV	Ultraviolet
WT	Wild Type

Summary

Eukaryotic cells rely on the mitogen-activated protein kinase (MAPK) pathways to respond to different stimuli and change their behaviour accordingly. Among the MAPKs, the p38 family is primarily activated by stress stimuli and includes four members: p38α, p38β, p38γ and p38δ, of which p38α is the most ubiquitously expressed and better characterized one. The ability of p38α signalling to regulate multiple cellular processes is of particular interest in cancer biology, as it has been described to have both tumour suppressive and tumour supportive roles in different models of tumorigenesis. Although p38α has been suggested as a potential target to impair tumour progression in certain tumour types, this is not a universal property and the contexts determining cancer cell-intrinsic p38α dependency are still elusive.

In an effort to investigate the p38α dependent cellular processes, we have performed a genome-wide CRISPR/Cas9 screening using a breast cancer model in which p38α depletion has been shown to be deleterious. We found that targeting Zcchc14 or p38δ increases the viability of the p38α KO cancer cells, identifying them as potential mediators of the deleterious effects observed in the absence of p38α. Among the factors that sensitize the cancer cells to the loss of p38α, we identified mTOR signalling and mitochondrial translation as two processes whose impairment enhances the deleterious effect of p38α downregulation. In parallel, we have leveraged the use of publicly available datasets and identified 75 cancer cell lines predicted to be dependent on p38α signalling. We have experimentally validated this dependency on p38α in the MIA PaCa-2 and SUP-T1 cancer cell lines, and identified the p38α activators MKK3 and MEKK4 as potential co-dependencies in a subset of the p38α dependent cancer cell lines.

In summary, we describe novel potential mediators of p38α MAPK functions in cancer cells, and new models of cancer cell dependency on p38α. Altogether, these results should allow a better characterization of the contexts in which p38α becomes critical for cancer cell fitness.

Resumen

Las células eucarióticas utilizan las vías de señalización de las MAPKs (de sus siglas en inglés *mitogen-activated protein kinases*) para responder a diferentes estímulos y cambiar su comportamiento en consecuencia. La familia de p38 MAPK se activa principalmente por estímulos de estrés e incluye cuatro miembros, p38α, p38β, p38γ y p38δ, de los cuales p38α es el que se expresa de manera más ubicua y está mejor caracterizado. La implicación de p38α en multitud de procesos celulares es especialmente relevante en el contexto de la biología del cáncer, ya que se ha descrito que tiene funciones tanto de supresión tumoral como de promotor del desarrollo tumoral en diferentes modelos de tumorigénesis. Por ello, aunque se ha sugerido que p38α es una potencial diana terapéutica en algunos tipos de tumores, ésta no es una propiedad universal, subrayando la necesidad de entender en qué situaciones la actividad de p38α puede ser importante para las células tumorales.

En un esfuerzo por esclarecer los procesos celulares que dependen de p38α, hemos realizado un cribado genético utilizando la tecnología CRISPR/Cas9 en un modelo de cáncer de mama en el cual se ha demostrado que la depleción de p38α reduce la viabilidad de las células. Ésta estrategia nos ha permitido identificar a Zcchc14 y p38δ como potenciales mediadores de los efectos nocivos que se producen al deplecionar p38α. También hemos observado que interfiriendo con la vía de señalización de mTOR o con la traducción mitocondrial se potencian los efectos perjudiciales de la depleción de p38α. En paralelo, y para completar el estudio de la importancia del contexto en el papel de p38α en cáncer, hemos usado las bases de datos públicas para identificar 75 líneas celulares tumorales cuya viabilidad dependería, según las predicciones, de esta vía de señalización. Hemos validado experimentalmente esta dependencia de p38α en las líneas celulares MIA PaCa-2 y SUP-T1, y hemos identificado los activadores de p38α MKK3 y MEKK4 como potenciales codependencias en un subgrupo de líneas celulares dependientes de p38α.

En resumen, hemos identificado potenciales mediadores de las funciones de p38α MAPK en células tumorales, y una serie de nuevos modelos celulares dependientes de p38α. Estos resultados deberían permitir una mejor caracterización de los contextos tumorales en los que p38α desempeña un papel crítico para la viabilidad de las células tumorales.

Introduction

The complexity of cancer phenotypes

In multicellular organisms homeostasis depends on the tightly regulated growth and function of individual cells. Cancer cells can circumvent the growth restraints and proliferate at the expense of neighbouring cells, disrupting the homeostasis of tissues and eventually impairing the function of the whole organism. The process in which the non-malignant cells acquire features that enable uncontrolled growth is known as malignant transformation. The transformation of non-malignant cells is a multistep process and the aberrations that drive the progression of tumorigenesis are heavily dependent on the context of the tissue. In this sense, every cancer is unique. There are over 100 different cancer types and subtypes described which is further complicated by observed heterogeneity both between different tumours and within the cellular composition of individual tumours. On top of that, tumours are not static as cancer cells continuously adapt to different challenges, further reshaping the tumour architecture. At a first glance, cancer biology resembles opening Pandora's Box. Fortunately, decades of research have identified unifying features that underlie cancer cell tumourigenicity.

The contemporary view of cancer as a disease of cells began in the 19th century, with Rudolf Virchow as one of the first proponents of the cellular origin of cancer. Although early on it became evident that cancer can occur upon exposure to different chemical compounds and toxins, the mechanisms of cancer initiation and progression were unknown. A major leap in our understanding of cancer initiation was instigated by the discovery of the Rous Sarcoma Virus (RSV), which could induce solid tumours from a cell free filtrate (Rous, 1911). A study published by Varmus and Bishop demonstrated that the *src* gene, previously reported to be an essential component of RSV for the induction of cell transformation (Duesberg & Vogt, 1970; Lai et al., 1973; L. H. Wang et al., 1975, 1976), was actually a gene that originates from the cellular genome (Stehelin et al., 1976). Discovery of *Src* was followed by the identification of other genes, such as *Myc* (Duesberg et al., 1977) and *ErbB* (Bister & Duesberg, 1979) in avian viruses, and *Ras* in murine

tumour viruses, eventually named oncogenes for their ability to induce malignant transformation. The identification of human *RAS* confirmed that cell intrinsic aberrations can in fact be the source of oncogenic potential (Parada et al., 1982; Santos et al., 1982). This placed the oncogenes into the spotlight of cancer research (Vogt, 2012).

On the other hand, fusion of normal and malignant cells indicated the existence of genes that can actively suppress the malignant potential of cancer cells (Harris et al., 1969; Stanbridge, 1976). The analysis of retinoblastoma tumours revealed that inactivation of both alleles of a gene later named RB1 drives the malignancy (Knudson, 1971). This was followed by identification of other tumour suppressor genes, such as *TP53* (Baker et al., 1989; Nigro et al., 1989), *PTEN* (J. Li et al., 1997) and *APC* (Laken et al., 1997).

The discovery of oncogenes and tumour suppressors suggested that amplification of the proliferation signal is a cell intrinsic driver of tumorigenesis. However, increased proliferation of cancer cells on its own is not sufficient in inducing tumorigenesis. It is now clear that cells harbouring genetic aberrations are common in ageing tissues (Martincorena, 2019). The cells that undergo oncogenic driver events are challenged by a plethora of protective mechanisms in place to limit the outgrowth of transformed clones. It is in fact the cumulative imbalance of cell intrinsic events together with the effect of the microenvironment and the immune system that drives the adaptation and rapid expansion of particular mutant cells (van Neerven & Vermeulen, 2022).

In 2000, Hanahan and Weinberg proposed a framework of principles that guide the malignant growth, which have so far withstood the test of time and further expanded to incorporate new findings (**Figure 1**). The initial six hallmarks of cancer encompassed sustaining proliferative signalling, evading growth suppression and cell death, enabling replicative immortality, inducing or accessing vasculature and activating invasion and metastasis (Hanahan & Weinberg, 2000). Ten years later, deregulating cellular metabolism and avoiding immune destruction were included as additional cancer cell abilities

(Hanahan & Weinberg, 2011), and in the latest review the phenotypic plasticity and the contribution of cellular senescence were recognized as new hallmarks (Hanahan, 2022). These cancer cell capabilities are facilitated by different enabling characteristics that include genome instability and mutation, tumour promoting inflammation, epigenetic reprogramming, and polymorphic biomes.

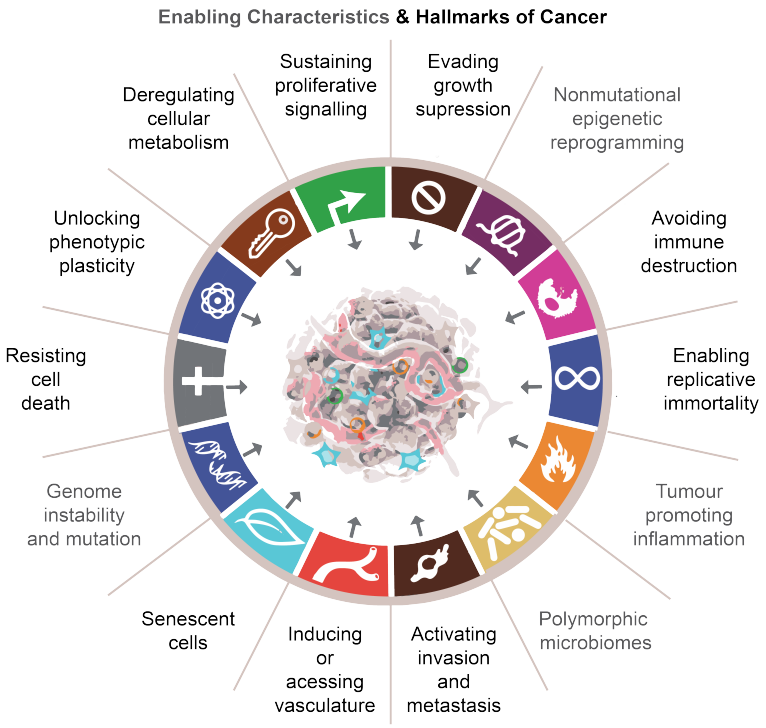

Figure 1. Hallmarks of cancer. Figure depicts enabling characteristic (grey) and hallmarks of cancer (black), modified from Hanahan, 2022.

Although the hallmarks of cancer represent conceptually distinct capabilities of cancer cells, they should not be perceived as independent phenomena. In fact, different oncogenic drivers can modulate cancer cells at multiple levels. For instance, mutated *KRAS* has been described to facilitate cancer cell escape from death through maintaining high levels of the inhibitor of apoptosis protein survivin (Tecleab & Sebti, 2013), or by rendering cells insensitive to the apoptosis induced by tumour necrosis factor-related-apoptosis-inducing-ligand (TRAIL) treatment (Sahu et al., 2011). On the other hand, *KRAS* can regulate metabolic programs by inducing autophagy

and thus promoting the survival of cancer cells upon starvation (Alves et al., 2015), or through promoting *de novo* lipid synthesis in breast epithelial cells (Ricoult et al., 2016). Similar observations have been made for other oncogenic drivers.

Overall, the enabling characteristics and hallmarks of cancer aim to create a blueprint of cancer research avenues as they systematise a vast amount of knowledge acquired over the years. Importantly, understanding the biology of tumorigenesis has paved the way for the development of improved therapies.

Exploiting cancer cell vulnerabilities

The increased understanding of cancer biology has fuelled the search for a silver bullet treatment - a way to target the cancer cells specifically and universally. It is unlikely that there will be a single compound or target that will ablate cancer cells universally, but a better understanding of this disease has uncovered a number of promising vulnerabilities. A clear distinction between malignant and normal cells is their propensity to proliferate, and this is what most cytotoxic compounds employed in cancer treatment target (**Figure 2**). Most cancer cells are sensitive to conventional chemotherapy. However, these drugs also exert a negative effect on non-malignant cells leading to a number of undesirable side effects (Nurgali et al., 2018).

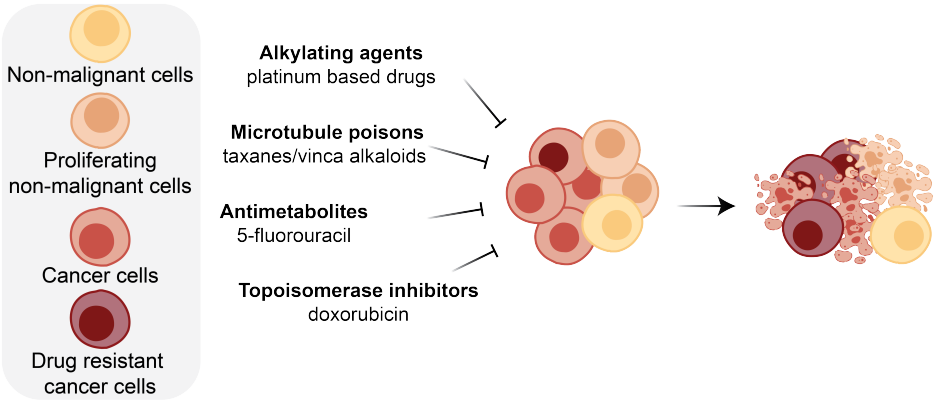

Figure 2. Conventional chemotherapy approaches. Increased proliferation of cancer cells confers specific vulnerabilities that are targeted by many first line chemotherapy agents. However, as these processes are universally essential in most cells, these compounds exert toxic effect on non-malignant cells. Their efficiency is also hindered by multiple drug resistance mechanisms that allow cancer cells to persevere.

Discovering inhibitors that can target the gain of function (GOF) alterations of different oncogenes has been an alluring strategy. However, not every tumour relies on a druggable oncogene. Although targeting the loss of function (LOF) alterations of tumour suppressor genes was less intuitive, the concepts of synthetic lethality and non-oncogene addiction have expanded the range of possible approaches.

Oncogene addiction

Targeting the increased activity of proteins encoded by oncogenes has been a successful therapeutic approach (**Figure 3**). In the 1980s, *HER2*, a member of the epidermal growth factor/HER tyrosine kinase family, was identified as an oncogene (Schechter et al., 1984). Further studies showed that the expression of *HER2* is increased in a number of breast cancer samples and correlates with worse prognosis (King et al., 1985). In the late 1990s, trastuzumab, a monoclonal antibody against HER2 was developed and approved for the treatment of breast cancer harbouring *HER2* amplification (Slamon et al., 2001). Importantly, stratification of patients with *HER2* amplification coupled with novel therapeutic approaches has resulted in dramatically increased survival rates (Swain et al., 2023).

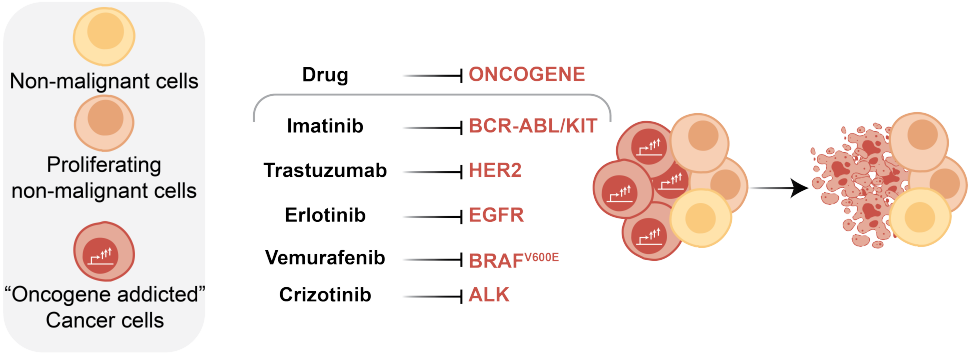

Figure 3. Targeting oncogene addiction. Figure shows several drugs used in clinic to target specific oncogenes. In comparison to the conventional chemotherapy, targeting oncogenes impairs cancer cells more specifically. However, not all tumours are driven by a druggable oncogene.

Another pivotal moment in cancer therapy was the characterization of the Philadelphia chromosome in chronic myelogenous leukaemia (CML) (Nowell & Hungerford, 1961; Tough et al., 1961). This led to the discovery of the *BCR-ABL* gene fusion as driver of CML (Daley et al., 1990). The search for a compound that was able to inhibit BCR-ABL identified imatinib, a PDGFR/KIT inhibitor, which also inhibited the BCR-ABL fusion protein (Druker et al., 1996). Imatinib was the first FDA approved kinase inhibitor for cancer therapy (Druker et al., 2001). It has often been described as a miracle drug as imatinib treatment increased the overall survival of CML patients (Savage & Antman, 2002).

Since imatinib discovery, there has been a number of inhibitors targeting GOF alterations in cancer cells, such as erlotinib for EGFR (Dowell et al., 2005), vemurafenib for BRAFV600E (Chapman et al., 2011) or crizotinib for ALK (Kwak et al., 2010). The inhibition of oncogenic proteins with GOF alterations has been the focus of many targeted therapy approaches. While the restoration of the protein function of tumour suppressors is more challenging, it is becoming evident that the LOF alterations in cancer cells also confer unique vulnerabilities with promising therapeutic potential.

Synthetic lethality

The concept that simultaneous mutation of two genes can cause cell lethality, while neither of the mutations alone has an adverse effect on cell viability was first described in *Drosophila melanogaster* by Calvin Bridges in 1922 (Bridges, 1922), and two decades later termed 'synthetic lethality' by Dobzhansky (Dobzhansky, 1946). In 1997, Hartwell and Friend proposed that uncovering synthetic lethal partners through genetic screens performed in *Saccharomyces cerevisiae* can be leveraged as a tool for tackling loss of function alterations in cancer cells. This is achieved by defining the precise molecular context of malignant cells in which inhibiting "secondary drug targets'' is detrimental for cancer cell viability (Hartwell et al., 1997). To this day, the concept of synthetic lethality guided therapy remains alluring, however it is becoming clear that its full potential can only be harnessed by carefully selecting the conditions in which this approach can be beneficial for the patients. In this line, the textbook example of synthetic lethality is the use of PARP1 inhibitors in BRCA1/2 deficient tumours (**Figure 4**).

Two seminal studies demonstrated that PARP1 inhibition or downregulation can selectively decrease the viability of BRCA1 or BRCA2 deficient cells and impair tumour progression (Bryant et al., 2005; Farmer et al., 2005). This discovery instigated a promising journey to translate PARP inhibitors (PARPi) into the clinic. While there have been studies showing a beneficial effect of PARPi on the overall survival of the patients with BRCA1/2 LOF (Poveda et al., 2020), a number of reports showing limited beneficial effects of PARPi along with the emergence of PARPi resistance are hampering the promise of

this synthetic lethality approach (Lord & Ashworth, 2017). On a more hopeful note, it seems likely that, at least in some instances, inaccurate stratification of patients could be the prime cause of low treatment efficacy, as the optimal use of PARPi in the clinic relies on the accurate assessment of BRCA1/2 inactivation (Setton et al., 2021).

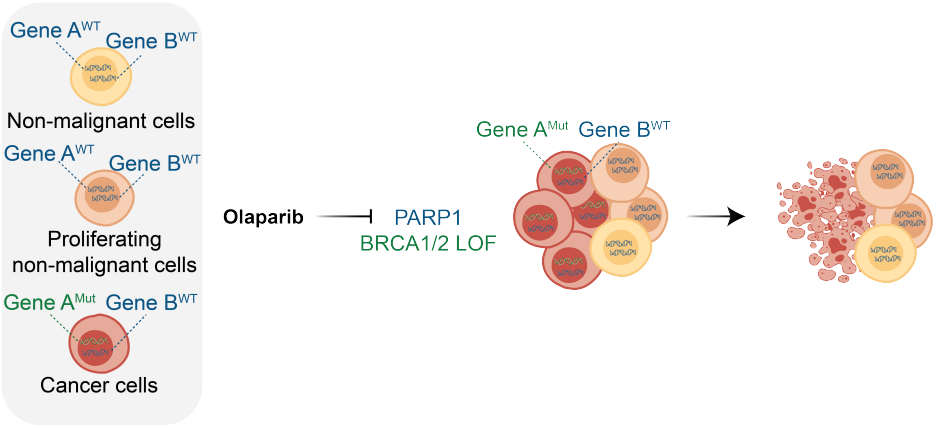

Figure 4. Targeting synthetic lethality. Targeting PARP1 in tumours with BRCA1/2 loss of function has been a prototypical example of synthetic lethality strategy in cancer therapy. It is important to note that its efficiency relies on the accurate detection of the BRCA1/2 status, and that several mechanisms of resistance to PARPi have been described, overall hindering their application in the clinic.

Overall, the promise of synthetic lethality guided approaches has fuelled research to identify partners and contexts that underlie specific vulnerabilities of cancer cells. Unsurprisingly, the progress vastly depends on the available cancer cell models as well as technological advances, which allow us to investigate the complexity of this disease in unprecedented detail. Thus, the emergence of new strategies to study genomic, transcriptomic, epigenetic and metabolic alterations of cancer cells is continuously adding new layers of information that can help to guide new therapeutic approaches. Furthermore, the development of high-throughput genome wide screens has enabled the functional assessment of potential context-specific vulnerabilities of cancer cells.

Mapping cancer cell dependencies

The promise of targeted therapy has motivated a number of studies aiming to elucidate the molecular characteristics of tumours. Perhaps the most illustrative is The Cancer Genome Atlas (TCGA) that generated genomic, transcriptomic, proteomic and epigenomic data for 33 cancer types with more than 10,000 cancer samples and matched normal samples (Cancer Genome Atlas Research Network et al., 2013). While the amount of patient data is increasing with time, established cancer cell lines and mouse models are to this day crucial in understanding the biology of cancer. The Cancer Cell Line Encyclopedia (CCLE) has provided in depth information on the expression, copy number alterations, methylation and mutational landscape of over 500 different cancer cell lines (Barretina et al., 2012; Ghandi et al., 2019). In addition, large drug screening efforts from the Broad (Corsello et al., 2020; Yu et al., 2016) and the Sanger (Yang et al., 2013) institutes have generated publicly available drug sensitivity data for a large number of compounds and cancer cell lines. Although molecular characterisation of tumours and cancer cell models has been invaluable, it does not paint a complete picture as it does not always indicates which genes are the main contributors in a particular cancer type or model. The most direct way of testing the essentiality of a gene is by perturbing its expression.

One of the first breakthroughs that enabled rapid loss-of-function screens in mammalian cells was the development of the RNAi technology. The screens performed with small interfering RNAs (siRNAs) or short hairpin RNAs (shRNAs) allowed genome-wide LOF analyses to directly identify genes involved in a particular process (Boutros & Ahringer, 2008). This approach made it possible to functionally test almost all genes in a desired context. One of the advantages often attributed to RNAi screens is that they mimic more closely the effect of chemical inhibitors, as there is never a complete depletion of the target (Mullenders & Bernards, 2009). On the downside, RNAi efficiency depends on the target transcript levels (Vu et al., 2015). Another major concern of the RNAi screens is the often fatal off-target toxicity due to oversaturation of the endogenous small RNA pathways (Grimm et al., 2006; Khan et al., 2009). The emergence of genome editing techniques has overcome some of these limitations.

The clustered regularly interspaced short palindromic repeat DNA sequences (CRISPR) and CRISPR-associated (Cas) proteins are components of the prokaryotic adaptive immunity system that is able to recognize and cleave foreign nucleic acids (Barrangou et al., 2007). The *Streptococcus pyogenes* CRISPR/Cas9 system is one of the first systems described for genome editing in mammalian cells (Cho et al., 2013; Cong et al., 2013; Jinek et al., 2013; Mali et al., 2013). The Cas9 DNA endonuclease can be targeted by a single guide RNA to any specific genomic loci containing an 'NGG' protospacer-adjacent motif (PAM) sequence (Jinek et al., 2012; Sapranauskas et al., 2011). Once targeted, it induces a blunt end double strand break, which is repaired by either homology-directed repair or, more commonly, the non-homologous end joining, an error-prone repair mechanisms that can lead to insertions or deletions disrupting the gene sequence and resulting in target loss of function (**Figure 5A**). Hence, unlike RNAi, the CRISPR/Cas9 system targets the DNA and is unaffected by differential transcript levels. Not surprisingly, genome wide CRISPR/Cas9 KO screens were soon shown to be an efficient strategy to perform loss of function screens as they made it possible to deplete many genes with higher efficiency compared to RNAi screens (Shalem et al., 2014; Wang et al., 2014).

CRISPR/Cas9 screens entail transduction of cells that express Cas9 with a pool of sgRNAs targeting genes of interest. By comparing the sgRNA populations before and after applying a selective pressure of interest, one can discriminate between genes that when depleted promote (positive selection) or impair (negative selection) the viability of cells (**Figure 5B**). CRISPR screens coupled with small molecule treatments have been extremely valuable in discovering genes that either confer resistance or further synergise with different chemical compounds (Noordermeer et al., 2018; Olivieri et al., 2020; Shalem et al., 2014; Wang et al., 2017; Wang et al., 2014). Importantly, endpoint screens for negative selection cannot discriminate between decreased cell proliferation and cell death as after several passages the sgRNAs that lead to lower proliferation or to cell death will likely be depleted from the population to a similar extent (Doench, 2018).

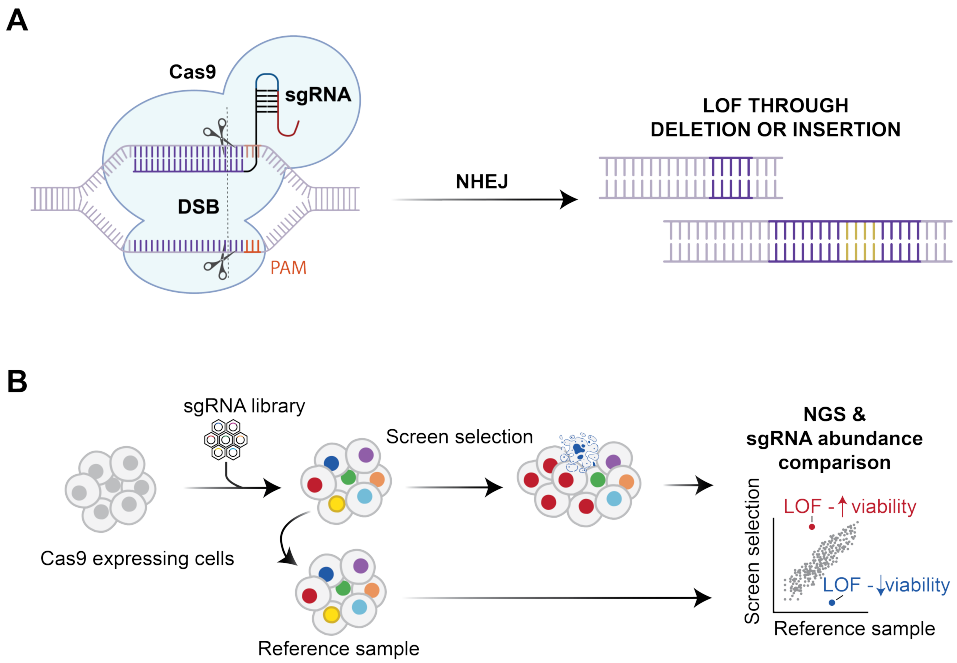

Figure 5. Application of CRISPR/Cas9 technology. (A) Scheme of the Cas9 mediated target gene disruption. A single guide RNA (sgRNA) complementary to the target gene sequence that contains a protospacer-adjacent motif (PAM) guides the Cas9 enzyme to introduce a double strand break. In most cases, the double strand break is repaired by the error-prone non-homologous end joining mechanism (NHEJ), resulting in deletions or insertions that lead to target gene disruption. **(B)** Overview of a basic CRISPR/Cas9 screen. A pool of sgRNAs targeting genes of interest is introduced into the cells expressing Cas9. Cells are then maintained under the selection of choice, e.g. drug treatment, and the effect of target disruption on cell viability is determined by comparing the sgRNA abundance at the end of the treatment with the reference sample by next generation sequencing (NGS).

While fitness screens in cell lines are extremely powerful for discovering new molecular players of different processes, what pushed the field forward were parallel screens performed in multiple cell lines. In 2014, Hart and colleagues defined a reference set of essential and non-essential genes. They described a 'Daisy Model' of gene dependencies where different cell lines and tissues confer context-specific dependencies while a core set of fitness genes, such as for instance ribosomal or tRNA metabolism genes, are essential regardless of the context (Hart et al., 2014). The context specific cancer cell dependencies are in some instances defined by the genotype, as in the case of the cells with *KRAS* or *BRAF* driver mutations that are more sensitive to depletion of other signalling cascade components, or by specific metabolic requirements (Hart et al., 2015). In a similar line, CRISPR/Cas9

screens performed in a panel of 14 human acute myeloid leukaemia cell lines underscored the ability of this approach to map protein networks essential for cell survival (Wang et al., 2017).

Genome wide RNAi and CRISPR/Cas9 loss of function screens have made it possible to characterise molecular cancer cell dependencies across many cell lines. Two major RNAi projects are Project Achilles from the Broad Institute that targeted 11,000 genes with shRNAs in a panel of around 500 cancer cell lines (Cowley et al., 2014; Tsherniak et al., 2017), and Project DRIVE by Novartis that employed shRNAs targeting almost 8,000 genes in 389 cancer cell lines (McDonald et al., 2017). These datasets have recently been complemented with genome-wide CRISPR/Cas9 KO screens performed in more than 1000 cancer cell lines, and are available in the Dependency Map (DepMap) portal (Dempster et al., 2021). By comparing genetic dependencies, molecular characteristics of cancer cells and drug sensitivity profiles, it is possible to elucidate context specific dependencies and potential biomarkers that can aid the patient stratification (**Figure 6A**).

The use of the DepMap data has helped to uncover a number of context specific vulnerabilities. Examples include the studies reporting that cancer cells deficient in the methylthioadenosine phosphorylase MTAP are more dependent on the loss of the arginine methyltransferase PRMT5 (Kryukov et al., 2016), that microsatellite instable cancer cells require the WRN helicase activity (Chan et al., 2019), that SMAD4 or CDH1 deficiency is synthetic lethal with the loss of the paralog enzymes VPS4A/B (Neggers et al., 2020), and that the PKMYT1 kinase is a vulnerability of cancer cells harbouring CCNE gene amplification (Gallo et al., 2022). In ovarian cancer cells, high expression of the phosphate importer SLC34A2 correlates with dependency on the phosphate exporter XPR1, making the XPR1–KIDINS220 complex a potential target for ovarian cancer treatment (Bondeson et al., 2022).

The DepMap data has also enabled the identification of cancer cell pan-essential genes, i.e. genes that when depleted show a lethal phenotype in the majority of the screened cancer cell lines. Interestingly, a number of compounds that are currently used in clinical trials, such as HDAC or PLK1

inhibitors, are targeting pan-essential genes. Despite showing promising effects in the preclinical models, these compounds had low success in the clinical trials, at least in part due to their high toxicity that can be attributed to the essentiality of the targets. In contrast, PI3Kα, EGFR and ALK inhibitors target context specific cancer cell vulnerabilities and several of them have managed to obtain FDA approval (**Figure 6B**) (Chang et al., 2021). This further illustrates the potential of the increasing knowledge of cancer cell models in prioritising more efficient therapy approaches.

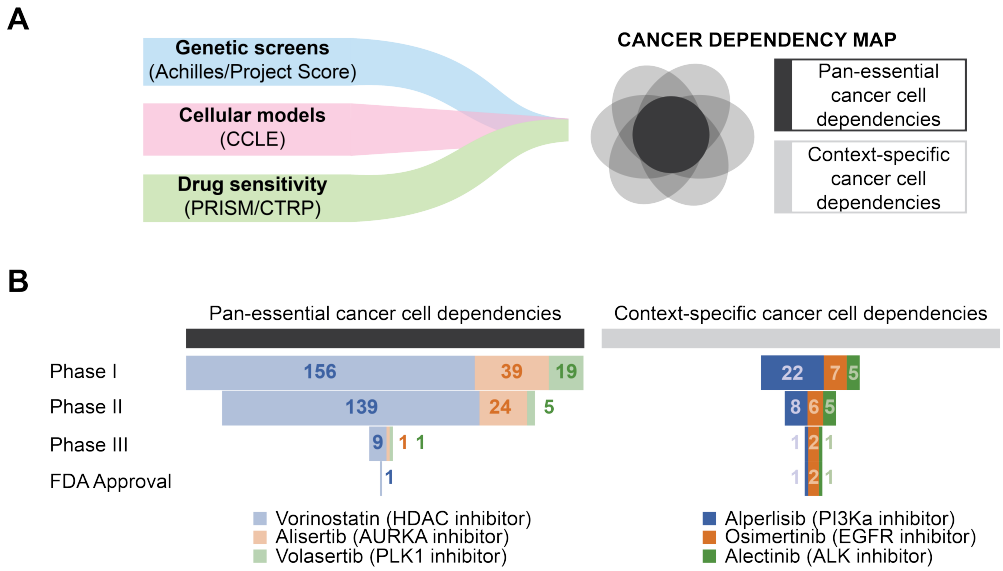

Figure 6. Pan-essential and context-specific cancer cell dependencies. (A) Databases such as DepMap contain a plethora of datasets characterising different cancer models. This enables identification of pan-essential cancer cell dependencies, i.e. genes that when disrupted will impair viability of the majority of cell lines tested. On the other hand, it also allows identification of context-specific dependencies that will efficiently target cell lines harbouring particular characteristics. Figure is made based on the DepMap website schematic. **(B)** Recent studies point to the promise of targeting context-specific dependencies, as this approach seems to identify compounds that pass the FDA approval with a higher frequency. Figure modified from Chang et al., 2021.

Non-oncogene addiction

Malignancy is an energetically expensive process and cancer cells have to endure high levels of different stresses. Many cellular pathways are rewired in cancer cells to support their proliferation and survival. This hinted that the metabolic and growth requirements of cancer cells might actually convey particular vulnerabilities that when targeted will preferentially affect the malignant cells. Enhanced activity of these targets in non-malignant cells does not usually show oncogenic potential, hence this phenomenon became known as 'non-oncogene addiction (**Figure 7**) (Solimini et al., 2007).

One of the first described non-oncogene addiction factors was heat-shock factor 1 (HSF1), a master regulator of heat-shock response. Loss of HSF1 can hinder the incidence and progression of *RAS* or *TP53* driven tumours. At the same time, depletion or overexpression of *HSF1* in non-malignant cells shows no oncogenic potential (Dai et al., 2007). Moreover, HSF1, together with other components of the cellular response to proteotoxic stress, was shown to be essential in the cellular response to diverse stresses. The components of these signalling pathways are seldom mutated, as often losing the precise regulation of their function is not beneficial for cancer cell survival.

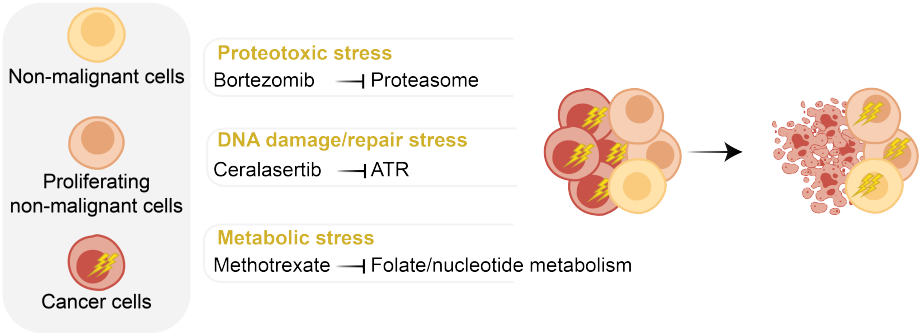

Figure 7. Targeting non-oncogene addiction. Targeting cell mechanisms that mitigate increased proteotoxic stress, DNA damage and repair, or the metabolic requirements of the cancer cells has been described as a promising approach to selectively eliminate cancer cells.

Building on the discovery of the HSF1 importance, several genome wide screens identified additional genes that regulate proteasomal degradation and protein folding as cancer cell dependencies (Marcotte et al., 2012; Martens-de Kemp et al., 2013; Nagel et al., 2015). Genetic alterations prevalent in cancer cells often lead to either improper folding or dysregulated dosage of different proteins, which can result in protein aggregations. Hence, cancer cells rely on the activity of heat-shock proteins and increased levels of proteasomal degradation (He et al., 2013; Jolly & Morimoto, 2000) and autophagy (Levy et al., 2017) in order to deal with their proteotoxic stress. Accordingly, the proteasome inhibitor bortezomib, has shown potential in treating some cancer types, especially those driven by *KRAS* (Luo et al., 2009).

Cancer cells also have to cope with increased levels of reactive oxygen species (ROS). The role of ROS in tumorigenesis is two sided. High levels of ROS in non-malignant cells leads to increased DNA damage and the accumulation of mutations. Accordingly, inactivating regulators of the cellular response to oxidative stress, such as MTH1 or NRF2, promotes tumour incidence in mouse models but is detrimental in cancer cells as they rely on these pathways to maintain manageable levels of ROS (Gad et al., 2014; Satoh et al., 2013). In the same line, treatment of cancer cells with ROS-inducing compounds such as piperlongumine and dichloroacetate shows anticancer effects (Bonnet et al., 2007; Trachootham et al., 2006). Interestingly, increased DNA damage levels have a similar effect as high ROS levels. Many tumour suppressor genes, such as *BRCA1/2*, *ATM* and Fanconi anaemia genes are key components of the DNA damage repair (DDR) pathway (D'Andrea & Grompe, 2003). However, while the proper functioning of DDR pathways prevents tumour initiation, they are essential to handle the increased levels of DNA damage occurring in tumour cells. In this line, targeting ataxia telangiectasia and Rad3-related protein (ATR), a key kinase for sensing the replication stress, and its downstream target checkpoint kinase 1 (CHEK1) has shown anticancer effect in preclinical models (Campaner & Amati, 2012; Murga et al., 2011).

Overall, non-oncogene addiction provides a possible way to target cancers driven by the so far undruggable oncogenes. In addition, some stress adaptation requirements of cancer cells are common across different oncogenic driver events. In this light, the protein kinase p38α, one of the master regulators of the cellular responses to a variety of stress stimuli, emerges as an attractive target for cancer treatment, since it has been shown to support progression of several tumour types, it is seldom mutated, and potent chemical inhibitors are available in the market.

The p38 MAPK signalling pathway

The adaptation of cells to the continuously changing environment hinges on their ability to recognize and adequately respond to pressures and stimuli, both intrinsic and extrinsic. This is achieved through different signalling cascades that connect the initial stimuli with the adequate response. Stimuli are sensed by the cell through receptor proteins, which in turn activate the intracellular signalling cascades that will activate the effector proteins and shape the final response of the cell. Protein kinases are important components of the cellular signalling pathways. They are enzymes that can modify other proteins by covalently adding phosphate groups. Kinases function as molecular switches that further relay the activation signal to their downstream targets resulting in a specific change of cellular behaviour. There are over 500 described human protein kinases encoded by ~2% of the human genes, highlighting the diversity of these signalling effectors (Manning et al., 2002).

Mitogen activated protein kinases (MAPKs) form one of the major protein kinase families. The MAPK signalling cascade classically comprises sequential activation of three protein kinases - a MAP kinase kinase kinase (MAP3K), which when activated phosphorylates and activates a map kinase kinase (MAP2K) that in turn phosphorylates and activates the MAPK, which transduces the signal to its wide range of substrates (**Figure 8A**). MAP3Ks belong to the tyrosine kinase-like family, MAP2Ks are serine-threonine kinases, and MAPKs belong to the CMGC kinase family, which also encompass cyclin-dependent kinases, glycogen synthase kinases and CDC-like kinase groups of protein kinases. The best characterised branches of the conventional MAPKs include the extracellular signal-regulated kinases (ERK)1/2, the c-JUN amino-terminal kinases (JNK)1/2/3, and the p38 MAPK subfamily (p38α/β/γ/δ). ERK5 is also considered a conventional MAPK, however, it is the least studied one.

Conventional MAPKs are activated by phosphorylation on their conserved T-X-Y motif within the activation loop. The atypical MAPKs ERK3/4 and Nemo-

like kinase (NLK) have the T-X-Y motif substituted by a single phospho-acceptor residue within an S-E-G motif. ERK7 contains a T-X-Y motif, same as ERK1/2 and ERK5, but it is considered an atypical MAPK, as it is much less conserved across species. For instance, the zebrafish ERK7 is only around 50% identical to the human ERK7, while zebrafish and human ERK1 are more than 90% identical (**Figure 8B**) (Coulombe & Meloche, 2007).

Contrary to the name of the family to which they belong, p38 MAPKs do not primarily respond to mitogens. While ERK1/2 are mainly activated by growth factors and mitogens (Lavoie et al., 2020), numerous stress-inducing stimuli can lead to the activation of both p38 MAPKs and JNKs, hence they are also known as stress-activated protein kinases (SAPKs).

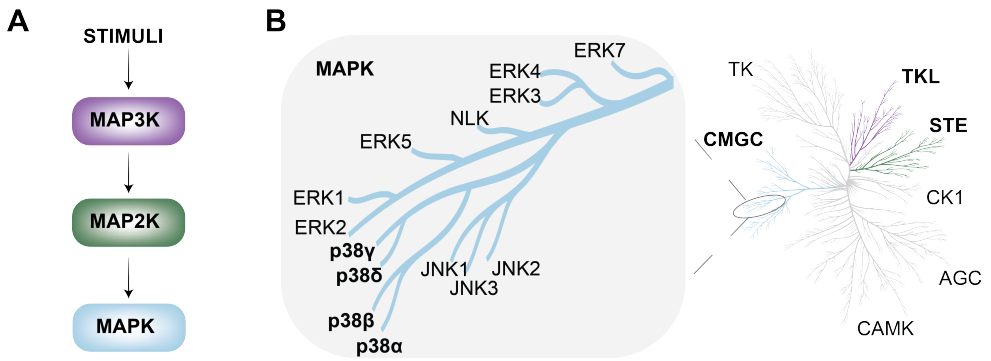

Figure 8. MAPKs. (A) Core components of a canonical MAPK activation cascade. Stimuli is sensed by the cell and relayed through phosphorylation events that lead to activation of a MAPK, which in turn orchestrates the cellular response to a given stimuli. **(B)** Human kinome tree (right) showing MAP3Ks that belong to the tyrosine-kinase like (TKL) family of proteins (purple), and MAP2Ks that are part of the serine-threonine kinase (STE) family (green). The branch of MAPKs that belong to the CMGC family (blue) is shown on the left. Kinome tree was created using Coral web application (Metz et al., 2018).

The first p38 MAPK family member was reported in several independent studies. Identified as a tyrosine phosphorylated protein in response to lipopolysaccharide (LPS) treatment (Han et al., 1994), a reactivating kinase (RK) that phosphorylates and activates MAPK-activated protein kinase 2 (MK2) upon osmotic stress, heat shock or sodium arsenite (Rouse et al.,

1994), a kinase activated in response to interleukin-1 (Freshney et al., 1994) and as a target of pyridinyl imidazole compounds (Lee et al., 1994). This p38 MAPK is today known as p38α, the most ubiquitously expressed p38 family member with high homology to the Hog1 MAPK in *S. cerevisiae*, which is important for osmostress response (de Nadal & Posas, 2022). Shortly after, the MAP2K family members MKK3, MKK4 and MKK6 were cloned and described as upstream activators of p38α (Dérijard et al., 1995; Han et al., 1996; Lin et al., 1995).

The discovery of p38α (encoded by *MAPK14*) was followed by the identification of three additional p38 MAPKs. p38β is encoded by *MAPK11* and was reported to be expressed in most tissues and sensitive to the inhibition by pyridinyl imidazole compounds, same as p38α (Jiang et al., 1996). p38γ is encoded by *MAPK12* and was described to be primarily expressed in muscle cells and, unlike the other two p38 kinases, insensitive to inhibition with pyridinyl imidazole compounds and unable to phosphorylate MK2 and ATF2 *in vitro* (Cuenda et al., 1997; Lechner et al., 1996; Li et al., 1996; Mertens et al., 1996). p38δ is encoded by *MAPK13* and is expressed at higher levels in pancreas, intestine, kidney, adrenal gland and heart, and is also not sensitive to pyridinyl imidazole compounds (Goedert et al., 1997; Jiang et al., 1996). The four p38 family members are around 60% identical in their amino acid sequence, with p38α and p38β being the most similar as they are 75% identical. Due to the sequence similarity, and the differential sensitivity to the pyridinyl imidazole compounds, the p38 kinases are often divided into two subgroups, p38α/β and p38γ/δ.

Activation of the p38 MAPK pathway

The p38 pathway can be activated in response to a wide range of stimuli, including different stresses, cytokines and G protein-coupled receptor (GPCR) agonists, which in most cases leads to the activation of the typical MAPK phosphorylation cascade known as the canonical pathway. The outcome of the pathway activation is shaped by the different molecular components of the cascade, and the extensive intermediary nodes between

the stimuli and the p38 MAPK underscore the complexity of this pathway, which is far from being completely understood (**Figure 9**).

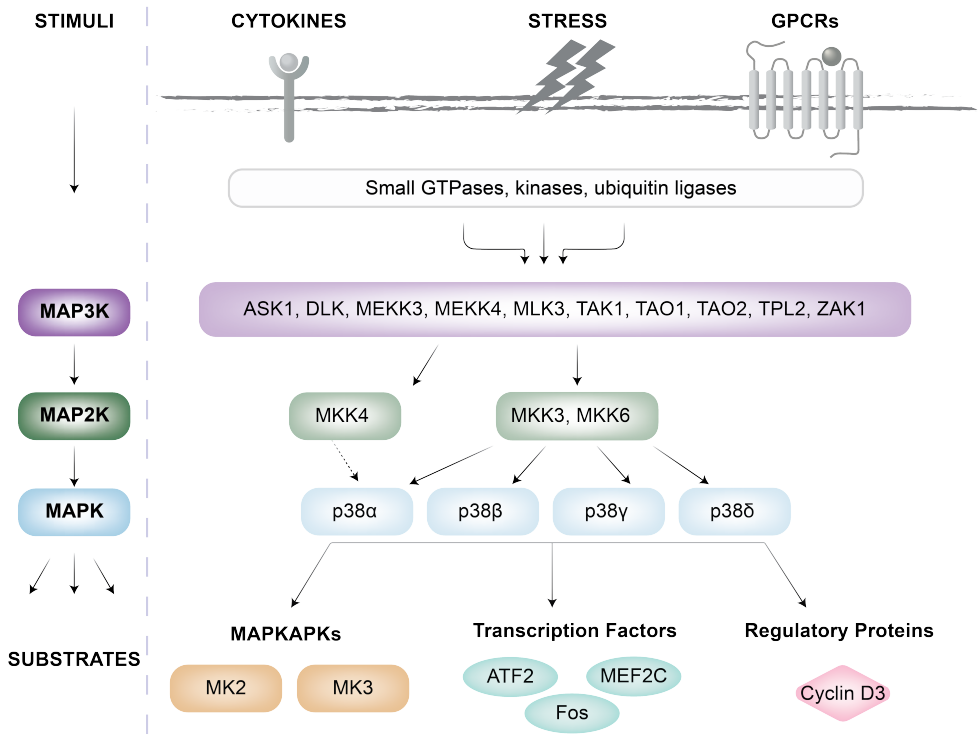

Figure 9. Activation of the p38 MAPK pathway. The canonical activation pathway is represented, together with some of the downstream substrates reported to be targeted by the four p38 MAPK family members.

Over the years, around ten different MAP3Ks have been described to trigger the p38 cascade activation. For example, TAO1/2 are activated in response to DNA damage (Chen et al., 1999; Hutchison et al., 1998; Raman et al., 2007), ZAK1 is activated in response to ribotoxic stress (Bloem et al., 2001; Jandhyala et al., 2008; Wang et al., 2005), oxidative stress leads to ASK1 activation (Ichijo et al., 1997) and TAK1 can be activated in response to TGF-β signalling (Moriguchi et al., 1996; Yamaguchi et al., 1995). Downstream of the MAP3Ks, two MAP2Ks are mostly responsible for phosphorylation and activation of p38 MAPKs: MKK3 (encoded by *MAP2K3*) and MKK6 (encoded by *MAP2K6*). Different MAP2Ks have distinct capacity to phosphorylate p38 family members, which also depends on the specific stimuli and cellular context (Enslen et al., 1998; Remy et al., 2010). For example, in mouse

embryonic fibroblasts (MEFs) treated with anisomycin, sorbitol or TNFα, depletion of both MKK3 and MKK6 was required to abolish p38α activation, but in response to UV treatment p38α was still activated in the absence of MKK3 and MKK6 (Remy et al., 2010), which is probably due to the ability of MKK4, an upstream MAP2K of the JNK pathway (Brancho et al., 2003), to at least partially activate p38α. Similarly, p38β phosphorylation was impaired only in the double MKK3/MKK6 KO cells upon all stimuli. In contrast, MKK6 deletion was sufficient to impair activation of p38γ, and MKK3 was crucial for p38δ activation. Together with other studies (Alonso et al., 2000; Brancho et al., 2003; Enslen et al., 1998), this illustrates the complexity of the system and the importance of the particular context in defining the connections in the p38 MAPK pathway.

In addition to the canonical activation cascade, two non-canonical pathways are described to activate p38α. T-cell receptor activation leads to ZAP70 phosphorylation of p38α on Tyr323, which in turn stimulates its autophosphorylation preferentially on Thr180 (Salvador et al., 2005). Interestingly, it has been reported that the mono-phosphorylated p38α shows different substrate specificity (Mittelstadt et al., 2009). Another non-canonical activation pathway is triggered by the binding to TAB1, which can induce p38α autophosphorylation (Ge et al., 2002).

Regulation and termination of p38 MAPK signalling

Fine tuning of the p38 pathway is achieved through different regulatory mechanisms that can overall impact the level of p38 activation. For instance, different scaffolding proteins can regulate p38 activation by binding to several components of the signalling cascade and bringing them into close proximity. Some examples are RACK1, AAPL1, JIP4 or OSM (Lin et al., 2015; Pinder et al., 2015; Uhlik et al., 2003; Xin et al., 2011). Different posttranslational modifications apart from the phosphorylation have also been shown to modulate the function of p38α, such as acetylation or arginine methylation (Brichkina et al., 2016; Jeong et al., 2020; Liu et al., 2020; Pillai et al., 2011).

Duration of the pathway activation is one of the most critical factors as it can determine the outcome of the p38α activity. Therefore, it is not surprising that several negative feedback loops and regulatory mechanisms that lead to p38 MAPK signal termination have been described so far. Once activated, p38α can limit its own activation by phosphorylating upstream cascade members, such as TAB1 (Cheung et al., 2003) and ZAP70 (Giardino Torchia et al., 2018) or by negatively regulating MKK6 mRNA stability (Ambrosino et al., 2003).

Signal termination can also be achieved through different serine/threonine, tyrosine and dual specificity phosphatases (DUSPs) that can inactivate p38α by dephosphorylating it. For instance, in response to UV, peroxide or cisplatin treatment, p38α activation increases the expression of DUSP1 through MSK1/2-CREBα axis, which in turn dephosphorylates both p38α, attenuating its activity, and JNK, thus promoting the survival of the cells (Staples et al., 2010). Interestingly, p38γ and p38δ are insensitive to DUSPs (Tanoue et al., 2001). Another negative feedback loop is triggered in response to genotoxic stresses, where p38α can increase the p53 activity, which in turn induces the expression of the Wip1 phosphatase, a member of the protein phosphatase type 2C family. Wip1 then inactivates the p38/p53 axis through dephosphorylation of both proteins, limiting the pathway activity during the cell recovery phase (Takekawa et al., 2000). Overall, the activation and termination of p38 MAPK signalling is tightly regulated by several processes that employ an extensive network of modulators.

Versatility of p38 functions

Although p38 MAPKs were initially described as kinases that primarily respond to stress stimuli such as UV, LPS, osmotic stress or heat shock, further studies have demonstrated the important roles of this kinase family in a variety of biological processes.

There are over 400 annotated putative p38α substrates, including kinases and transcriptional factors that modulate diverse cellular events such as cell proliferation, migration or survival (**Figure 10**) (Cuadrado & Nebreda, 2010; Han et al., 2020; Martínez-Limón et al., 2020; Trempolec et al., 2013).

Several of the MAP3Ks described to activate the p38 signalling cascade have also been reported to activate ERK1/2 and JNK signalling in response to specific stimuli. Hence, the outcome of p38α activation is not only shaped by a specific combination of upstream activators, downstream targets and different regulatory mechanisms, but also by the crosstalk with other signalling pathways that adds an additional layer of complexity to p38 MAPK signalling.

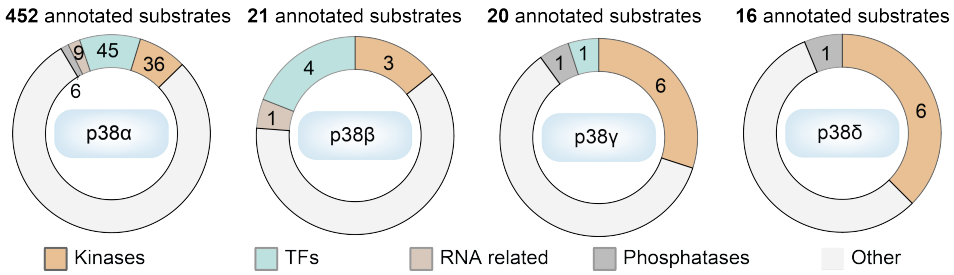

Figure 10. p38α is the best characterised p38 MAPK. Figure shows annotated substrates of different p38 MAPKs retrieved from the KEA substrates of kinases (Lachmann & Ma'ayan, 2009) and PhophoSitePlus Substrates of Kinases (Hornbeck et al., 2004, 2015) datasets. There are over 400 annotated p38α substrates compared to around 20 reported for the other p38 MAPK family members. Legend indicates substrates that are other kinases (orange), transcription factors (TFs, teal), RNA related proteins (beige) and phosphatases (grey).

During embryonic development, p38α is the only essential p38 MAPK, as p38α KO mice are embryonic lethal due to defects in placental development (Adams et al., 2000; Mudgett et al., 2000). Studies with conditional depletion of p38α restricted to embryonic tissues showed that loss of p38α is fatal during postnatal development (Hui et al., 2007). While genetic models of p38β depletion demonstrated no adverse effects on embryonic development (Beardmore et al., 2005), combined depletion of both p38α and p38β resulted in embryonic lethality with major cardiac defects detected as well as other phenotypes not observed in individual KO mice, indicating that p38β can compensate for loss of p38α in specific processes. However, expression of p38β under the p38α promoter was not able to rescue neither placental development nor cardiac defects, suggesting distinct roles of each p38 MAPK (del Barco Barrantes et al., 2011). In contrast, p38γ, p38δ and double p38γ/δ KO mice have been shown to be viable and fertile, with no major defects during development (Sabio et al., 2005).

The necessity of p38α during embryo development hints at the important role of this kinase in regulating essential cellular processes. This is in part achieved through the variety of downstream substrates, among which are also several protein kinases such as MK2/3/5, MSK1/2 and MNK1/2. MK2 can regulate the actin filament remodelling through phosphorylation of Hsp27 (Guay et al., 1997), and can modulate post-transcriptional events through phosphorylation of different adenylate–uridylate-rich element (ARE)-binding proteins such as tristetraprolin (TTP) and Human antigen R (HuR) (Soni et al., 2019). MSK1 and MSK2 have diverse roles in the control of the gene transcription activation (Reyskens & Arthur, 2016), and MNK1 and MNK2 are described to regulate protein translation through phosphorylation of the initiation factor eIF4E in response to activation by p38α (Wang et al., 1998). Interestingly, both MSK1/2 as well as MNK1/2 can also be activated by ERK1/2 signalling. p38α also has an important role in cell cycle progression. In G1/S, p38α can induce cell cycle arrest through down-regulation of cyclin D1, activation of the p53/p21Cip1 pathway or transcriptional up-regulation of p16INK4a (Casanovas et al., 2000; Goloudina et al., 2003; G.-Y. Kim et al., 2002; J. N. Lavoie et al., 1996). In G2/M, p38α mediates cell cycle arrest either through MK2 activation or by directly phosphorylating Cdc25B and Cdc25C (Donzelli & Draetta, 2003; Lemaire et al., 2006; Manke et al., 2005). The induction of cell cycle arrest as well as upregulation of the anti-apoptotic BCL-2 proteins (Phong et al., 2010), are examples of the pro-survival functions that p38α can perform in the cellular response to different genotoxic stresses.

An additional layer of complexity comes from the crosstalk with other signaling pathways. For instance, a number of the upstream activators and substrates of p38α overlap with those of other protein kinases. An interesting example is the cross-talk with the JNK pathway. The p38 and JNK pathways are often simultaneously activated, despite this, in some systems the JNK pathway is negatively regulated by p38α, as downregulation of p38α leads to increased levels of JNK activation (Batlle et al., 2019; Hu et al., 2018). A recent study that examined the dynamics of the p38 and JNK activation at a single cell level demonstrated that in a population of cells,

p38α can mediate cell survival by activating DUSP1, which then inactivates the pro-apoptotic JNK signalling. Interestingly, this p38α induced *DUSP1* expression was present in a subset of cells, and seems to be a consequence of stochastic events, although this is not entirely clear (Miura et al., 2018).

The interplay of different p38 family members in determining the outcome of the p38 MAPK pathway activation has also been reported. This can be due to distinct activation patterns, as in endothelial cells where TGF-β1 activates p38α that leads to increased levels of apoptosis, while VEGF activates p38β, promoting cell survival (Ferrari et al., 2012). In other cases, the endogenous levels of different p38 MAPKs shape their function, as in the regulation of the AP-1 transcription factor, a dimeric complex that contains members of the JUN, FOS, ATF and MAF protein families (Jochum et al., 2001). Thus, the activation of p38β by MKK6 stimulates AP-1 dependent transcription in murine NIH3T3 cells that express low levels of p38δ, but not in p38δ expressing EMT-6 murine cells (Pramanik et al., 2003). A direct link between different p38 MAPKs has also been reported, as the negative regulation of p38δ activity by p38α to supress the brown adipose tissue thermogenesis (Matesanz et al., 2018). Nevertheless, most of the studies investigating the functions of p38 MAPKs focus implicitly on the p38α, and the same applies to the publications that specify the isoform studied (**Figure 11A**).

Of note, these are just a few illustrative examples meant to showcase the complexity of this signalling pathway and by no means encompass all the reported biological functions of p38 MAPKs. An important point is that many studies reporting particular roles for p38 MAPKs base their conclusions solely on the use of chemical inhibitors (**Figure 11B**). While valuable, p38 inhibitors have a number of limitations. On one hand, they often do not discriminate between different p38 family members, as is the case with the ATP-competitive inhibitor BIRB769, which at higher doses inhibits all four p38 MAPKs (Kuma et al., 2005). This makes it difficult to distinguish individual contributions of different family members to the phenotypes reported. In addition, the concentrations of the inhibitors used in many studies are often unnecessarily high, increasing the probability of potential off-target effects (He et al., 2013; Menon et al., 2011). The drawbacks of

some p38 inhibitors emphasise the importance of genetic tools to study the p38 MAPK pathway.

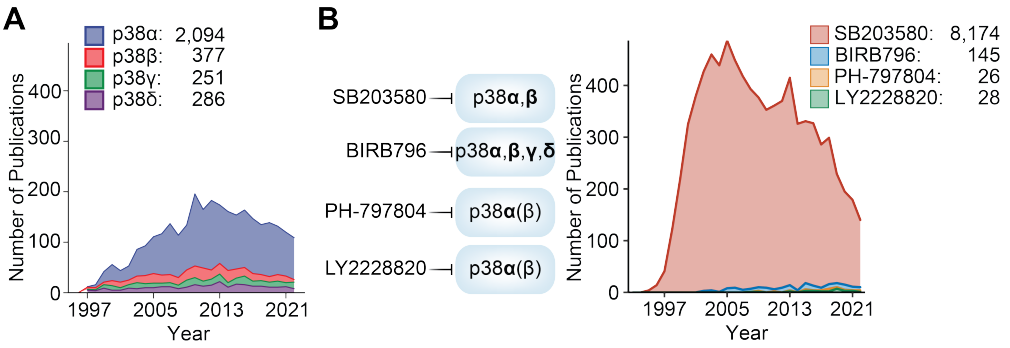

Figure 11. PubMed entries for p38 MAPK inhibitors. Results of PubMed queries for the indicated p38 family members **(A)** and p38 inhibitors **(B)** reported until 2022.

A number of studies have been performed describing different functions of p38α. Despite this, the complexity of this pathway still leaves many questions unanswered. It is however clear that p38α is a central modulator of many homeostatic functions, some of which are dysregulated in different pathological contexts, explaining the interest in studying the role of p38α in diseases such as cancer.

Context dependent role of p38α in cancer cells

The p38α kinase is important in several cancer cell types and has specific functions not only in the cancer cells but also in different components of the tumour microenvironment, such as fibroblasts and endothelial cells, as well as in different immune cell populations.

p38α was initially described as a tumour suppressor as its activity was reported to limit the oncogene-induced malignant transformation. For instance, p38α can negatively regulate the *H-Ras*-induced malignant transformation of fibroblasts through induction of premature senescence (Wang et al., 2002), induction of p53 dependent cell cycle arrest (Bulavin et al., 2002) or upregulation of cell cycle inhibitors (Nicke et al., 2005). Some of the inhibitory effects are due to the p38α mediated induction of apoptosis and prevention of ROS accumulation in the early stages of transformation (Dolado et al., 2007). Different mouse models have provided *in vivo* evidence further emphasising the importance of p38α in suppressing tumour initiation. Mice deficient in Wip1 phosphatase show increased p38α activation levels and reduced tumorigenesis of breast cancer upon *Erbb2* or *H-Ras* expression, while treatment with the p38 inhibitor SB203580 rescues *Erbb2* driven tumorigenesis of Wip1 KO mice (Bulavin et al., 2004). Depleting Gadd45α, an activator of the p38 MAPK pathway, reduces p38α activation and breast tumorigenesis induced by *Ras* (Tront et al., 2006). Consistent with an important role of p38α in lung homeostasis, depleting p38α in adult mice increases proliferation and impairs differentiation of the lung stem and progenitor cells, leading to increased incidence of oncogenic *K-Ras G12V* induced tumours (Ventura et al., 2007). In the liver, loss of p38α increases hepatocyte proliferation through increased activation of the JNK pathway resulting in increased development of chemically induced liver cancer (Hui et al., 2007). Similarly, deletion of p38α in intestinal epithelial cells increases the tumour development induced by azoxymethane/dextran sodium sulphate treatment (Gupta et al., 2014; Wakeman et al., 2012). Overall, p38α activity is important for homeostasis and limits malignant transformation of different tissues. However, there are many reports showing that once the tumours are

formed, established cancer cells can become dependent on p38α for their survival. Hence it seems that once the cells are transformed, this pathway can be hijacked in order to sustain cancer cell survival.

Accordingly, inhibition or deletion of p38α impairs viability of established colon cancer cell lines and reduces tumour growth both in models of xenografts in nude mice as well as in azoxymethane-treated *Apc*^{Min} mice (Chiacchiera et al., 2009; Comes et al., 2007). This dual role of p38α was demonstrated in a model of chemically-induced colon cancer, in which p38α loss in the epithelial intestinal cells promotes tumour formation, while deletion of p38α after tumours are formed reduces cancer cell proliferation and increases apoptosis, thus reducing the tumour burden (Gupta et al., 2014). In a *K-Ras G12V*-driven lung cancer model, p38α also promotes the proliferation of cancer cells through regulation of a metallopeptidase inhibitor TIMP-1, and the deletion or inhibition of p38α impairs tumour progression (Vitos-Faleato et al., 2020). This cancer cell dependence on p38α has also been observed in models of multiple myeloma (Medicherla et al., 2008; Vanderkerken et al., 2007), head and neck squamous cell carcinoma (Leelahavanichkul et al., 2014) and UV induced skin tumorigenesis (Dickinson et al., 2011; Liu et al., 2013), or in ER negative p53 mutant breast cancer cell lines (Chen et al., 2009). Moreover, a study investigating the p38α inhibitor LY2228820, reported beneficial effects of p38α inhibition in models of melanoma, non-small cell lung cancer, ovarian, glioma, myeloma and breast cancer (Campbell et al., 2014).

When it comes to the chemotherapy response, many first line chemotherapeutic drugs elicit p38α activation. Again, the outcome of the p38α activity depends both on the cellular context and on the drug used, and there are even reports describing opposing roles of this kinase in response to the same drug. The activity of p38α is reported to be essential for the cytotoxic effect of oxaliplatin in human colorectal adenocarcinoma cells (Rasmussen et al., 2016), or imatinib in the chronic myeloid leukaemia cell line K562 (Maia et al., 2009). Treatment with cisplatin, a platinum-based drug often used in a number of cancers, can lead to activation of p38α which in some models results in p53 activation (Bragado et al., 2007) or EGFR

internalisation (Zwang & Yarden, 2006), thus mediating *in vitro* cytotoxicity of cisplatin. On the other hand, the inhibition of p38α in a mouse model of polyoma middle T (PyMT) induced mammary tumours can synergise with cisplatin treatment by increasing ROS accumulation (Pereira et al., 2013). A number of studies also reported beneficial effects of p38α inhibition in combination with MEK inhibitors in colorectal cancer (Chiacchiera et al., 2012; Lepore Signorile et al., 2021; van Houdt et al., 2010), non-small cell lung cancer (Sunaga et al., 2019) and hepatocellular carcinoma models (Rudalska et al., 2014). In glioma cancer cells, inhibiting p38α synergises with the methylating agent temozolomide (Gao et al., 2022; Hirose et al., 2003).

Altogether, p38α seems to function as a non-oncogene addiction factor that is seldom mutated in cancer cells supporting their viability once the tumours are established. Of note, a recent study reported that high concentrations of p38α inhibitors can decrease the viability of established cancer cell lines even after deletion of p38α, while deleting p38α on its own has no effect, suggesting that the cytotoxicity observed (at very high concentrations) is due to the off-target effects of the inhibitor (Lin et al., 2019). This further emphasises the importance of combining chemical inhibitors with the genetic perturbation of p38α to study p38α cancer cell dependency.

An interesting model to address this issue was described by Cánovas *et al*., which showed that p38α is essential for the progression of PyMT-induced mouse mammary tumours, as genetic KO of p38α leads to tumour regression (Cánovas et al., 2018). Importantly, the effect of p38α was cancer cell autonomous. In cultured epithelial cells established from these tumours, p38α restricts DNA damage and genome instability, supporting cancer cell survival and proliferation. Accordingly, p38α deletion in these cells results in increased cell death and enhanced levels of DNA damage compared to the wild type (WT) tumour cells, in part due to impaired CtIP phosphorylation and DNA repair. In this model, inhibition of p38α in combination with taxanes, which are known to promote chromosomal instability, shows increased cytotoxicity, further supporting the role of p38α in genome integrity maintenance. The same effect of potentiating taxane treatment was

observed in patient derived xenografts, unravelling a promising context in which p38α inhibition could be of clinical relevance.

To this day, p38α remains the most studied p38 MAPK family member and this also applies to the context of cancer cell biology. Accordingly, a number of clinical trials has been performed to test the potential of p38α inhibitors in cancer treatment, however with limited success, which is in most cases could be caused by off-target toxicity (**Figure 12A**) (Cánovas & Nebreda, 2021). Development of more specific and potent inhibitors is without a question invaluable to potential uses in the clinic. However, in addition to having the right tools for targeting p38α, it will be crucial to understand when and why the loss of p38α activity is detrimental to cancer cells.

In summary, while p38α represents an attractive therapeutic target, it is clear that its tumour supporting role is not a universal property. The nature of the p38α pathway and the particular cellular context shape the consequences of the p38α activity. Hence, deciphering the molecular cues that determine cancer cell dependency on p38α would be crucial to understand the potential beneficial effect of p38α inhibition for cancer therapy (**Figure 12B**).

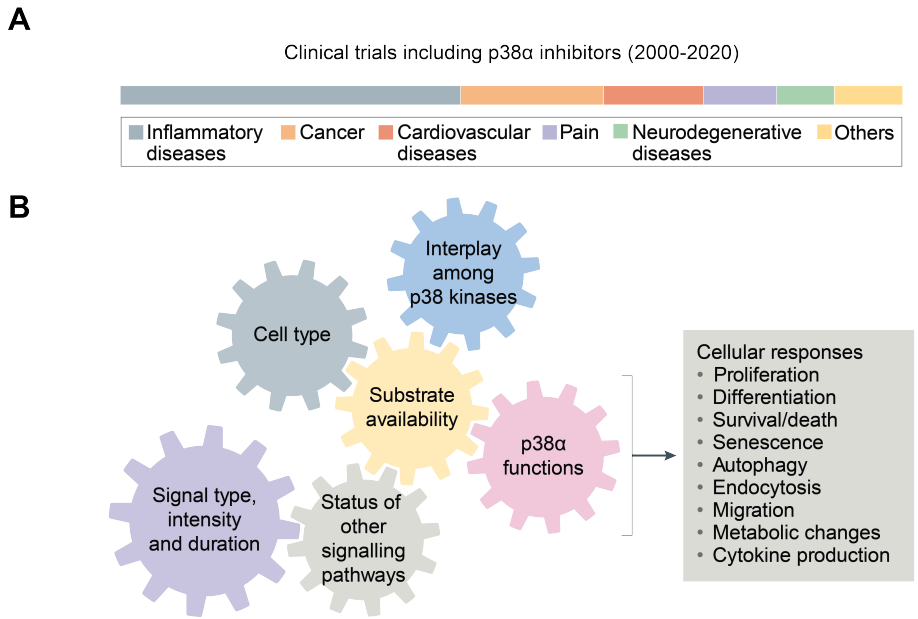

Figure 12. p38α as a therapeutic target in cancer. (A) Overview of the clinical trials with p38 MAPK inhibitors over the past two decades. **(B)** Scheme of molecular determinants that shape the function of p38α. Figure adapted from Cánovas & Nebreda 2021.

Objectives

Our group and others have shown the beneficial effect of p38α kinase pharmacological inhibition in the response of cancer cells to chemotherapeutic drugs. However, the effect of p38α inhibition is heavily dependent on the cell type and stimulus, emphasizing the need to further understand the underlying mechanisms in order to exploit the full potential of targeting the p38α pathway for cancer treatment. To gain insights into the molecular basis of the cancer cell dependency on p38α, we have performed a genome wide CRISPR/Cas9 screen using a breast cancer model that is sensitive to p38α depletion with the following specific aims:

- Identify targets that mediate the p38α functions

- Elucidate processes that synergise with p38α depletion

- Explore the relationship of p38α with other components of the p38 MAPK pathway

- Analyse the publicly available datasets to extend the observations to other cellular models.

Materials & Methods

Materials

General buffers and solutions

Buffers and solutions used in this thesis are specified below.

10X PBS
1.37 M NaCl
27 mM KCl
100 mM Na_2HPO_4
17.5 mM KH_2PO_4
pH 7.4

10X TBS
0.2 M Trizma base
1.5 M NaCl
pH 7.5

10X Electrophoresis running buffer
0.25 M Tris base
2 M glycine
1% SDS
pH 8.3

10X Immunoblotting transfer buffer
0.2 M Tris base
1.5 M glycine

Ponceau Red
0.1% Ponceau Red powder
5% acetic acid

RIPA buffer
50 mM TRIS-HCl pH 8.0
100 mM NaCl
0,1% (w/v) SDS
1% (v/v) NP40
0,5% (w/v) DOC (Deoxycholic acid)
5 mM EDTA
PhosSTOP™
cOmplete™, EDTA-free Protease Inhibitor Cocktail

5X Protein loading buffer
250 mM Tris pH 6.8
50% glycerol
250 mM DTT
10% SDS
0.1% bromophenol blue

2X HBS buffer
50 mM HEPES
280 mM NaCl
1.5 mM Na_2HPO_4
pH 7.12

Commercial reagents and kits

Cell culture

Table 1 | Cell culture reagents

Reagent	Company	Reference
(5Z)-7-Oxozeaenol	Sigma	O9890
4-hydroxytamoxifen	Sigma	H7904
Anisomycin	Sigma	L4005
Blasticidin S HCl	Invitrogen	A11139-03
Calcium chloride	Sigma	449709
Chloramphenicol	Sigma	C0378
DMEM	Sigma	5796
DMSO	Sigma	D8418
FBS	Life Technologies	10500064
L-Glutamine 200mM	Labclinics	X0550
LY2228820	Selleckchem	S1494
Mr. Frosty freezing container	ThermoFisher	5100-0001
Opti-MEM	ThermoFisher	31985070
PBS 10X	Sigma	D1408
PEI MAX	Polysciences	24765-100
Penicillin/Streptomycin	LabClinics	L0022
PH-797804	Selleckchem	S2726
Polybrene	Sigma	TR-1003-G
Puromycin	Sigma	P9620
Rapamycin	Santa Cruz	sc-3504
RPMI-1640	Sigma	R8758
TC10 Cell Counting Slides	BioRad	145-0011
Trypsin	Sigma	T3924

Commercial kits

Table 2 | Commercial kits

Kit	Company	Reference
Cell proliferation Assay Kit I (MTT)	Sigma	11465007001
Click-iT™ Plus EdU Alexa Fluor™ 647 Flow Cytometry Assay Kit	Sigma	C10635
GenElute Plasmid miniprep kit	Sigma	PLN350-1KT
MycoAlert Mycoplasma Detection Kit	Cultek	H3LT07-418
PureLink on column DNAse	Invitrogen	121-85-010
QIAamp DNA Blood Maxi Kit	Qiagen	51192
QIAquick Gel Extraction Kit	QIAGEN	28704
RC DC protein assay kit II	BioRad	5000122
RealTime-Glo™ MT Cell Viability Assay	Promega	G9713
RNA PureLink Minikit	Ambion	12183018A

Cellular and molecular biology

Table 3 | Cellular and molecular biology reagents

Reagent	Company	Reference
Acetic acid	Panreac	131008.1611
Acrylamide 40% 29:1	BioRad	161-0146
Agarose	Conda	8019
Ammonium persulfate (APS)	Sigma	A3678
Ampicillin	Vitro	CAY-14417
Bromophenol blue	Sigma	B8026
BSA	Sigma	A7906
cOmplete™ Protease Inhibitor Cocktail	Roche	11873580001
Crystal Violet	Sigma	HT90132
DAPI	Life Technologies	P36935
DTT	GE Healthcare	17-1318-02
EDTA	Sigma	E46758

Ethanol 96%	Panreac	141085
Ethanol absolute	Panreac	141086
FastAP	ThermoFisher	EF0651
FastDigest Esp3I	ThermoFisher	FD0454
Glycerol	Sigma	G5516
Luria Broth Base 2500g	Invitrogen	12795-084
Methanol	Panreac	131091
Nitrocellulose Membrane 0.2 µm	Protran	10600001
NP-40	AppliChem	A1694
PFA 16%	EMS	15710
PhosSTOP™	Roche	4906845001
Ponceau Red	Sigma	P3504
Propidium Iodide	Sigma	P4864
qScript cDNA SuperMix	Quantabio	95048
Quick Ligase	NEB	M2200S
RNase A	Qiagen	19101
SDS	Sigma	71725
Sodium chloride	Sigma	433209
SYBR Select Master Mix for CFX	ThermoFisher	4472954
SYBR™ Safe DNA Gel Stain	ThermoFisher	S33102
T4 DNA ligase buffer	NEB	B0202S
T4 PNK	NEB	M0201S
TaKaRa Ex Taq® DNA Polymerase	Clonotech	RR001A
TEMED	Sigma	T9281
TRIZMA-base	Sigma	T6066
TRIZMA-HCl	Sigma	T3253
Trizol	ThermoFisher	15596026
Tween 20	Sigma	P7949

Methods

Cell culture

Cell lines

The BBL358 cell line was previously described (Cánovas et al., 2018). This is an epithelial cancer cell line derived from PyMT-induced mammary tumors in mice with Ubc-Cre-ERT2 and floxed alleles of the p38α-encoding gene *Mapk14*, which allows the 4-hydroxytamoxifen (4-OHT) inducible deletion of p38α.

Adherent BBL358, HEK293T and MIA PaCa-2 cells were grown in Dulbecco's modified eagle media (DMEM) supplemented with 10% foetal bovine serum (FBS), 1% Penicillin/Streptomycin and 1% glutamine. For sub-culturing, the growth media was aspirated and cells were washed once with 1x PBS and incubated with 1 ml trypsin at 37°C until detached. Cells were then collected in complete media, diluted 1/12 (BBL358), 1/8 (HEK293T) or 1/6 (MIA PaCa-2) and re-plated in a new culture dish.

SUP-T1 cells were grown in suspension in RPMI media supplemented with 10% FBS, 1% Penicillin/Streptomycin and 1% glutamine. For sub-culturing, liquid cultures were diluted 1/4 with fresh complete growth media and transferred to a new culture dish.

All cell lines were maintained in complete media at 37°C and with 5% CO_2.

Cell counting

Cells were trypsinized, collected in a final volume of 5 ml of complete fresh media, and then were resuspended carefully and 10 μl of cell solution transferred to a BioRad counting slide. Cell numbers were determined using a BioRad TC10 Automated cell counter.

Cryopreservation of mammalian cells

Cells were collected by trypsinization, centrifuged for 5 min at 200 xg, resuspended in 10% DMSO/FBS freezing solution at $2x10^6$ cells/ml and

transferred to 1.5 ml cryo-tubes. Cryo-tubes were stored in a Mr. Frosty container at -80°C for up to one week and then transferred to liquid nitrogen for long-term storage.

To start cell cultures from frozen aliquots, cells were quickly thawed in a 37°C water bath, and resuspended in 5 ml of fresh complete growth media followed by centrifugation for 5 min at 200 xg. Media containing DMSO was then carefully removed and cells were plated in an appropriate culture dish.

Mycoplasma detection

Cells were routinely tested for mycoplasma using a Mycoplasma Detection Kit. After 72 h of cell growth, 500 μl of the cell media was collected, centrifuged for 5 min at 200 xg and 100 μl of the supernatant transferred to a clean test tube. Then 100 μl of MycoAlert reagent was added, incubated for 5 min at room temperature (RT) after which the luminescence was measured and the value A recorded. Next, 100 μl of MycoAlert substrate was added, luminescence was measured after 10 min of incubation at RT and the value B was recorded. The ratio of B/A was used to determine the mycoplasma status according to manufacturer´s parameters, with B/A < 1 indicating mycoplasma negative status of the samples.

Cell treatments

4-OHT

4-OHT is the active metabolite of tamoxifen. 4-OHT binds to a modified fragment of the estrogen receptor (ER), which allows the Cre-ERT2 recombinase to relocate into the nucleus where it induces the recombination of loxP sites. In our case, the activation of Cre-ERT2-induces the deletion of the *Mapk14* gene that is flanked by loxP sites. To induce p38α downregulation, BBL358 cells were treated with 100 nM 4-OHT for 48 h. A 10 mM stock was prepared in ethanol and stored at -20°C.

Inhibitors of p38α MAPK

PH-797804 is an ATP-competitive inhibitor that can target p38α and p38β with higher selectivity for p38α (Hope et al., 2009). Cells were treated with 2 μM PH-797804. A 2 mM stock was prepared in DMSO and stored at -20°C.

LY2228820 is an ATP-competitive inhibitor highly selective for p38α and p38β, with higher selectivity for p38α (Campbell et al., 2014). Cells were treated with 200 nM LY2228820. A 200 μM stock was prepared in DMSO and stored at -20°C.

Rapamycin

Rapamycin is an allosteric inhibitor of the mTOR complex (Heitman et al., 1991; Sehgal et al., 1975). Cells were treated with the indicated concentrations of rapamycin. A 100 μM stock was prepared in DMSO and stored at -20°C

Chloramphenicol

Chloramphenicol is a synthetic antibiotic that can inhibit mitochondrial protein synthesis by inducing the stalling of mitochondrial ribosomes (Richter et al., 2013) Cells were treated with the indicated concentrations of chloramphenicol. A 100 mM stock was prepared in ethanol and stored at 4°C.

5Z-7-oxozeaenol

5Z-7-oxozeaenol is an ATP-competitive irreversible inhibitor of TAK1 (Ninomiya-Tsuji et al., 2003). Cells were treated with the indicated concentrations of 5Z-7-oxozeaenol. A 10 mM stock solution was prepared in DMSO and stored at -20°C

Calcium chloride transfection of HEK293T cells

For the calcium chloride transfection, HEK293T cells were grown in 10 cm culture plates with 10 ml of growth media. Cells were plated in order to reach 70% confluence at the moment of transfection. Briefly, 10 μg of DNA were dissolved in 450 μl of water to which 50 μl of $CaCl_2$ were added in a dropwise manner and incubated at RT for 5 min. Then, 500 μl of 2 x HBS were added dropwise, the mixture was incubated for 20 min at RT, and then added dropwise to the cells that were in complete DMEM and incubated overnight. The following day, media was replaced with fresh growth media.

PEI transfection of HEK293T cells

For polyethylenimine (PEI) transfection, HEK293T cells were cultured in 6 well plates. A day before transfection, $5.5x10^5$ cells were plated per well in 2 ml of complete growth media. The following day, 2 μg of DNA in 150 μl of Opti-MEM and 5 μl of PEI MAX reagent in 150 μl of Opti-MEM were incubated at RT for 5 min, then were combined and vortexed well, followed by a brief spin and incubation at RT for 40 min. The mixture was then added to the cells in a dropwise manner, and the media was replaced with fresh growth media 10-16 h after transfection.

Lentivirus production

For lentivirus production, the packaging plasmids VSV-G and Δ89 were mixed with the target DNA in a 0.1:0.9:1 ratio (**Table 4**), and HEK293T cells were transfected as described above depending on the culture dish format. Media containing viruses was collected 48 and 72 h after transfection and, unless indicated otherwise, pooled, centrifuged for 14 min at 200 xg and either used immediately or aliquoted and stored at -80°C.

Table 4 | Amounts of DNA used for lentivirus packaging.

	10 cm plate ($CaCl_2$)	6 well plate (PEI)
VSV-G	0.5 μg	0.1 μg
Δ89	4.5 μg	0.9 μg
DNA	5 μg	1 μg

Generation of the BBL358-Cas9 cell line

BBL358 cells were transduced with lentiviruses containing the Cas9-Blast construct (Addgene, #52962). Lentiviruses were generated in HEK293T cells using the calcium phosphate transfection and two rounds of infection (48 h and 72 h of virus generation) were performed in the presence of 8 μg/ml polybrene. After 48 h of infection, cells were split, selected with 5 μg/ml blasticidin, and Cas9 activity was assayed before further application.

Cas9 activity assay in BBL358-Cas9 cells

The Cas9 activity in the BBL358-Cas9 cells was assayed using the pXPR-011-EGFP reporter (Addgene, #59702) as described previously (Doench et al., 2014). This reporter plasmid drives the constitutive expression of both EGFP and an EGFP-targeting sgRNA. Cells transduced with the reporter are EGFP positive and puromycin resistant. When a cell also expresses active Cas9, the EGFP-targeting sgRNA allows the cleavage of the EGFP encoding sequence, disrupting its expression and abolishing cell fluorescence. The fraction of cells that are puromycin resistant but do not express EGFP indicate the cells expressing active Cas9.

BBL358-Cas9 cells were transduced with lentiviruses containing the pXPR-011-EGFP reporter. Lentiviruses were generated in HEK293T cells using calcium phosphate transfection and two rounds of infection (48 h and 72 h of virus generation) were performed in the presence of 8 μg/ml polybrene. Cells were then selected for 48 h with 3 μg/ml puromycin and assayed by flow cytometry 10 days after transduction. Non-transduced BBL358-Cas9 cells were used as a negative control, and parental BBL358 cells transduced with the reporter (BBL358-XPR) as a positive control.

Generation of mammalian knock-out cells using CRISPR/Cas9

The DNA corresponding to a sgRNA targeting the gene of interest was cloned into the plasmids Lenti_sgRNA_EFS_GFP (Addgene #65656), pLenti-Puro-GFP or pLenti-Puro-mCherry (Noordermeer et al., 2018). First, sgRNA oligos were phosphorylated and annealed in a 10 μl reaction containing 1 μl of forward and reverse sgRNA oligos (100 μM stock, **Table 5**), 1 μl of 10x T4 Ligation buffer (NEB, B0202) and 1 μl of T4 PNK (NEB, M0201) using the following thermocycler program:

37°C for 30 min
95°C for 5 min
Ramp down to 25°C at 5°C/min

Table 5 | sgRNA oligos used in this study.

sgRNA	Forward	Reverse
sg1-Zcchc14	CACCGTGTGGACATCCATGTCGAG	AAACCTCGACATGGATGTCCACAC
sg2-Zcchc14	CACCGTTGAAAAGATAGACCTGAA	AAACTTCAGGTCTATCTTTTCAAC
sg3-Zcchc14	CACCGAATCTGGGCCAGCCAAGCA	AAACTGCTTGGCTGGCCCAGATTC
sg1-Rptor	CACCGAAGCAGCTTCAGTACATAG	AAACCTATGTACTGAAGCTGCTTC
sg2-Rptor	CACCGAACTTCGACTCTGCAAGA	AAACTCTTGCAGAGTCGAAGTTC
sg1-Rictor	CACCGCTTCAGGAACGAGACAGAA	AAACTTCTGTCTCGTTCCTGAAGC
sg2-Rictor	CACCGACAGTTGGAGGCTTTCCGA	AAACTCGGAAAGCCTCCAACTGTC
sg1-Mrpl28	CACCGAAGCCACAGCTGTTCACTC	AAACGAGTGAACAGCTGTGGCTTC
sg2-Mrpl28	CACCGAGGCAGAGGCCGAGTGGGT	AAACACCCACTCGGCCTCTGCCTC
sg1-Mapk11	CACCGTCCAATCGCTGATCCACGCG	AAACCGCGTGGATCAGCGATTGGAC
sg1-Mapk12	CACCGCAGCCGCACTGGCAACAAGG	AAACCCTTGTTGCCAGTGCGGCTGC
sg1-Mapk13	CACCGCATGGGGATGGAATTCAGCG	AAACCGCTGAATTCCATCCCCATGC
sg2-Mapk13	CACCGCAGCTCGGCCATCGACAAG	AAACCTTGTCGATGGCCGAGCTGC
sg3-Mapk13	CACCGGGCTATGTGGTGACCCGC	AAACGCGGGTCACCACATAGCCC
sg1-Mapk14	CACCGCAGGCTACGTGGCTACCAGG	AAACCCTGGTAGCCACGTAGCCTGC

sg1-Lmx1a	CACCGGGTGGGGTGAGACCCTGT	AAACACAGGGTCTCACCCCACCC
sg1-Afm	CACCGCAGGTTGTTACCGCCATG	AAACCATGGCGGTAACAACCTGC
sg1-Adcy6	CACCGAGACCCGAGGTTACATCC	AAACGGATGTAACCTCGGGTCTC
sg1-Hc	CACCGTAGAAGAAAATGATTACAC	AAACGTGTAATCATTTTCTTCTAC
sg1-Igf2bp2	CACCGTTGGCTGAATATGGGACAG	AAACCTGTCCCATATTCAGCCAAC
sg2-Igf2bp2	CACCGCATAATCTCAAGAATCATG	AAACCATGATTCTTGAGATTATGC
sg1-Ranbp2	CACCGATGGAAGAGCAAAATACT	AAACAGTATTTTGCTCTTCCATC
sg2-Ranbp2	CACCGACTCACCAGCATAATCGG	AAACCCGATTATGCTGGTGAGTC
sg2-Ccnb2	CACCGCTCGCCTTAAGAAGTGAAG	AAACCTTCACTTCTTAAGGCGAGC
sg1-Gbgt1	CACCGACGATGGGTGCCAACCACG	AAACCGTGGTTGGCACCCATCGTC
sg2-Gbgt1	CACCGCTGCTGACACTTACCCCG	AAACCGGGGTAAGTGTCAGCAGC
sg1-P2ry1	CACCGGCTTCCTAGGCAACAGCG	AAACCGCTGTTGCCTAGGAAGCC
sg2-P2ry1	CACCGTTGAAATCACACATTTCTG	AAACCAGAAATGTGTGATTTCAAC
sg1-Cuedc2	CACCGGCAGGTGTGCCTGAACGA	AAACTCGTTCAGGCACACCTGCC
sg2-Cuedc2	CACCGCTTTGGCCAGCACCCACT	AAACAGTGGGTGCTGGCCAAAGC
sgRosa26	CACCGACTCCAGTCTTTCTAGAAGA	AAACTCTTCTAGAAAGACTGGAGTC

For cloning, 3 μg of the expression plasmid were digested with FastDigest Esp3I and gel purified using QIAquick Gel Extraction Kit following the manufacturer's instructions. The ligation mixture containing 50 ng of digested plasmid, 1 μl of diluted (1:200) oligo duplex, 5 μl of 2x Quick Ligase buffer and 1 μl of Quick ligase in a final volume of 10 μl was incubated for 10 min at RT and then used to transform DH5α competent *E.coli* cells. Ampicillin resistant clones were selected, expanded and DNA extracted with a GenElute plasmid miniprep kit. The correct insertion of the sgRNA sequence was confirmed by sequencing the sgRNA plasmid with the U6 Forward primer (GAGGGCCTATTTCCCATGATT).

Lentiviruses were generated in HEK293T cells using either calcium phosphate or PEI transfection. BBL358-Cas9 cells were infected for 48 h in the presence of 8 μg/mL polybrene, selected with 3 μg/ml puromycin for 48 h and then used for further analysis. The only exception was the sg1-Zcchc14 sgRNA cloned into the Lenti_sgRNA_EFS_GFP, which does not express the puromycin resistance cassette. In this case, BBL358-Cas9 cells were transduced with sg1-Zcchc14, harvested 72 h post-infection, and the top 20% of the GFP expressing cells were sorted in a BD FACSAria Fusion Cell Sorter and then re-plated for further experiments.

Cell viability assays

Colony formation assay

For colony formation assay, 1,200 cells in a 60 mm dish or 200 cells per well in a 12 well plate were plated. Treatment was added 24 h after plating and the cells were allowed to grow until visible colonies were formed (7-10 days depending on the treatment). Then, cells were washed with 1x PBS and stained with Crystal Violet by gently shaking at RT for 30 min. Afterwards the samples were rinsed at least 3 times with distilled water and left to dry. The colony area was measured using ImageJ.

EdU labelling assay

The EdU labelling assay allows the quantification of the percentage of cells undergoing proliferation. It relies on the incorporation of the thymidine

analogue 5-Ethynyl-2'-deoxyuridine (EdU) into the DNA of proliferating cells.

Cells were incubated with 10 μM EdU for 1 h at 37°C and then processed according to the manufacturer's instructions. Briefly, cells were collected by trypsinisation, washed with 1% BSA/PBS and fixed in 100 μl of 4% PFA for 15 min at RT. Samples were then washed again with 1% BSA/PBS, and the cell pellets were resuspended in 100 μl of Click-IT reaction cocktail and incubated for 30 min at RT protected from light. Cells were then washed once with permeabilization and wash reagent and resuspended in PI staining solution containing 20 μg/ml propidium iodide and 0.1 mg/ml RNase A. Samples were analysed in a Gallios Flow Cytometer (Beckman Coulter) and using the FlowJo v10.7.1 software.

Metabolic viability assays

MTT assay

600 BBL358 cells, 12,500 MIA PaCa-2 cells or 12,500 SUP-T1 cells per well were seeded in a 96 well plate in a final volume of 100 μl. Treatment with compounds was done 24 h after plating. After the desired incubation times, cell viability was determined with the MTT Cell Growth Assay following the manufacturer's instructions. Briefly, 10 μl of reagent 1 was added to every well, incubated 4 h at 37°C followed by addition of 100 μl of solubilisation reagent 2 per well. The following day, the absorbance at 570 nm was read with a spectrophotometer (BioTek, #FLx800), and data was analysed with the GraphPad software. The absorbance from wells with no cells but with reagents added was used for baseline subtraction. For IC50 calculation, background subtracted data was fit with a nonlinear inhibitor vs response (variable slope) model with bottom constrained to 0.

Real Time Glo assay

The RealTime-Glo™ (RTG) Cell Viability Assay is a non-lytic bioluminescent method to determine cell viability in real time by measuring the reducing potential of cells. While conceptually similar to the MTT assay, it allows measuring cell viability over time as it is not toxic to cells.

Briefly, 600 BBL358 cells or 12,500 SUP-T1 cells were plated per well in a 96 well plate in complete media supplemented with 1x RTG reagents. Luminescence measurements were then acquired daily by BioTek Synergy H1 plate reader. Data was normalised to the first time point (24 h).

Cell death assay

To measure cell death, cells were plated, treated the following day, and after 72 h of treatment both growth media and adherent cells were collected by trypsinisation. Samples were washed once with 1x PBS and resuspended in 1x PBS containing 40 μg/ml DAPI. Samples were analysed in a Gallios Flow Cytometer (Beckman Coulter) and using the FlowJo v10.7.1 software.

Bright-field microscopy

To acquire bright-field images, cells were imaged with a DMi8 Leica microscope and the obtained images were processed with ImageJ.

Competitive proliferation assay

Flow cytometry

To assay the effect of target downregulation on cell viability, cells were infected with the sgRNA targeting a gene of interest in a construct that also expresses GFP. Transduction was done under conditions that result in less than 60% of cells infected. Without selection, this mix of cells that are transduced (express GFP) and non-transduced (no fluorescence) was split into two pools, one of which was treated with 4-OHT to induce p38α downregulation and the other left untreated as a WT control. Samples were then passaged every 2-3 days at a 1:12 dilution and the percentage of GFP positive cells was measured in a Gallios Flow Cytometer (Beckman Coulter) and analysed with FlowJo v10.7.1 software.

Time-lapse imaging

The time-lapse competitive proliferation assay was performed with the help of the IRB advanced digital microscopy facility. Cells were transduced with the targeting sgRNA plasmid expressing GFP or with a control sgRNA targeting the Rosa26 locus and expressing mCherry. After selection for 48 h

with 3 μg/ml puromycin, cells were treated for 48 h with 4-OHT (p38α KO) or left untreated (WT). Then, both p38α KO and WT cells with either targeting or control sgRNAs were mixed 1:1 and plated in a glass-bottom 96 well plate. Starting the following day (24 h later), images were acquired every 12 h over 72 h using the Nikon Lipsi high content cell imaging platform, capturing a 3x3 grid at a 10x magnification and acquiring red and green fluorescence channels. The number of nuclei in each channel was quantified for each time point with ImageJ software using the StarDist plugin (Schmidt et al., 2018) and normalised to the nuclei count detected at the first time point.

Molecular biology

Protein detection by western blotting

Protein extraction

For extracting total protein, cell plates were processed on ice by washing twice with ice-cold 1x PBS and scraping the cells in 100 μl of RIPA lysis buffer. Cell lysates were then transferred to a 1.5 ml tube, vortexed well and incubated on ice for 30 min followed by 20 min centrifugation at 4°C and 12,000 x g. The supernatant containing protein extract was then transferred to a new pre-chilled 1.5 ml Eppendorf tube and quantified.

Determination of protein concentration

Total protein concentration was quantified using the Lowry-based colorimetric quantification DC Protein Assay kit from Bio-Rad following the manufacturer's instructions. The assay was performed in a microplate format. Briefly, reagent S and reagent A were pre-mixed (20 μl of reagent S added per 1 ml of reagent A) and 25 μl added to 2 μl of the protein sample pipetted per well in duplicates. Then 200 μl of the reagent B was added to each well and the plate incubated at RT for 15 min. Absorbance at 750 nm was read with spectrophotometer (BioTek, #FLx800) and protein concentration determined based on the BSA standard curve.

Western Blotting

For western blotting, 40 µg of the total protein lysate were mixed with protein loading buffer (1x final concentration), boiled for 5 min at 95°C, centrifuged briefly and chilled on ice before loading the sample on an SDS-PAGE gel of the desired acrylamide percentage (**Table 6**)**.** Proteins were then separated for 1.5 h at 130 V and transferred from the gel to a nitrocellulose membrane using a wet blotting transfer system (Bio-Rad) for 1.5 h at constant amperage (300 mA).

Table 6 | Laemmli SDS-polyacrylamide gel preparation

	UNIT	RESOLVING GEL				STACKING GEL
% Acrylamide		**8%**	**10%**	**12%**	**14%**	**5%**
Milli-Q Water	ml	12.7	11.5	10.3	9.1	5.8
Acrylamide 40% 29:1	ml	4.8	6	7.2	8.4	1
1.5M Tris pH 8.8 (RESOLVING) 1M Tris pH 6.8 (STACKING)	ml	6	6	6	6	1
SDS 10%	µl	240	240	240	240	80
APS 10%	µl	240	240	240	240	80
TEMED	µl	24	24	24	24	8

After transfer, the membrane was dried for 10 min at 37°C, then rehydrated by 5 min incubation in 1x TBS. Efficient protein transfer was confirmed with Ponceau red staining. The membrane was then rinsed in 1x TBS and blocked in 5% non-fat dry milk diluted in 1x TBS gently shaking for 1 h at RT. After a brief rinse in 1x TBS, the primary antibody diluted with 5% BSA in TBS-0.1%Tween (TBST) was incubated overnight at 4°C. The following day, the membrane was washed 3 x 5 min in TBST and incubated with the fluorophore-conjugated secondary antibody diluted in 5% BSA/TBST gently shaking for 1 h at RT and protected from light. Finally, the membrane was washed 2 x 5 min in TBST followed by one last wash for 5 min in 1x TBS and imaged using the Odyssey Infrared Imaging System. The antibodies used in this study are indicated in **Table 7**.

Table 7 | Antibodies used for western blotting

Antibody	Host	Dilution	Company	Reference
p38 MAPK, Phospho T180/Y182 (Figures 1A and 18A)	Rabbit	1:1,000	CST	9211
p38 MAPK, Phospho T180/Y182	Mouse	1:1,000	BD	612288
p38α	Mouse	1:1,000	Santa Cruz	sc-535
p38α (Figure 1A)	Rabbit	1:1,000	CST	9218
p38γ	Rabbit	1:1,000	CST	2307
p38δ	Rabbit	1:1,000	CST	2308
MK2, Phospho T334	Rabbit	1:1,000	CST	3007
MK2	Rabbit	1:1,000	CST	3042
HSP27, Phospho S82	Rabbit	1:1,000	CST	2401
HSP27	Goat	1:1,000	Santa Cruz	sc-1049
Tubulin	Mouse	1:10,000	Sigma	T9026
GAPDH	Mouse	1:1,000	Sigma	G8795
Donkey anti-Goat IgG, Alexa Fluor 680	Donkey	1:10,000	Invitrogen	A21084
Goat anti-Rabbit IgG (H+L), DyLight 680	Goat	1:10,000	Invitrogen	35568
Goat anti-Mouse IgG, Alexa Fluor 680	Goat	1:10,000	Invitrogen	A21057
Goat anti-Rabbit IgG (H+L), DyLight 800	Goat	1:10,000	Invitrogen	SA5-35571
Goat anti-Mouse IgG (H+L, DyLight 800	Goat	1:10,000	Invitrogen	SA5-35521

qRT-PCR analysis of gene expression

RNA extraction

Cell plates were washed once with 1x PBS and then cells were collected in a 1.5 ml Eppendorf tube with 500 µl of Trizol reagent. To each sample, 100 µl of chloroform were added and samples were vortexed briefly and centrifuged 15 min at 4°C and 12,000 x g. The aqueous phase was transferred to a new tube and mixed 1:1 with freshly prepared 70% ethanol. The RNA extraction was then performed using RNA Purelink MiniKit coupled with PureLink on column DNase treatment for residual DNA digestion

following manufacturer´s instructions. Samples were eluted in 30µl of RNase free water and the concentration was determined by measuring the absorbance at 260 and 280 nM using NanoDrop 2000 spectrophotometer (ThermoScientific). Samples were then either stored at -80°C or used directly for cDNA synthesis.

cDNA synthesis

The cDNA synthesis was performed with the qScript SuperMix following manufacturer´s instructions. Briefly, 1µg of RNA was mixed with 2 µl of 5x qScript SuperMix in a 10 µl reaction and the following thermocycler program was used:

5 min at 25°C
30 min at 42°C
5 min at 85°C
∞4°C

Quantitative real time PCR

For mRNA expression analysis, 20 ng of cDNA were mixed with 5 µl of SYBR Select Master Mix for CFX reagent and 0.25 µl of gene specific Forward and Reverse primers (10 µM stock solution) in a 10 µl final volume. The assay was performed in a 384-well plate with technical triplicates for each sample. The plate was sealed, centrifuged for 1 min at 200 ×g and run in QuantStudio™ 6 Flex Real-Time PCR System with the following program:

50°C for 2 min
95°C for 10 min
40 cycles of:
    denaturation at 95°C for 15 s
    annealing and elongation at 60°C for 1 min
95°C for 15 s
60°C for 1 min
95°C for 15 s

Relative mRNA levels were determined with the Comparative Ct method using the QuantStudio Real-Time PCR Software v1.3, and *Gapdh* and *Hprt* as endogenous controls. Primers used are shown in **Table 8**.

Table 8 | Primers used for qRT-PCR analyses

Gene	Forward sequence 5'-3'	Reverse sequence 5'-3'
Hprt	GAGAGCGTTGGGCTTACCTC	ATCGCTAATCACGACGCTGG
Gapdh	CTTCACCACCATGGAGGAGGC	GGCATGGACTGTGGTCATGAG
Mapk12	GCGGGATTCTACCGGCAAG	GCGAGACAGCTTCTTTACAGC
Mapk13	ATGAGCCTCACTCGGAAAAGG	GCATGTGCTTCAAGAGCAGAA
Map2k3	ACTCCCGGACCTTCATCACTA	ATGCCGCACTTTCTCTACCAC
Map2k6	ATGTCTCAGTCGAAAGGCAAG	TTGGAGTCTAAATCCCGAGGC

Genome-wide CRISPR/Cas9 screen

Screen conditions

We used the lentiviral Brie CRISPR Pooled Library that targets 19,674 genes and contains 78,638 targeting sgRNAs and 1,000 non-targeting control sgRNAs (Addgene, 73633-LV).

To determine the optimal virus volume in order to achieve a multiplicity of infection (MOI) close to 0.3, a trial infection experiment was performed. This step is important to minimise the possibility of a single cell being transduced with more than one sgRNA. Briefly, $3x10^6$ cells were plated in 15 cm plates and transduced with several virus volumes (25 µl, 50 µl and 100 µl). After 24 h, equal numbers of cells from each condition were split into two new 15 cm plates, one containing complete medium and the other one containing complete medium supplemented with 3 µg/ml puromycin. The infection efficiency was determined based on the ratio of live cells after 48 h of puromycin addition compared to the non-treated control. Based on this trial, 100 µl was selected as the volume expected to infect ~ 30% of the cells.

For the screen, $1.2x10^8$ cells were transduced in 15 cm plates, each containing $3x10^6$ cells, 100 µl of virus and complete medium to a final volume of 12 ml per plate supplemented with 8 µg/ml polybrene. After 24 h

of infection, the media was replaced with fresh complete medium supplemented with 3 μg/ml puromycin. During the selection, cells were passaged every two days always maintaining at least $4x10^7$ cells in total, which accounts for a 500x coverage. After 10 days of puromycin selection, $4x10^7$ cells were collected, centrifuged and stored at -80°C for DNA extraction as Day 0 sample. The rest of the cells were split into two groups with $4x10^7$ cells per group. After letting the cells attach for 24 h, one group was treated with 100 nM 4-OHT in order to induce p38α deletion while the other group was left untreated as a WT control. After 48 h, $4x10^7$ cells per condition were plated and the leftover cell suspensions were centrifuged and used for p38α deletion confirmation by western blotting. Cells were passaged every 2-3 days maintaining the 500x representation. After 7, 14 and 21 days of the screening, 4 x 10^7 WT and the same number of p38α KO cells were collected, centrifuged and stored at -80°C for subsequent DNA isolation.

sgRNA amplification and sequencing

Genomic DNA was extracted from cell pellets using the Blood & Cell Culture DNA Maxi Kit following the manufacturer's instructions. Approximately $4x10^7$ cells were loaded per column for each of the three samples, and sgRNAs were amplified with a two-step PCR. For each sample, 186 μg of genomic DNA were amplified in 10 PCR1 reactions (**Table 9**).

Table 9 | Composition of the PCR1 reaction

Reagent	(μl)
Takara ExTaq	0.5
10x ExTaq Buffer	10
dNTP mix	8
10 μM Primer Forward	7.5
10 μM Primer Reverse	7.5
H_2O	36.5
DNA	30

PCR1 program:

95°C for 1 min
11 cycles of:
95°C for 30 sec
55°C for 30 sec
72°C for 30 sec
72°C for 10 min

The PCR1 products were further processed by the CCiTUB Genomics Unit. Briefly, the PCR1 products of each sample were pooled and quantified with the Invitrogen Qubit dsDNA HS Assay Kit (Invitrogen, Q3285) to ensure proper amplification. The PCR2 reaction, in which the unique indexes for each library were added, was then performed with a 5 µl aliquot per sample taken from the pools of the PCR1 products.

The conditions of the PCR2 were the same as for PCR1 except for the number of cycles. The optimal number of cycles for the PCR2 was determined using qPCR with SYBR-green. PCR2 products were then purified with Mag-Bind® Total Pure NGS (Omega BIO-TEK) beads in a PCR product-to bead ratio of 1:1.1. Primers used are shown in **Table 10.**

Table 10 | Primers used in sgRNA amplification PCR reactions

Primer	Sequence 5'-3'
PCR1-Forward	AATGATACGGCGACCACCGAGATCTCGATTTCTTGGC TTTATATATCTTGTGGAAAGGACG
PCR1-Reverse	GTGACTGGAGTTCAGACGTGTGCTCTTCCGATCTT CTACTATTCTTTCCCCTGCACTGT
PCR2-P5-Forward	AATGATACGGCGACCACCGAGATCT
PCR2-NEBNext adaptor-Reverse	CAAGCAGAAGACGGCATACGAGAT**index**GTGA CTGGACTTCAGACGTGTGCTCTTCCGATC

The resulting libraries were quantified with the Invitrogen Qubit dsDNA HS Assay, and the concentration and sizes were determined by electrophoresis with Agilent DNA 1000 chips. The PCR2 products were then sent to the CNAG-CRG sequencing facility where the final concentration of the library was quantified and similar quantities of different Day 0, WT Day 14 and KO Day 14 sample libraries were sequenced as a pool on Illumina HiSeq2500 by 50-bp single-end sequencing. Due to the same sequencing platform being unavailable at the time of the Day 7 sample sequencing, WT Day 7 and KO Day 7 sample libraries were sequenced by 50-bp single-end sequencing on Illumina NextSeq v2.5 together with the previously prepared Day 0 library in order to account for possible technical variability. Target coverage was $4x10^7$ reads per sample.

CRISPR screen data analysis

The initial analysis was performed by the IRB Biostatistics Unit. Reads were pre-processed by removing adapters using cutadapt (Martin, 2011) with parameters:
"-e 0.2 –a GTTTTAGAGCTAGAAATAGCAAGTTAAAAT -m 18".

Processed reads were aligned to both sgRNA probe sequences and controls using bowtie (v.0.12.9) with 0 mismatches allowed (Langmead et al., 2009). The number of reads aligning to each probe and sample were computed in R (R Core Team, 2008). The count matrix was normalized using the "varianceStabilizingTransformation" function from the DESeq2 R package (Love et al., 2014). Only control guides were considered in the size factor calculations (median ratio method (W. Li et al., 2014)). Top 50 hits are shown in **Appendix Table 1**.

Gene set enrichment analysis (GSEA) was performed using the maxmean test statistic under restandardization (Efron & Tibshirani, 2007) on the observed log_2FCs. Gene permutations were done to approximate statistical significance.

Custom analysis

To facilitate target prioritisation, datasets obtained from the analysis described above were further processed as following. First, for every gene, sgRNAs were categorized as enriched (KO > WT) or depleted (WT > KO) by comparing normalized counts in the two samples. The KO vs WT log_2FC was determined by the average difference of normalized counts between KO and WT samples across the 4 sgRNAs. Each sgRNA was considered to follow the same trend as the gene if it matched the KO vs WT log_2FC sign (>0 enriched and <0 depleted). We filtered out target genes with low counts in the Day 0 sample (Day 0 sgRNA count lower than 50) (Behan et al., 2019). Genes that had absolute KO vs WT log_2FC higher than 1.5, with at least 2 out of the 4 sgRNAs following the gene global trend were classified as following:

Group A

No effect in the WT and overrepresented in the KO sample:

|WT vs Day 0 log_2FC| < 1.5 & KO vs Day 0 log_2FC > 1.5

Group B

No effect in the WT and underrepresented in the KO sample:

|WT vs Day 0 log_2FC| < 1.5 & KO vs Day 0 log_2FC < -1.5

Group C

Underrepresented in the WT and no effect in the KO sample:

WT vs Day 0 log_2FC < -1.5 & |KO vs Day 0 log_2FC | < 1.5

Group Co

Underrepresented in the WT and overrepresented in the KO sample:

WT vs Day 0 log_2FC < -1.5 & KO vs Day 0 log_2FC > 1.5

Group D

Overrepresented in the WT and no effect in the KO sample:

WT vs Day 0 log_2FC > 1.5 & |KO vs Day 0 log_2FC | < 1.5

Group Do

Overrepresented in the WT and underrepresented in the KO sample:

WT vs Day 0 log_2FC > 1.5 & KO vs Day 0 log_2FC < -1.5

Group E

Overrepresented in both samples, but more so in the KO sample:

WT vs Day 0 log_2FC > 1.5 & KO vs WT log_2FC > 1.5

Group F

Underrepresented in both samples, but more so in the KO sample:

WT vs Day 0 log_2FC < -1.5 & KO vs WT log_2FC < -1.5

For group level hypergeometric test (HGT) enrichment analysis, mouse gene symbols were converted to human and EnrichAnalyzer function from MAGeCKFlute R package was used (B. Wang et al., 2019). From the results obtained, only GO terms for which 4 or more genes are detected with adjusted p-value lower than 0.05 were taken into consideration.

MAGeCK analysis

Raw data obtained from the sequencing of Day 7 samples was processed together with the raw data of previously analysed Day 14 samples using MAGeCK algorithm. FASTQ files were mapped using MAGeCK (v0.5.9.2.)

"*count*" command with 0 mismatches allowed and counts normalised to control sgRNAs with "*--norm-method control*" parameter. Further analysis was performed in R. Principal Component analysis was performed using biplot function with $\log_2$ (normalised count+1) values of each sample. Next, sgRNAs with 50 or less counts detected in either of the replicates of Day 0 sample were removed from the analysis and $\log_2$FC per gene for the desired comparison calculated as mean of $\log_2$ (normalized counts condition A +1 /normalized counts condition B +1). In each case, pseudo count 1 was added to avoid calculating $\log_2$ (0).

To define a more stringent threshold, the number of enriched or depleted sgRNAs per gene was defined as number of sgRNAs out of 4 with $\log_2$FC higher or lower than 1 for a given comparison and targets were assigned to custom groups as described above. Enrichment analysis was performed with MAGeCK Flute package.

DepMap data analysis

CRISPR Chronos gene effect, Chronos gene dependency, CCLE expression and sample info datasets were downloaded from the 2022 Q2 DepMap release using the Broad Institute's DepMap portal (Dempster et al., 2021). Cell lines were characterized as dependent on a gene of interest if the gene dependency probability was higher or equal to 0.5. The *MAPK14* gene effect was correlated to the gene effect score of all the other genes in the dataset across 1,086 cell lines. Pearson's correlations were performed in R using the cor.test function followed by correction for false discovery using the Benjamini-Hochberg method of the p.adjust function in R and $-\log_{10}$ normalisation of obtained values. The Wilcoxon test was used to compare the mRNA levels of different p38 MAPKs between p38α-Dependent (Dep) and Non-Dependent (NonDep) cell lines.

Statistical analysis

Data are represented as mean ± SD and statistical significance determined using Graph Pad Prism software by unpaired two-tailed Student´s test or two-way ANOVA with Dunnett's multiple comparisons test unless indicated otherwise. All p-values < 0.05 were considered statistically different.

Results

Genome-wide CRISPR/Cas9 screen

To understand the molecular mechanisms underlying the p38α dependency of cancer cells, we performed a genome-wide CRISPR/Cas9 screen using the cancer cell line BBL358, previously described by our group to be dependent on p38α. These cells were derived from PyMT-induced mouse mammary tumours, and allow the 4-OHT-inducible and Cre mediated deletion of p38α. We chose this particular cell line for the CRISPR/Cas9 screen as it allows the efficient deletion of p38α and consistently exhibits impaired proliferation upon both p38α deletion and treatment with p38 inhibitors (Cánovas et al., 2018).

Treatment with 4-OHT led to the downregulation of p38α levels in these cells without affecting the protein levels of other p38 family members, although we consistently observed increased phosphorylation levels of either p38γ or p38δ (**Figure 13A**). Deletion of p38α impaired growth of BBL358 cells (**Figure 13B**), and this effect was maintained throughout several passages (**Figure 13C**). We also treated this cell line with two different p38α inhibitors, PH-797804 (PH) and LY2228820 (LY), and examined the pathway activation in response to anisomycin. As expected, anisomycin treatment led to increased phosphorylation levels of the p38α downstream cascade components MK2 and HSP27. Both p38α deletion and treatment with p38α inhibitors efficiently prevented the increased phosphorylation of MK2 and HSP27 (**Figure 13D**). In addition, PH or LY treatment had a negative effect on the proliferation of BBL358 cells (**Figure 13E**). Thus, we selected BBL358 cells as a robust cellular model of p38α dependency. The advantage of the genome wide CRISPR/Cas9 screen is the simultaneous functional testing of the effect of depleting the majority of the known protein coding genes. This can help us better understand the molecular mechanisms driving the cancer cell dependency on p38α.

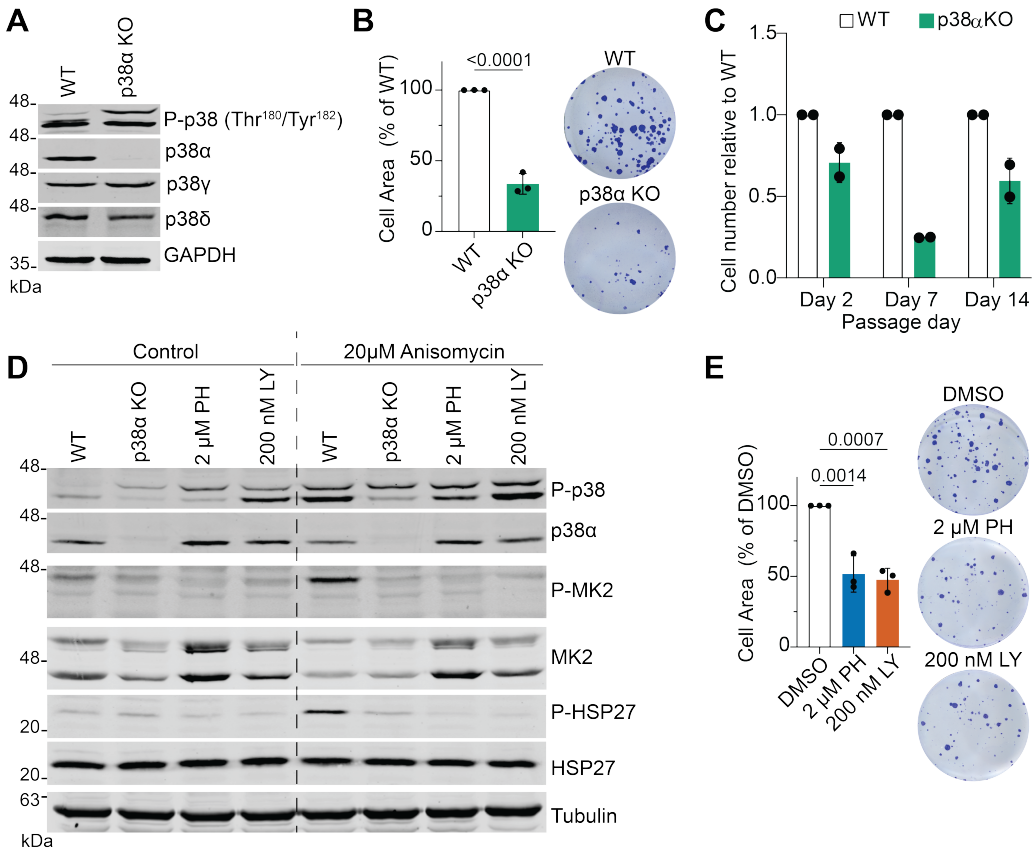

Figure 13. PyMT derived breast cancer cells are p38α dependent. (A) 4-OHT treatment decreases p38α protein levels without affecting other p38 family members. Murine PyMT-derived BBL358 cancer cells were treated for 48 h with 100 nM 4-hydroxytamoxifen (4-OHT) to induce p38α KO or left untreated (WT). Cell lysates were analysed by western blotting using the indicated antibodies. **(B)** Loss of p38α reduces colony formation capacity. Quantification (left) and representative images (right) of WT and p38α KO colony formation assays. After 48 h of 4-OHT treatment, cells were re-plated at low density, cultured for 7 days and stained with crystal violet. Statistical significance was determined with unpaired two-tailed t-test. Plot shows mean values of independent experiments (points) ± SD. **(C)** Deleterious effect of p38α depletion persists over several passages. Following 4-OHT treatment, WT and p38α KO cells were kept in culture for 2 weeks, counting the cells upon every passage. Plot shows cell numbers relative to WT cells at different days of subculturing as means of two biological replicates (points) ± SD. **(D)** The p38α deletion or inhibition abrogates downstream signalling. Cells were pre-treated for 48 h with 4-OHT, the p38α inhibitors 2 μM PH-797804 and 200 nM LY2228820 or left untreated (WT), and then were treated for 40 min with 20 μM anisomycin. Cell lysates were analysed by western blotting using the indicated antibodies. **(E)** The inhibition of p38α impairs colony formation by BBL358 cells. Quantification (left) and representative images (right) of cell area upon p38α inhibition. Cells were plated at low density, treated with PH, LY or DMSO as control and stained with crystal violet after 7 days of plating. Statistical significance was determined with two-way ANOVA Dunnett's multiple comparisons test. Plot shows mean values of independent experiments (points) ± SD.

To perform a genome-wide CRISPR/Cas9 screen in the isogenic WT and p38α KO BBL358 cells, aiming at the unbiased identification of targets that when depleted either boost or compromise the proliferation of p38α KO cells specifically, we chose the Brie mouse knockout (KO) pooled library (Doench et al., 2016).

The first step was to establish BBL358 cells that stably express the active form of Cas9. To achieve this, we transduced the parental BBL358 cells with the lentiCas9-Blast construct (Sanjana et al., 2014). To ensure that the cells express an active form of Cas9, we transduced BBL358-Cas9 cells with the pXPR-011 EGFP reporter (Doench et al., 2014). This reporter constitutively expresses EGFP as well as an sgRNA that targets EGFP. In the presence of a functional Cas9 enzyme, EGFP is cleaved and the fluorescence is lost (**Figure 14A**). We assayed the percentage of GFP negative cells 10 days after transduction with the reporter, using non-transduced BBL358-Cas9 cells as a negative control that does not express EGFP and parental BBL358 cells that do not express Cas9, but are transduced with the reporter construct as a positive control. Based on the flow cytometry analysis, 70% of the BBL358-Cas9 cells lost the EGFP expression, indicating that the majority of BBL358-Cas9 cells express an active Cas9 (**Figure 14B**).

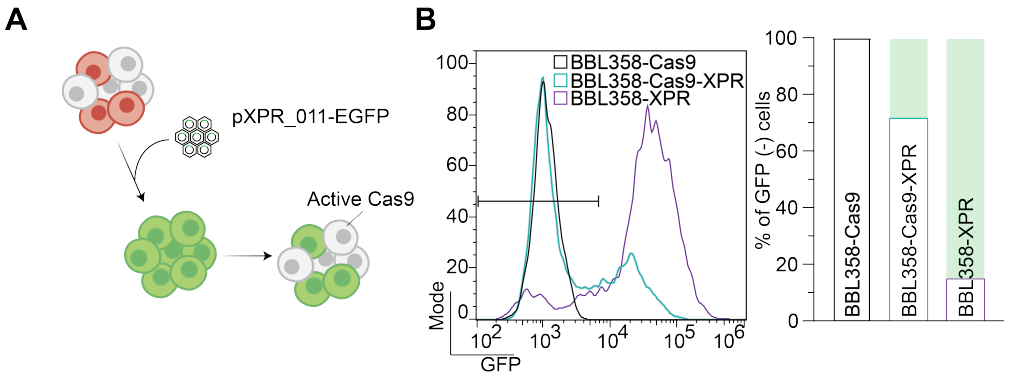

Figure 14. BBL358-Cas9 cells express active Cas9. (A) Scheme of the Cas9 activity assay. **(B)** The majority of BBL358-Cas9 cells express active Cas9. BBL358-Cas9 cells were transduced with the pXPR-011-EGFP reporter, which in the presence of active Cas9 loses green fluorescence. Cells were assayed by flow cytometry 10 days after transduction. Non-transduced BBL358-Cas9 were used as a negative and parental BBL358 transduced with the reporter (BBL358-XPR) as a positive control. Histogram (left) and percentage of GFP negative (-) cells (right) show that around 70% of BBL358-Cas9 cells express active Cas9.

The general strategy that we undertook for the CRISPR/Cas9 screen is shown in **Figure 15**. Briefly, we infected 120 million BBL358-Cas9 cells to obtain 40 million infected cells in order to ensure transduction of 500 cells per sgRNA (500x coverage). Cells were infected for 24 h and then selected for 10 days, splitting when necessary and always maintaining enough cells in culture to retain the 500x library representation. After 10 days of selection, 40 million cells were collected as a Day 0 and the remaining cells were split into two groups, one was kept as WT control, and in the other p38α deletion was induced with 4-OHT treatment. After two weeks of splitting the cells every 2-3 days (around 20 cell doublings), WT and p38α KO cells were collected for DNA extraction, sgRNA amplification and sequencing.

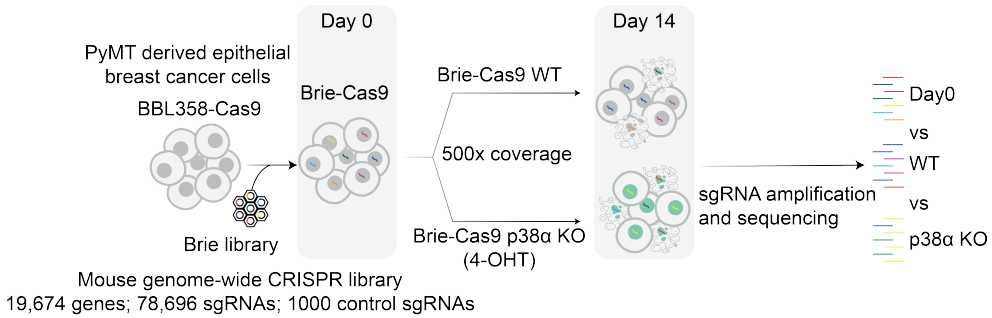

Figure 15. Scheme of the genome-wide CRISPR/Cas9 screen. $1.2x10^8$ BBL358-Cas9 cells were transduced for 24 h with 100 μl of the Brie genome-wide library. After 10 days of puromycin (3 μg/ml) selection, Day 0 sample was collected and the remaining cells were split into WT and p38α KO groups in which p38α was depleted by treating 48 h with 100 nM 4-hydroxytamoxifen (4-OHT). Cells were cultured for 14 days, and then WT and p38α KO samples were collected for DNA isolation, sgRNA amplification and sequencing. At every passage and sample collection, the coverage of $40x10^6$ cells per group was maintained to ensure the 500 cells per sgRNA (500x) representation.

In order to follow any potential changes in the growth of the cells, we performed several assays throughout the screening. First, we confirmed by western blotting that p38α was indeed deleted in the KO cells, and that this downregulation was maintained until the end of the screen (**Figure 16A**). Next, we evaluated by EdU incorporation assay the percentage of proliferating cells in the different samples. We observed that, while in the initial time point p38α KO cells had a lower percentage of proliferating EdU^+ cells, this difference was lost after two weeks of culturing, as both control

(BBL358-Cas9) and library infected (Brie-Cas9) p38α KO cells had similar percentage of proliferating EdU⁺ cells relative to their WT controls (**Figure 16B**). Similar results were observed in colony formation assays. In this case, while the control BBL358-Cas9 cells were still affected by the absence of p38α after two weeks in culture, we could no observe no differences in the colony formation ability of the library transduced WT and p38α KO cells (**Figure 16C**).

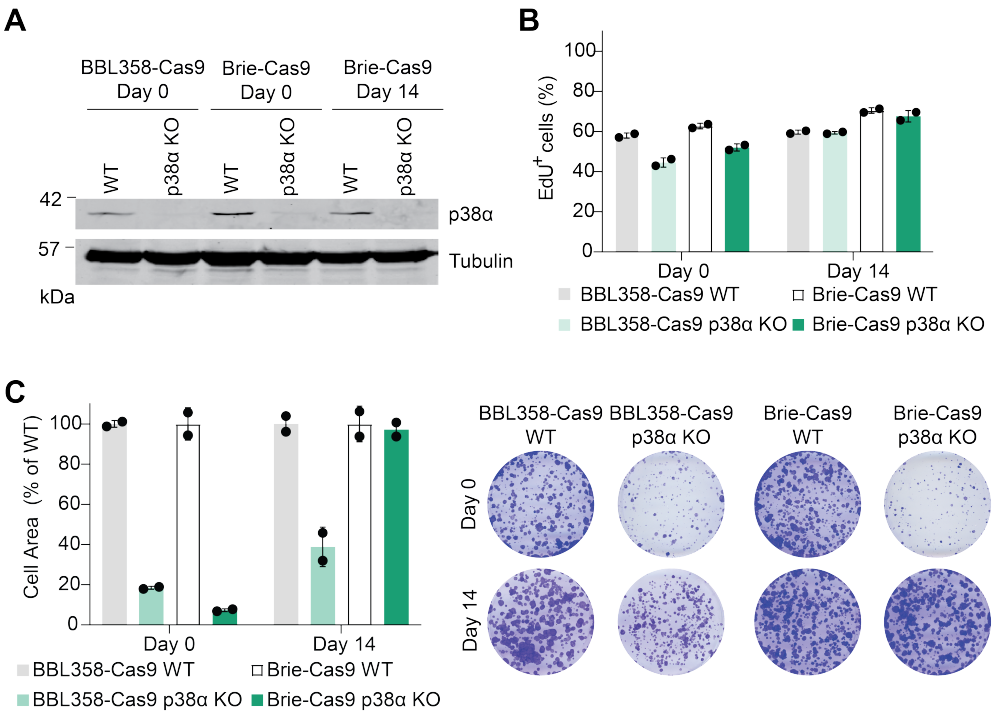

Figure 16. Proliferation of CRISPR library-infected cells increases by the end of the screen. (A) Protein levels of p38α are depleted throughout the screening. Western blot analysis of total p38α levels in WT and p38α KO cells either before (BBL358-Cas9) or after library infection (Brie-Cas9), and collected after 48 h of 100 nM 4-hydroxytamoxifen (4-OHT) treatment (Day 0) or after two weeks of culturing (Day 14). **(B)** The decreased percentage of EdU⁺ proliferating cells induced by p38α depletion is not observed after 2 weeks of culturing. Control BBL358-Cas9 or library transduced Brie-Cas9 cells were plated for 48 h after 4-OHT treatment (Day 0) or after 2 weeks of passaging (Day 14), grown for another 48 h, pulsed with EdU and analysed by flow cytometry. The plot shows the mean percentage of EdU⁺ cells of two biological replicates ± SD. **(C)** Library transduced p38α KO cells regain colony formation capacity. Control BBL358-Cas9 or library transduced Brie-Cas9 cells were plated at low density either 48 h after 4-OHT treatment (Day 0) or after 2 weeks of passaging (Day 14) and stained with crystal violet 7 days later. The plot shows mean cell area as percentage of the respective WT samples in two biological replicates ± SD. Representative images are shown in the right.

CRISPR/Cas9 screen data analysis

The analysis of the reads obtained from sequencing Day 0, WT and p38α KO samples indicated that more than 60% of the obtained reads were mapped to a sgRNA without any mismatch allowed (**Figure 17A**). Gini index (describing the sgRNA distribution inequality) was 0.06 for the initial Day 0 sample and 0.14 for the endpoint WT sample, both within acceptable range based on the previous literature (Wang et al., 2019), while 0.25 in the KO sample indicated slightly higher heterogeneity of the read count distribution (**Figure 17B**). Similarly, the percentage of sgRNAs not detected (zero count sgRNAs) was higher in the endpoint samples (**Figure 17C**).

We first looked at the raw counts for sgRNAs targeting p38α (*Mapk14*) and found that 3 out of 4 sgRNAs were depleted in the WT sample while the 4th sgRNA was detected at very low levels in the initial sample, indicating a deleterious effect of p38α depletion in this cell line as expected. However, a similar behaviour was observed in the KO sample, which was a bit surprising as we would expect no effect in the p38α KO cells (**Figure 17D**).

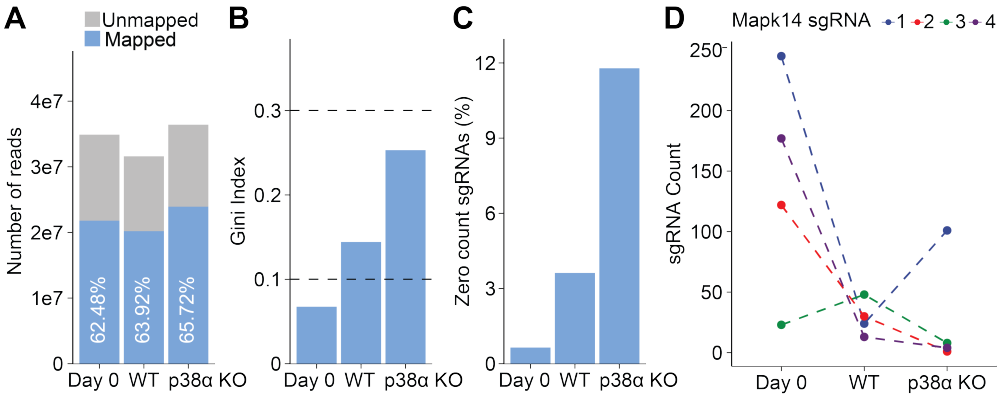

Figure 17. Quality control of CRISPR/Cas9 screen. (A) Sufficient number of reads was successfully mapped to a sgRNA. Bar plots show the total number of reads (grey) and percentage of mapped reads (blue) obtained for Day 0 sample and Day 14 WT and p38α KO samples. **(B)** The sgRNA distribution evenness is decreased at the final time point. Bar plot shows Gini index of sgRNA counts in Day 0, WT and p38α KO samples. **(C)** Proportion of non-detected sgRNAs increases in the endpoint samples. Bar plot shows the percentage of all sgRNAs present in the library not detected. **(D)** p38α (*Mapk14*) targeting sgRNAs are lost in the WT sample. Plot shows raw sgRNA counts of 4 individual sgRNAs across Day 0, WT and p38α KO samples. Dashed line connects the same sgRNA.

Next, raw counts were normalised using DESeq2 and the $\log_2$FC values were calculated. Gene set enrichment analysis (GSEA) of targets differentially

enriched in the p38α KO compared to the WT sample identified DNA repair, G2/M checkpoint and chromosome segregation as processes enriched in targets that synergize with the p38α KO, further recapitulating the results of Cánovas et al. (2018). Additional processes found in this group were mTOR signalling and RNA processing. Fewer terms were found enriched among the processes predicted to increase the viability of p38α KO cells, suggesting that there are few processes whose downregulation can rescue the deleterious effect of p38α KO in our model (**Figure 18A, B**).

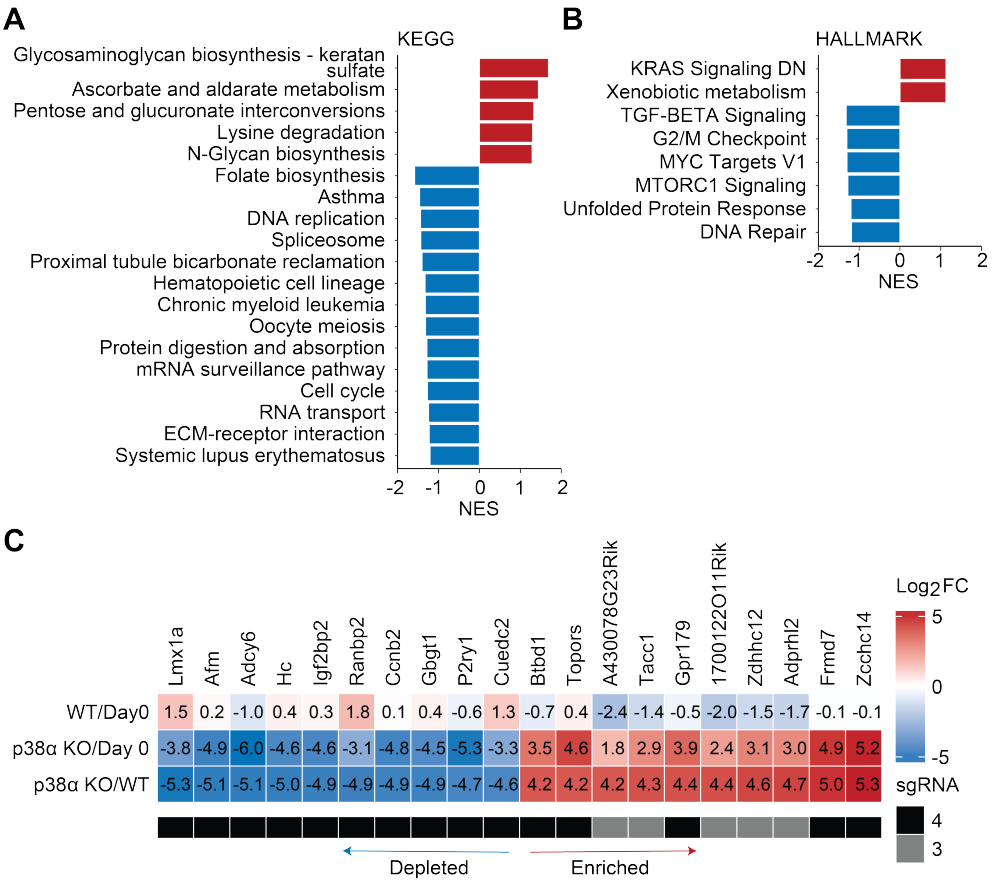

Figure 18. Top processes and targets enriched in the p38α KO sample. (A)(B) Gene set enrichment analysis (GSEA) of the comparison between p38α KO and WT cells querying **(A)** KEGG or **(B)** HALLMARK databases. Most significantly enriched (red) or depleted (blue) terms with |NES| > 1 and p-value < 0.05 are shown. **(C)** Heatmap showing the top 10 targets with sgRNAs enriched (red) or depleted (blue) in p38α KO compared to the WT cells. Targets were sorted based on the KO vs WT log_2FC values and the top 10 enriched or depleted targets were plotted. Numbers in the heatmap represent the log_2FC of the target comparing WT to Day 0 (WT/Day 0), KO to Day 0 (p38α KO/Day0) or KO to WT samples (p38α KO/WT). sgRNA legend indicates the number of sgRNAs (out of 4) that show the same phenotype.

Looking at the top 10 enriched or depleted hits, we identified *Zcchc14* as the top enriched target, with 4 sgRNAs overrepresented in the KO sample, while *Lmx1a* was the top depleted target, with all 4 sgRNAs lost in the KO sample compared to the WT. Curiously, the effect of depleting these targets in the WT cells varied, as loss of some of the targets is predicted to increase the viability of WT cells while being lethal in the p38α KO background (e.g. *Lmx1a*, *Ranbp2*). In contrast, some of the sgRNAs enriched in the KO sample were underrepresented in the WT sample (e.g. *Adprhl2*, *Zdhhc12*) (**Figure 18C**). This observation motivated us to further classify the putative hits based on the effect they might have in WT cells.

We defined several subgroups among putative hits based on the effect that their downregulation had in WT cells (**Figure 19A**). By comparing WT and p38α KO cells with the Day 0 sample, we defined targets with absolute log_2FC higher than 1.5 as differentially enriched, and assigned them to distinct groups. This approach retrieved 977 genes whose downregulation promoted viability (group A) and 1901 genes that were essential (group B) exclusively in the p38α KO background. We could also define a group of targets for which the p38α KO rescued the deleterious (Group C - 415 hits) or beneficial (Group D - 184 hits) effect observed in the WT sample. In addition, we detected a small group of genes that had opposite effects in the p38α KO cells compared to the WT cells, i.e., depletion of these targets impaired the viability of WT cells but promoted the viability of the KO cells (group Co - 26 genes), or vice versa, target lost decreased the viability of p38α KO cells but enhanced viability in the WT cells (group Do - 20 targets). Finally, we also identified targets that were either enriched (group E, 23 genes) or depleted (Group F - 152 genes) in both p38α KO and WT cells, but displayed a stronger effect in the p38α KO (**Figure 19B).**

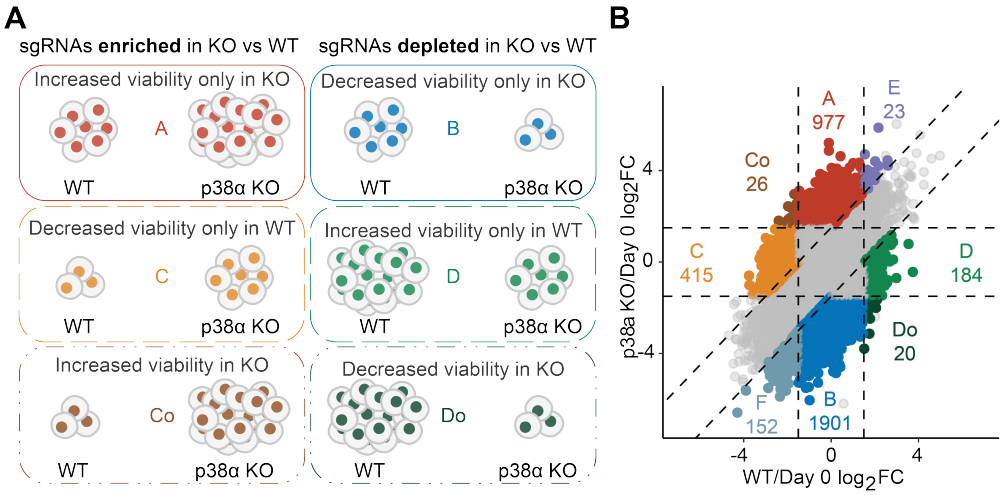

Figure 19. Classification of hits according to the DESeq2 custom analysis. (A) Scheme showing the expected phenotypes of targets found in the different groups defined in the custom analysis. **(B)** Scatter plot showing the number of targets detected in each of the groups. Only the targets with 2 or more sgRNAs following the same trend and log_2FC higher than 1.5 or lower than -1.5 were considered as differentially enriched. Groups A and B consist of targets differentially enriched exclusively in the p38α KO cells. Depleting targets in groups C, Co, D and Do only affects the WT cells. Groups E and F contain targets that are enriched or depleted in both samples but have a more extreme phenotype in the p38α KO cells.

To get a better idea of the processes found in each of the groups, we performed a hypergeometric test (HGT) enrichment analysis querying gene ontology (GO), KEGG and REACTOME databases (**Figure 20**). Among the targets enriched only in the p38α KO background, histone H3-K9 demethylation was detected as a potentially interesting enriched term. The majority of other terms enriched in the targets with increased viability in the p38α KO cells compared to the WT cells were coming from group C, targets that have no effect on the p38α KO cells but are detrimental to the viability of WT cells. Terms enriched in this group included oxidative phosphorylation and respiratory electron transport, indicating that perhaps p38α depletion renders cells less sensitive to OXPHOS disruption. We further found that genes in the group B, which are expected to be deleterious only in the p38α KO cells, were related to DNA replication and RNA processing, in line with the previous GSEA analysis results (shown in **Figure 18A,B**). Interestingly, mitochondrial translation was also found enriched in this group (**Figure 20C**).

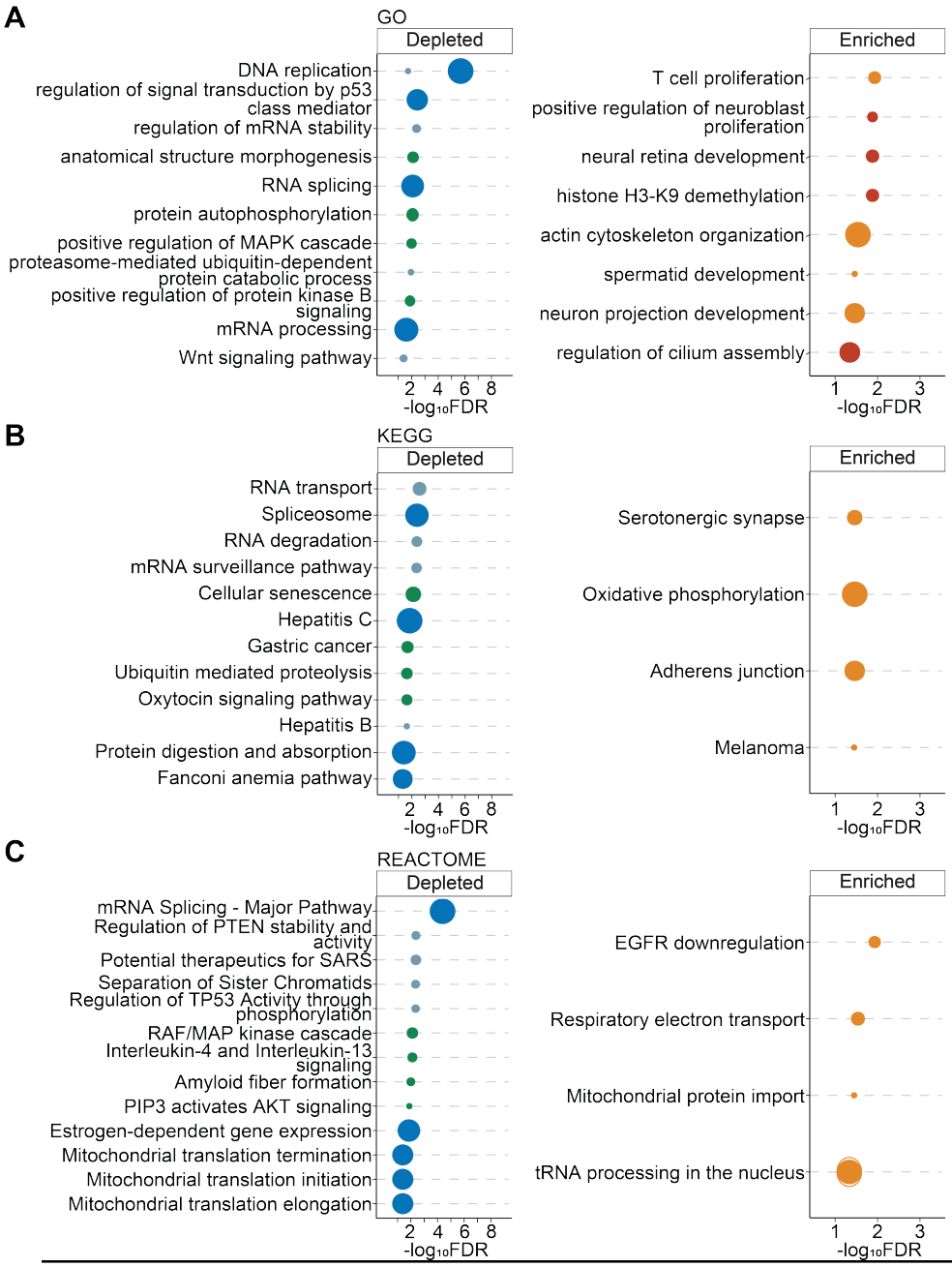

Figure 20. Enriched processes in the custom analysis. Enrichment of gene sets in the previously defined groups of interest were detected by hypergeometric test (HGT) enrichment analysis querying Gene Ontology **(A),** KEGG **(B),** and REACTOME **(C)** databases. Top enriched terms with normalised enrichment score |NES| > 1 and p-value < 0.05 are shown. Size of the point corresponds to NES and colour to the groups described in Figure 19.

Next, we looked at the top 10 enriched or depleted genes in each of the groups (**Figure 21**). Among the overall top targets some were supposed to have an effect only in the p38α KO cells, and were categorised in groups A and B, for instance *Zcchc14* the most enriched target, which falls in the group A and is expected to have an effect only in the p38α KO cells (**Figure 21A,B**). However, other targets seemed to exert opposite effects when depleted in the p38α KO cells compared to the WT cells. These include the previously identified top depleted target *Lmx1a,* which is assigned to group Do and its loss is expected to increase the viability of WT cells, while being detrimental in the p38α KO cells.

Overall, we detected several targets and processes potentially interconnected with p38α function. We decided to prioritise *Zcchc14* as the top enriched target, and mTOR signalling and mitochondrial translation as processes whose disruption is expected to sensitise cells to p38α depletion.

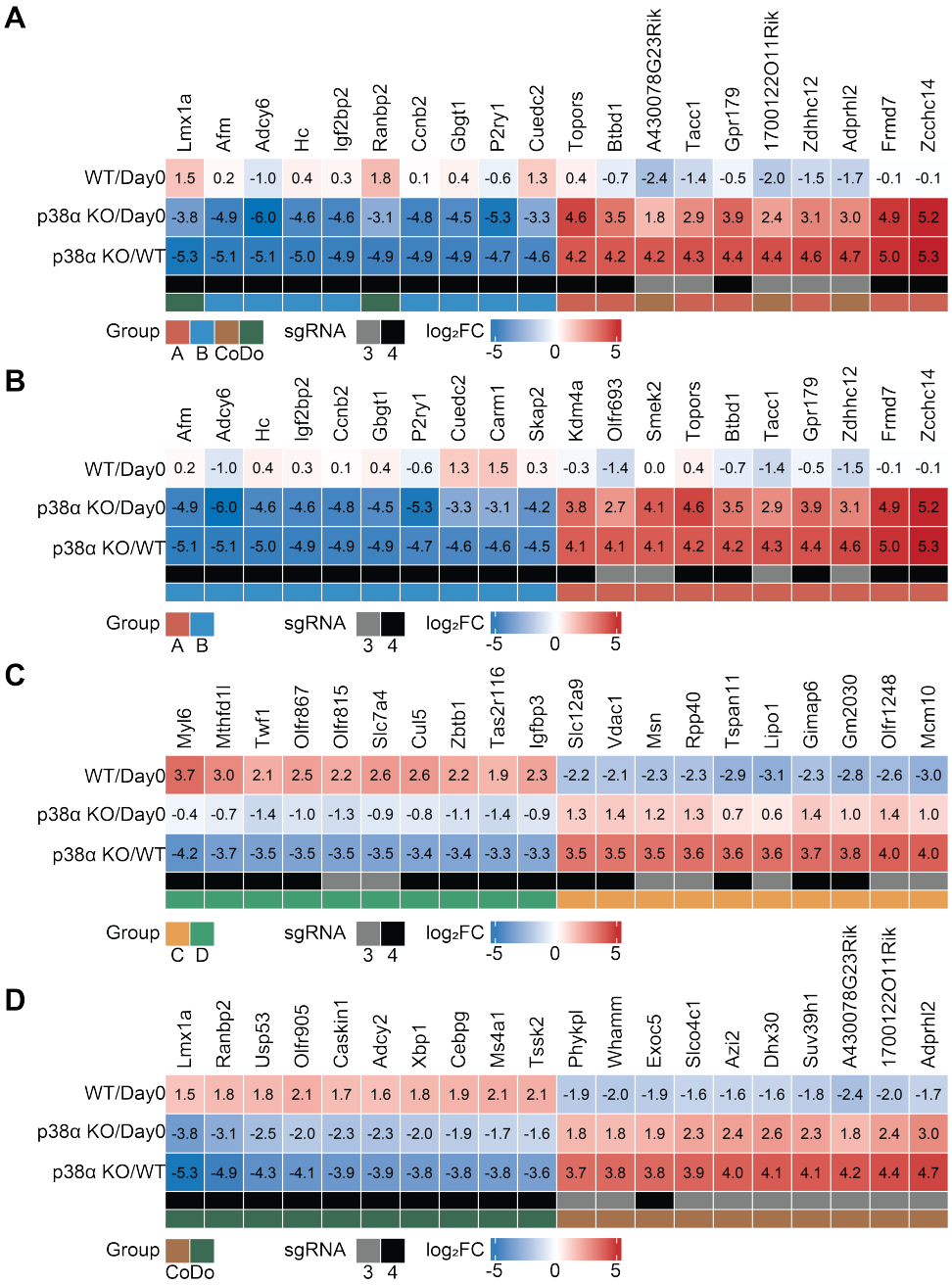

Figure 21. Top 10 enriched or depleted genes in the custom analysis. Top 10 genes regardless of the group **(A),** and top 10 enriched or depleted genes in groups A and B **(B)**, C and D **(C)** and Co and Do **(D)**. Numbers indicate log_2FC and the sgRNA legend indicates the number of the sgRNAs with the same phenotype.

Validation of the CRISPR/Cas9 screen hits

In order to assess the effect of putative targets on the viability of the p38α KO cells, we decided to employ parallel approaches to increase the probability of obtaining reliable results. For testing the effect of deleting individual genes, we cloned sgRNAs targeting the gene of interest in a lentiviral sgRNA expression plasmid that also expresses a fluorescent protein, thus facilitating the detection of cells with incorporated sgRNAs either by flow cytometry or microscopy. In addition to testing the cell viability, the fluorescently labelled cells allowed us to perform competitive proliferation assays. This approach entails mixing the cells infected with the GFP expressing sgRNA plasmid together with the mCherry expressing control cells and splitting them into 2 groups, one in which p38α KO is induced and the other WT. This mimics the CRISPR screen performed as it allows us to track the growth dynamics of the mixed population over time to learn whether loss of the target gene affects the competitive advantage of the p38α KO cells relative to the control cells. When possible, these analyses were complemented with the use of available chemical inhibitors against targets of interest.

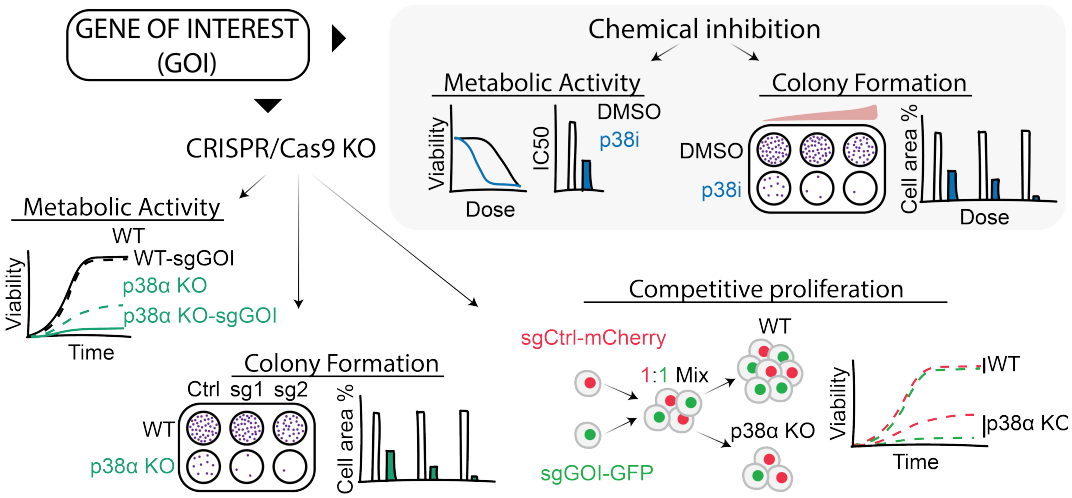

Figure 22. Assays used for the validation of CRISPR/Cas9 screen hits. GOI – Gene Of Interest, p38i – p38α inhibitor, sg – sgRNA; IC50-half maximal inhibitory concentration.

Depleting Zcchc14 increases viability of p38α KO cells

We first focused on the top enriched target *Zcchc14*, which encodes a Smaug-like RNA binding protein with a SAM domain that facilitates binding to common stem-loop elements of target mRNAs (Aviv et al., 2003). It belongs to the zinc finger CCHC-type superfamily (Wang et al., 2021), and has recently been identified as an essential host factor that forms a complex with noncanonical poly(A) polymerases TENT4A and TENT4B (Papd7 and Papd5), which generate a mixed poly(A) tail with intermittent non-adenosine residues such as guanosine, facilitating viral infection (Hyrina et al., 2019; Kim et al., 2020; Kulsuptrakul et al., 2021). Interestingly, our screening showed that both *Papd7* and *Papd5* sgRNAs were enriched in the p38α KO cells, although to a lesser extent than *Zcchc14*, suggesting a potential role of this complex in the deleterious effect of p38α depletion in cancer cells (**Figure 23A**).

Depleting Zcchc14 is expected to boost the proliferation of p38α KO cells while having no effect in the WT cells. To test this, we transduced BBL358-Cas9 cells with a sgRNA targeting *Zcchc14* (sg1-Zcchc14). Colony formation assays showed increased viability of sg1-Zcchc14 transduced cells upon treatment with the p38α inhibitor LY compared to the control cells (**Figure 23B**). We repeated the transduction with sg1-Zcchc14 and without selecting the transduced cells, split the cells into two pools. In one we induced the p38α KO with 4-OHT treatment while the other was left untreated as WT control. As comparison we used cells transduced with a sgRNA that targets p38β (*Mapk11*), as we expected that depleting p38β in this model has no effect on proliferation of p38α KO cells. As the sgRNA transduced cells also express GFP, we assayed the percentage of GFP+ sgRNA transduced cells by flow cytometry at 1, 4 and 8 days after p38α deletion. No selection for the cells that express the sgRNA allowed us to directly compare sg1-Zcchc14 transduced cells that are GFP+ with the control non-fluorescent cells. While the percentage of the control sgMapk11 cells and sgZcchc14 transduced WT cells did not change through the course of the assay, the population of sgZcchc14-p38α KO cells increased by the end of experiment suggesting that deleting Zcchc14 conferred a competitive advantage to the p38α KO cells (**Figure 23C**).

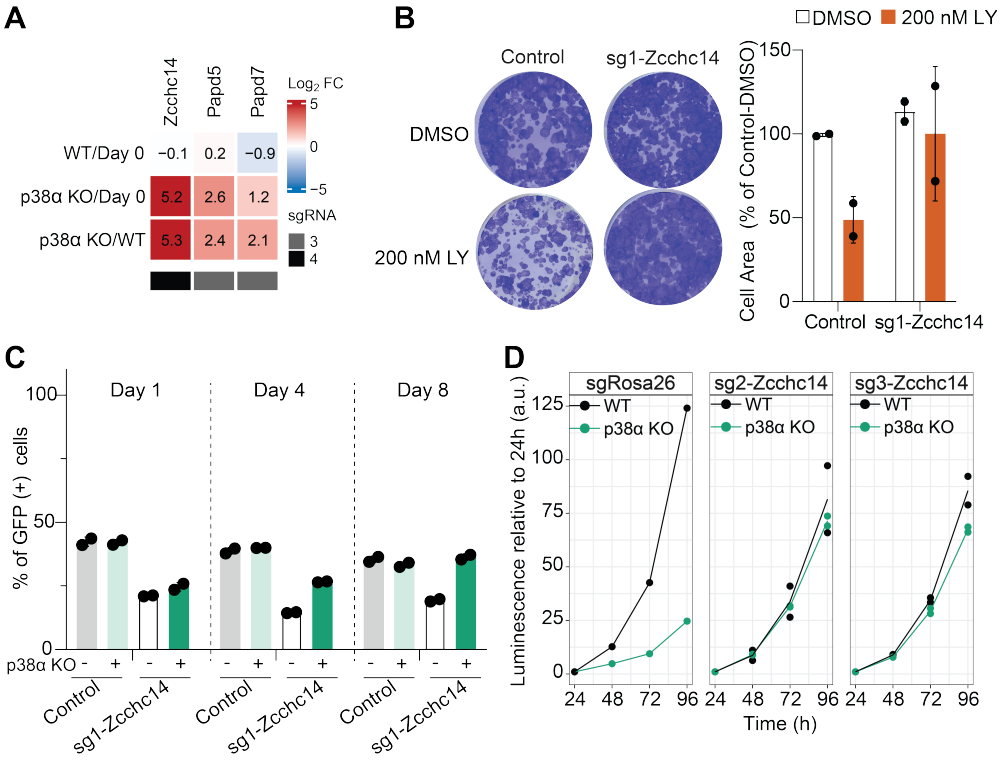

Figure 23. Targeting Zcchc14 increases the viability of p38α KO cells. (A) Heatmap showing the enrichment of sgRNAs targeting the Papd5 and Papd7 noncanonical poly(A) polymerases. Numbers in the heatmap show the log_2FC of the indicated comparisons. The sgRNA legend states the number of sgRNAs (out of 4) with the same phenotype. **(B)** BBL358-Cas9 cells were transduced with a lentivirus expressing GFP and a sgRNA targeting *Zcchc14* (sg1-Zcchc14), and 48 h later GFP+ cells were sorted by FACS and expanded. For colony formation assays, cells were plated at low density, treated with 200 nM LY2228820 (LY) or DMSO as control, and stained with crystal violet 7 days later. Representative images (left) and quantification of two independent experiments (right) shown as percentage of the control DMSO treated sample. **(C)** BBL358-Cas9 cells were transduced with vectors expressing GFP and either sg1-Zcchc14 or a sgRNA targeting *Mapk11* (Control), treated with 4-hydroxytamoxifen (4-OHT) for 48 h to induce p38α KO or left untreated, replated and passaged every 2-3 days. The GFP+ population was measured by flow cytometry after 1, 4 and 8 days of growth. Plot shows the mean of two technical replicates ± SD.**(D)** Viability of BBL358-Cas9 cells transduced with two independent sgRNAs targeting *Zcchc14* (sg2-Zcchc14 and sg3-Zcchc14) or the Rosa26 locus (sgRosa26) as control was measured by RealTime-Glo (RTG) assay. After infection with the sgRNA expressing plasmids, cells were selected for 48 h with 3 μg/ml puromycin, and then either treated for 48 h with 4-OHT (p38α KO) or left untreated (WT) and replated in media supplemented with the RTG reagents. Cell metabolic activity was followed by daily measurement of luminescence levels. Plots show luminescence levels relative to the signal detected after 24 h of growth. Lines connect the means of two technical replicates.

To further confirm these observations, we designed two additional *Zcchc14* targeting sgRNAs, and also included a Rosa26 targeting sgRNA as a control that leads to a genomic DNA cut in a 'safe-harbour' location in the genome, mimicking the DNA damage effect of the CRISPR/Cas9 system without targeting any particular gene (Friedrich & Soriano, 1991). Following the metabolic activity of the cells, we observed increased viability of the p38α KO cells transduced with the two sgZcchc14 constructs, while the control sgRosa26-expressing cells exhibited the expected decrease of growth upon p38α depletion (**Figure 23D**).

Additionally, we infected BBL358-Cas9 cells with the sgRosa26 cloned into an mCherry expressing plasmid and mixed them 1:1 with the sgZcchc14-GFP expressing cells. After 48 h of 4-OHT treatment, we imaged the mixed populations over 72 h, acquiring images every 12 h. The results again showed an increased proliferation of the p38α KO cells upon targeting Zcchc14. Indeed, by the end of the experiment, sgZcchc14 transduced cells represented the majority of cells detected in the p38α KO wells, further confirming that Zcchc14 depletion rescues the effect of p38α deletion (**Figure 24A,B**).

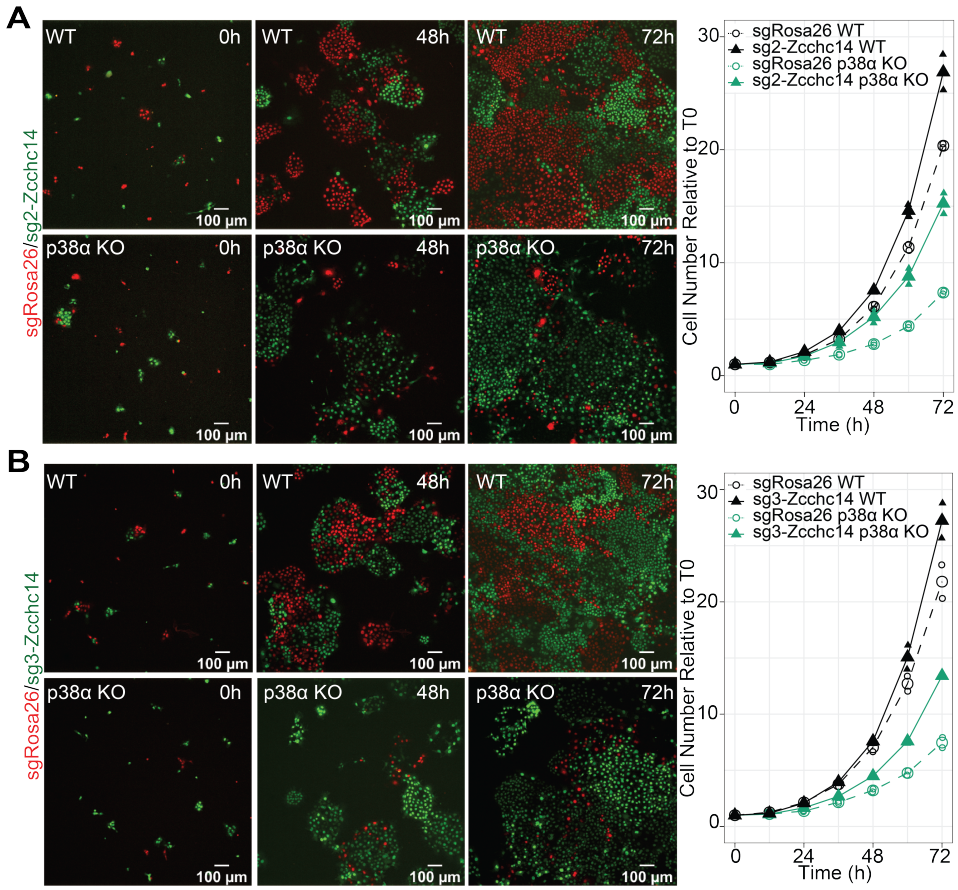

Figure 24. Targeting Zcchc14 increases the proliferation of p38α KO cells. BBL358-Cas9 cells were transduced with sg2-Zcchc14-GFP **(A)** or sg3-Zcchc14-GFP **(B)** and with control sgRosa26-mCherry, selected for 48 h with puromycin, and treated for another 48 h with 4-OHT (p38α KO) or left untreated (WT). Both p38α KO and WT cells expressing with sg-Zcchc14 (green) or sgRosa26 (red) were mixed 1:1, plated and 24 h later were imaged every 12 h over 72 h. The number of nuclei in each channel was quantified for each time point and normalised to the cell count detected at the first imaging time point (T0). Representative images (left) and quantification (right) of the time-lapse imaging are shown. Lines and larger symbols indicate mean values of two technical replicates (smaller symbols).

Inhibiting p38α potentiates the effect of mTOR inhibition

Although p38α has been reported to activate mTOR signalling (Cully et al., 2010; Hernández et al., 2011), the extent of the crosstalk between p38α and mTOR is not clear. Based on the CRISPR screen, disrupting the mTOR signalling was predicted to sensitise cells to p38α depletion, hence we set out to test this using rapamycin, an mTOR inhibitor.

After 72 h of combined treatment with p38α inhibitors and rapamycin, we observed a consistent decrease of cell viability compared to the rapamycin treatment alone (**Figure 25A**). This was reflected in decreased IC50 values as inhibiting p38α reduced the concentration of rapamycin necessary to achieve 50% of viability decrease (**Figure 25B**). Of note, rapamycin had a very striking effect on the viability of WT cells at doses as low as 1 nM. To test if the observed decrease in viability was due to lower cell survival, we performed a cell death assay after 72 h of treatment with rapamycin in combination with p38α inhibitors or DMSO as control. However, we observed no increase in DAPI+ dead cells upon rapamycin treatment and no effect of p38α inhibition (**Figure 25C**), but we cannot exclude the possibility of increased cell death levels at later time points. On the other hand, colony formation assays showed decreased cell area after two weeks of treatment with both mTOR and p38α inhibitors compared to the effect of single inhibitor treatment (**Figure 25D**). Overall, these results suggest that impairing mTOR signalling potentiates the deleterious effect of p38α inhibition in our cancer cell model.

Rapamycin inhibits mTOR signalling by forming a complex with the prolyl-isomerase FKBP12 which then sequesters and inhibits mTOR activity. While rapamycin is able to target mTOR in the mTORC1 complex, in the mTORC2 complex the rapamycin-FKBP12 binding site is protected by the scaffold protein RICTOR. In this line, mTORC1 and mTORC2 are often described as rapamycin-sensitive and rapamycin-resistant, respectively. Although rapamycin cannot bind directly to mTOR while it is forming the mTORC2 complex, it has been shown that prolonged treatment with rapamycin does lead to mTORC2 inhibition (Lamming et al., 2012; Sarbassov et al., 2006).

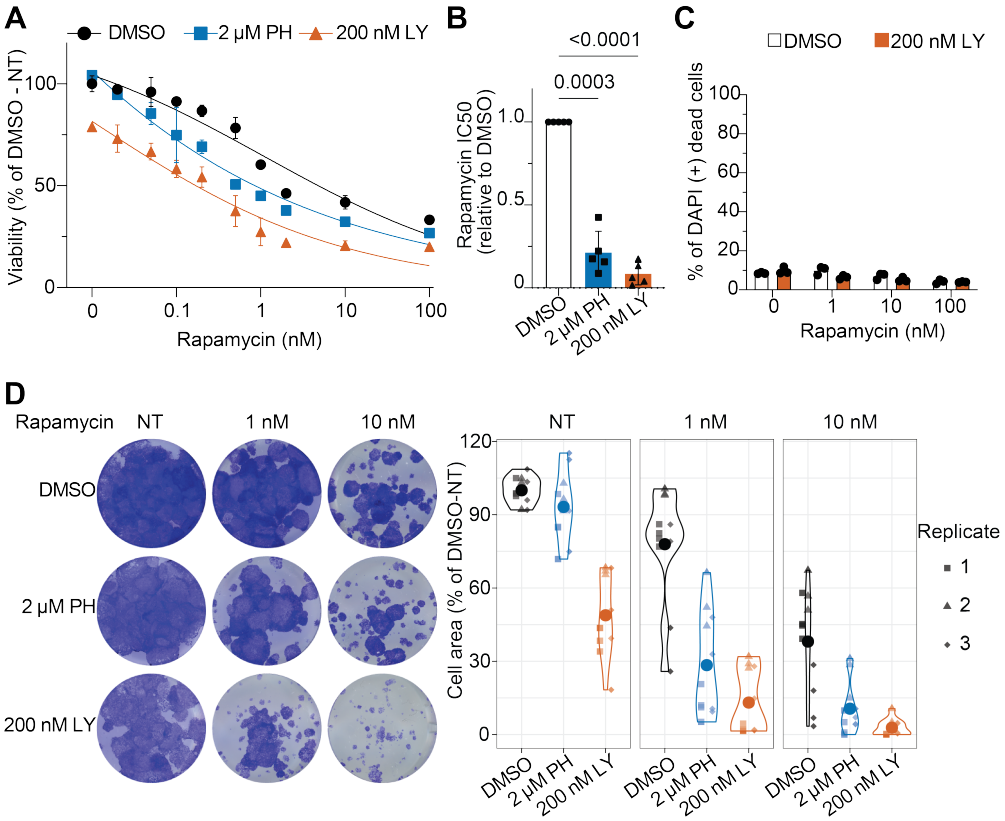

Figure 25. Inhibiting p38α potentiates the cytostatic effect of mTOR inhibition. **(A)** Combined p38α and mTOR inhibition decreases BBL358 cancer cell viability. Representative dose-response curve of an MTT assay performed after 72 h of treatment with increasing doses of the mTOR inhibitor rapamycin in combination with the p38α inhibitors 2 μM PH-797804 (PH), 200 nM LY2228820 (LY) or DMSO as control. Data represent mean ± SD of the measured viability normalised to DMSO non-treated (DMSO-NT) sample. **(B)** Inhibiting p38α decreases rapamycin IC50 values. Bar plots show mean IC50 values normalised to DMSO from 5 independent MTT experiments performed after 72 h of treatment ± SD. Statistical significance was determined using one-way ANOVA Dunnett multiple comparison test. **(C)** Inhibiting both mTOR and p38α has no effect on cell death levels. Cells were plated and treated the following day with the indicated doses of rapamycin in combination with 200 nM LY for 72 h, then collected and stained with DAPI. Plot shows the mean percentages of DAPI+ dead cells in the two technical replicates of the indicated samples. **(D)** Colony formation potential is impaired upon treatment with p38α inhibitors and rapamycin. Cells were plated at low density and treated with the indicated concentrations of rapamycin together with the p38α inhibitors PH and LY or with DMSO as a control, and stained with crystal violet two weeks later. Representative images are shown in the left and quantification of three independent experiments (right) shows the cell area percentage normalised to the DMSO-NT samples. Distinct point shapes indicate technical replicates from the same experiment.

In order to investigate which of the two complexes might be responsible for the observed effect, we first looked at the CRISPR screen enrichment values of different core components and downstream targets of mTORC1 and mTORC2. Both complexes contain the core components mTOR and mLST8, and a complex specific scaffold unit named RAPTOR (*Rptor*, mTORC1) or RICTOR (*Rictor*, mTORC2). PRAS40 (*Akt1s1*) is a Raptor-interacting protein that can inhibit mTORC1, while DEPTOR (*Deptor*) is an endogenous inhibitor of both mTORC1 and mTORC2. Activated mTORC1 can phosphorylate S6K1 (*Rps6kb1*) or 4E-BP1 (*Eif4Ebp1*), while AKT (*Akt1*) and SGK1 (*Sgk1*) are phosphorylated by mTORC2 **(Figure 26A**). Based on our analysis, depleting mTOR or mLST8 should be deleterious in both WT and p38α KO cells, while depleting RICTOR or SGK1, a scaffolding unit and a downstream target of mTORC2, respectively, is predicted to have a deleterious effect only in the p38α KO cells, suggesting that perhaps inhibiting the mTORC2 complex increases the sensitivity to p38α inhibition (**Figure 26B**).

To test this, we decided to target the RAPTOR subunit of mTORC1 and the RICTOR subunit of mTORC2 with sgRNAs. We observed decreased viability of both sgRptor and sgRictor transduced cells upon p38α deletion or treatment with the p38α inhibitor LY, although the WT cells transduced with sgRNAs also had reduced colony formation potential. Of note, we have not confirmed downregulation of the targeted genes and it is possible that the observed phenotypes are due to incomplete target downregulation.

Altogether, it seems that the effect of mTOR pathway disruption is potentiated by p38α depletion or inhibition, however further experiments would be needed to elucidate the underlying mechanism.

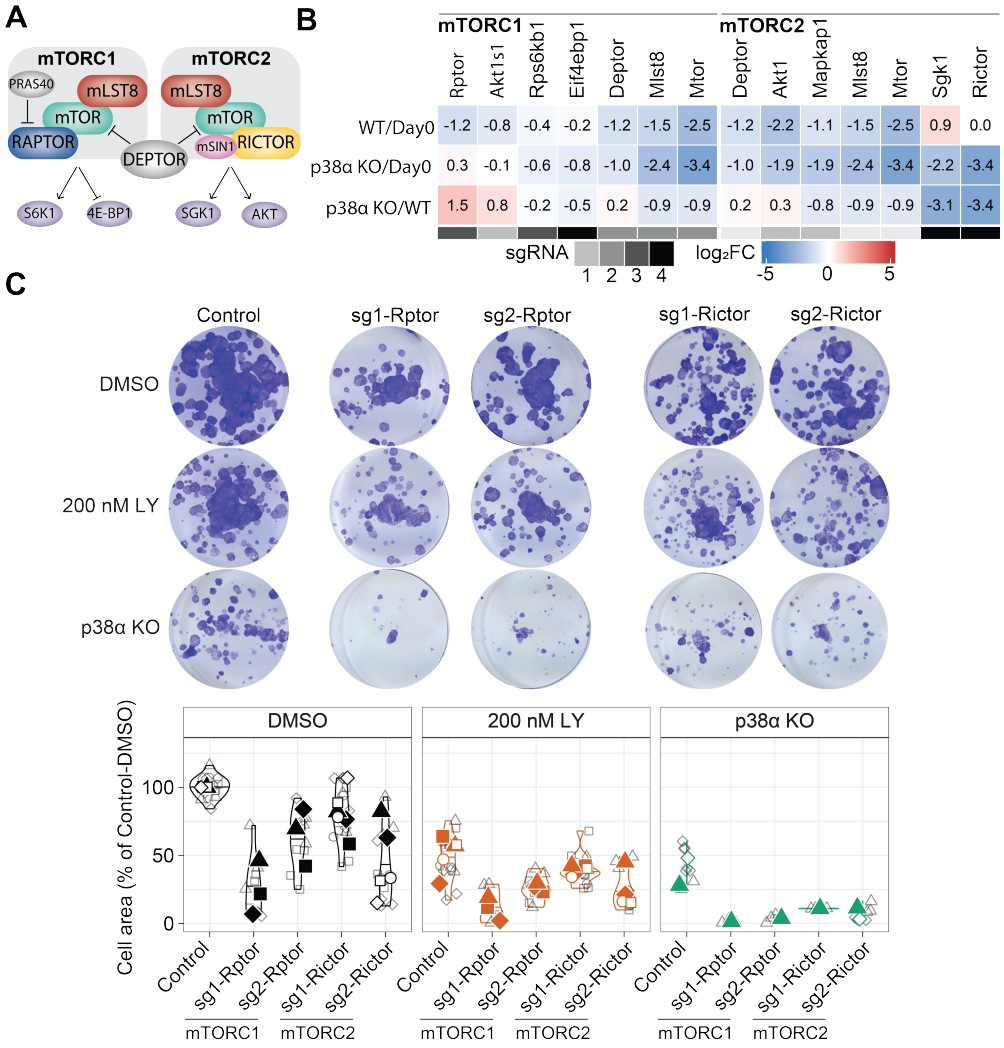

Figure 26. Targeting mTORC1 or mTORC2 is lethal for BBL358 cells. (A) Scheme showing the known components and downstream targets of the mTOR complex 1 (mTORC1) and mTOR complex 2 (mTORC2). Figure adapted from (Liu & Sabatini, 2020). **(B)** Heatmap showing the enrichment of sgRNAs targeting genes encoding components and downstream substrates of mTORC1 (left) and mTORC2 (right). Numbers in the heatmap show the log_2FC of the indicated comparisons. The sgRNA legend states the number of sgRNAs (out of 4) with the same phenotype. **(C)** Targeting RAPTOR (*Rptor)* or RICTOR (*Rictor*) impairs BBL358 cell viability. BBL358-Cas9 cells were transduced with two independent sgRNAs targeting *Rptor* (sg1-Rptor, sg2-Rptor), *Rictor* (sg1-Rictor, sg2-Rictor) or a control Rosa26-sgRNA, and were selected for 48 h with 3 μg/ml puromycin. After 48 h of treatment with 4-hydroxytamoxifen, to induce the p38α KO , or with 200 nM of the p38α inhibitor LY2228820 (LY) or DMSO as control, cells were plated at low density and stained with crystal violet 7 days later. Representative images (above) and quantification (below) are shown as the cell area percentage of DMSO treated control sample. Shape denotes biological replicates.

p38α KO cells are sensitized to mitochondrial translation inhibition

To check if impairing mitochondrial translation synergises with p38α inhibition as expected based on the CRISPR screen analysis, we first performed experiments with chloramphenicol, an antibiotic described to inhibit mitochondrial translation (Richter et al., 2013).

We observed a consistent decrease in viability when chloramphenicol was combined with p38α inhibitors, which was further reflected in decreased IC50 values (**Figure 27A,B**). To test if the observed decrease in viability was due to a decrease in cell survival, we tested the cell death levels after 72h of treatment. However no difference in cell death levels was observed, suggesting that neither chloramphenicol treatment increases cell death levels at this time point nor this changes upon p38α inhibition (**Figure 27C**). Next, we looked at the colony formation capacity of cells and found that treatment with chloramphenicol decreased the colony area and the combined treatment with p38α inhibitors slightly potentiated this effect.

In order to disrupt mitochondrial translation, we targeted one of the genes that in our CRISPR screen analysis was preferentially depleted in the p38α KO cells. Based on the sgRNA enrichment scores of targets found in the mitochondrial translation related gene ontology groups (**Figure 28A**), we decided to focus on *Mrpl28*, which encodes the mitochondrial large ribosomal subunit protein L28. Targeting this gene is predicted to be detrimental to the viability of p38α KO cells while having no effect on the WT cells. We transduced BBL358-Cas9 cells with two independent sgRNAs targeting *Mrpl28* (sg1-Mrpl28 and sg2-Mrpl28) and performed a colony formation assay. The results showed a deleterious effect of targeting Mrpl28 in the WT cells, and we could observe a further decrease in colony formation ability when combining both Mrpl28 disruption with p38α inhibition or depletion **(Figure 28B**).

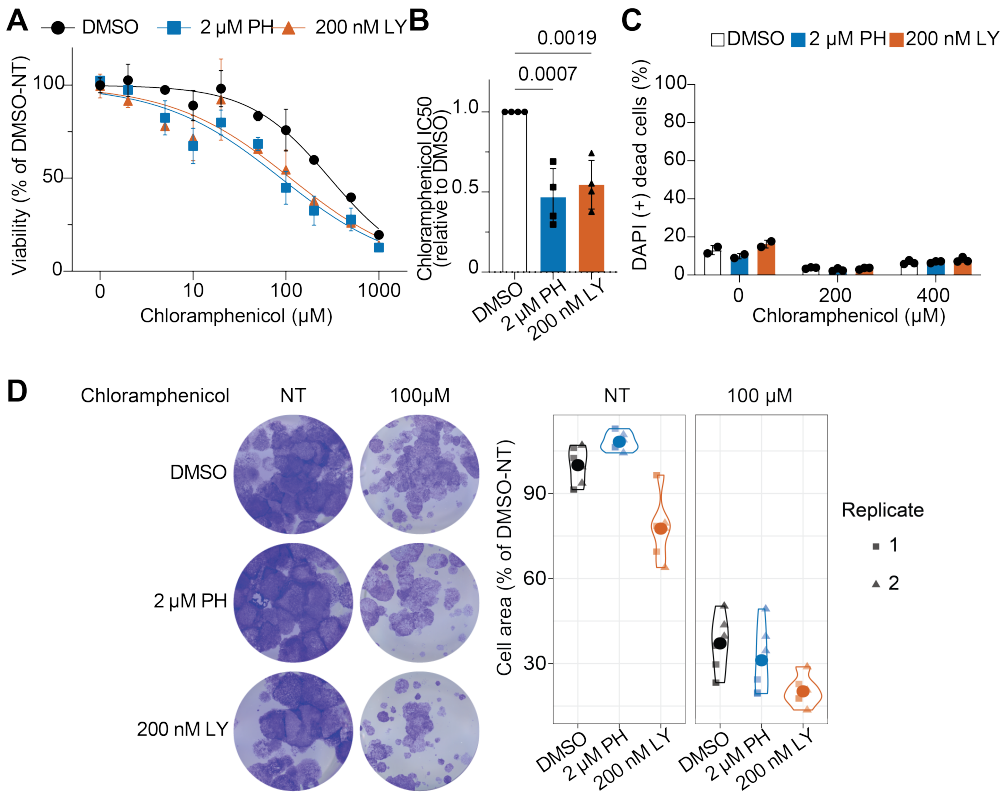

Figure 27. The inhibition of p38α in combination with chloramphenicol treatment decreases cell viability. (A) Representative dose-response curve of an MTT assay performed after 72 h of treatment with increasing doses of the mitochondrial translation inhibitor chloramphenicol in combination with the p38α inhibitors 2 μM PH-797804 (PH) and 200 nM LY2228820 (LY), or DMSO as control. Data represent mean of the viability normalised to DMSO non-treated (DMSO-NT) sample ± SD. **(B)** Bar plots show mean IC50 values normalised to DMSO from 4 independent MTT experiments performed after 72h of treatment ± SD. Statistical significance was determined using one-way ANOVA Dunnett multiple comparison test. **(C)** Inhibiting both mitochondrial translation and p38α has no effect on cell death levels. Cells were plated and treated the following day with indicated doses of chloramphenicol in combination with 200 nM LY for 72 h, then collected and stained with DAPI. Plot shows mean percentage of DAPI+ dead cells in two technical replicates. **(D)** The combined treatment with chloramphenicol and p38α inhibitors has a small effect on colony formation potential. Cells were plated at low density and treated with the indicated concentrations of chloramphenicol together with the p38α inhibitors PH and LY, or with DMSO as control, and two weeks later were stained with crystal violet. Representative images are shown in the left and quantification of two independent experiments (right) shows the cell area percentage normalised to the DMSO-NT samples. Distinct shapes indicate technical replicates from the same experiment.

Overall it seems that impairing mitochondrial translation, either by chemical inhibition or genetic depletion of one of the mitochondrial ribosomal subunits, indeed sensitises the cells to p38α inhibition or depletion. However, disrupting this process also impairs the viability of the WT cells, contrary to the expected outcome based on the CRISPR screen analysis.

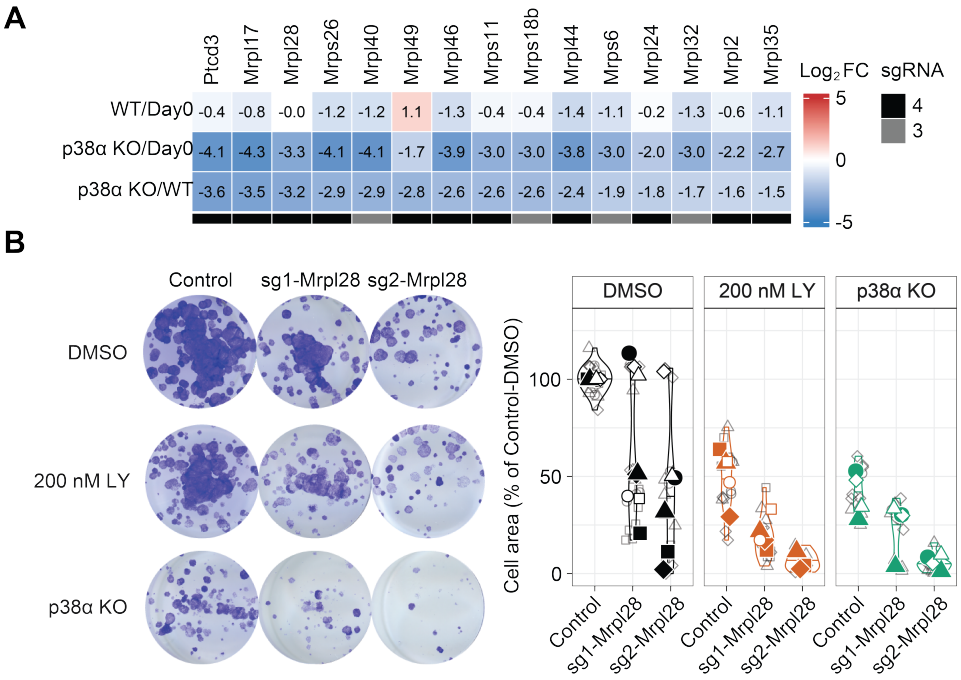

Figure 28. Depleting *Mrpl28* impairs cell viability. (A) Heatmap showing the enrichment of sgRNAs targeting genes that encode mitochondrial ribosomal subunits. Numbers in the heatmap show the log_2FC of the indicated comparisons. The sgRNA legend states the number of sgRNAs (out of 4) with the same phenotype. **(B)** Targeting *Mrpl28* impairs colony formation potential. BBL358-Cas9 cells were transduced with two independent sgRNAs targeting *Mrpl28* (sg1-Mrpl28 and sg2-Mrpl28) or the Rosa26 locus (Control) and selected 48 h with 3 μg/ml puromycin. After 48 h, cells were treated with 4-hydroxytamoxifen, to induce p38α KO, or with 200 nM of the p38α inhibitor LY2228820 (LY), or with DMSO as control, and then were plated at low density and stained with crystal violet 7 days later. Representative images (left) and quantification of the indicated number of experiments for each of the sgRNAs (right) shown as percentage of control DMSO treated sample. Different shapes indicate biological replicates.

Role of other p38 MAPK pathway components

The dependency of BBL358 cancer cells on the p38α pathway is not a universal phenomenon, as not every cancer cell line relies on p38α for survival. An interesting possibility is that this dependency on p38α could be driven by dysregulation of a particular branch of the p38 MAPK signalling. To further explore this, we looked at the CRISPR screen effect of depleting different MAP3Ks and MAP2Ks described previously as upstream activators of p38α, as well as other p38 MAPK family members (**Figure 29**). This analysis identified TAK1 (*Map3k7*) as a gene whose depletion should have a more deleterious effect in the p38α KO background. Interestingly, depleting MEKK3 (*Map3k5*) or MKK3 (*Map2k3*) is predicted to impair the viability of WT, but not p38α KO cells. In contrast to MKK3, targeting MKK6 (*Map2k6*) is expected to increase the proliferation of WT cells, suggesting a potential opposing role of these two kinases. When looking at different p38 family members, we were surprised to see enrichment of sgRNAs targeting p38δ in the p38α KO cells. If true, this would suggest a role for p38δ in mediating the deleterious effect of p38α depletion. Hence, we set out to test the effect of disrupting p38δ or chemically inhibiting TAK1.

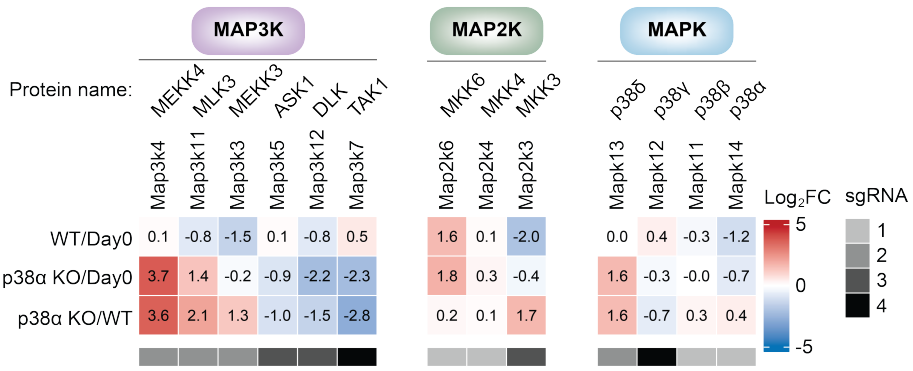

Figure 29. Representation of different MAP3K, MAP2K and MAPK family members in the CRISPR screen analysis. Heatmaps showing the enrichment of sgRNAs targeting genes encoding MAP3Ks or MAP2Ks reported to function upstream of p38α and the four p38 MAPK family members detected in the CRISPR screen dataset. Numbers in the heatmap show the log_2FC of the indicated comparisons and the sgRNA legend states the number of sgRNAs (out of 4) with the same phenotype.

Downregulation of p38δ rescues the effect of p38α deletion

To investigate the effect of depleting different p38 family members observed in the CRISPR screen analysis, we transduced cells with sgRNAs targeting the four p38 MAPKs. Targeting p38α decreased cell viability as expected. However, while guides targeting p38β and p38γ had no effect on cell viability, depleting p38δ increased the viability of p38α KO cells and rendered them less sensitive to treatment with the p38α inhibitor LY (**Figure 30**).

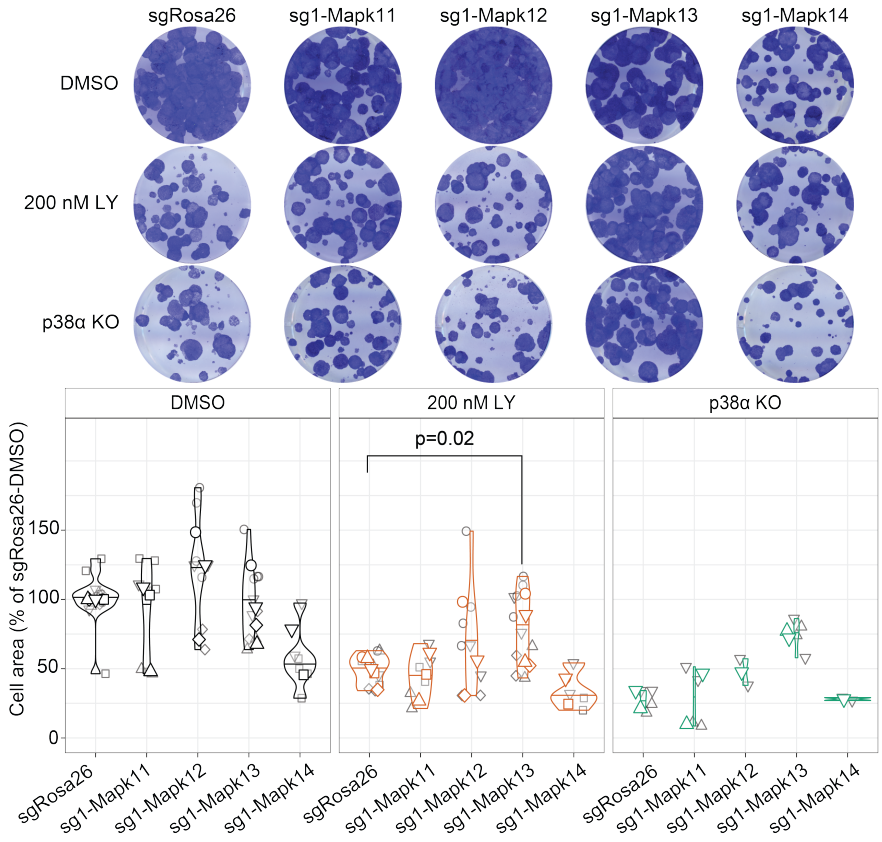

Figure 30. Effect of depleting different p38 family members in BBL358 cell viability. Representative images of colony formation assays (upper panel) performed with BBL358-Cas9 cells transduced with sgRNAs targeting p38α (sg1-Mapk14), p38β (sg1-Mapk11), p38γ (sg1-Mapk12), p38δ (sg1-Mapk13) or the Rosa26 locus (sgRosa26) as control. Cells were infected, selected for 48 h with 3 µg/ml puromycin, treated for 48 h with 4-hydroxytamoxifen, to induce p38α KO, or with 200 nM of the p38α inhibitor LY2228820 (LY), or with DMSO as control, and then were plated at low density and stained with crystal violet 7 days later. The lower panels show the quantification of the experiments performed. Plots indicate the cell area as percentage of the sgRosa26 DMSO treated sample. Independent experiments are denoted with different point shapes. Statistical significance was determined for samples with at least two biological replicates using multiple t-tests followed by Benjamini-Hochberg p-value adjustment.

Western blot analysis of cells transduced with sg1-Mapk13 indeed showed decreased total protein levels of p38δ (**Figure 31A**).

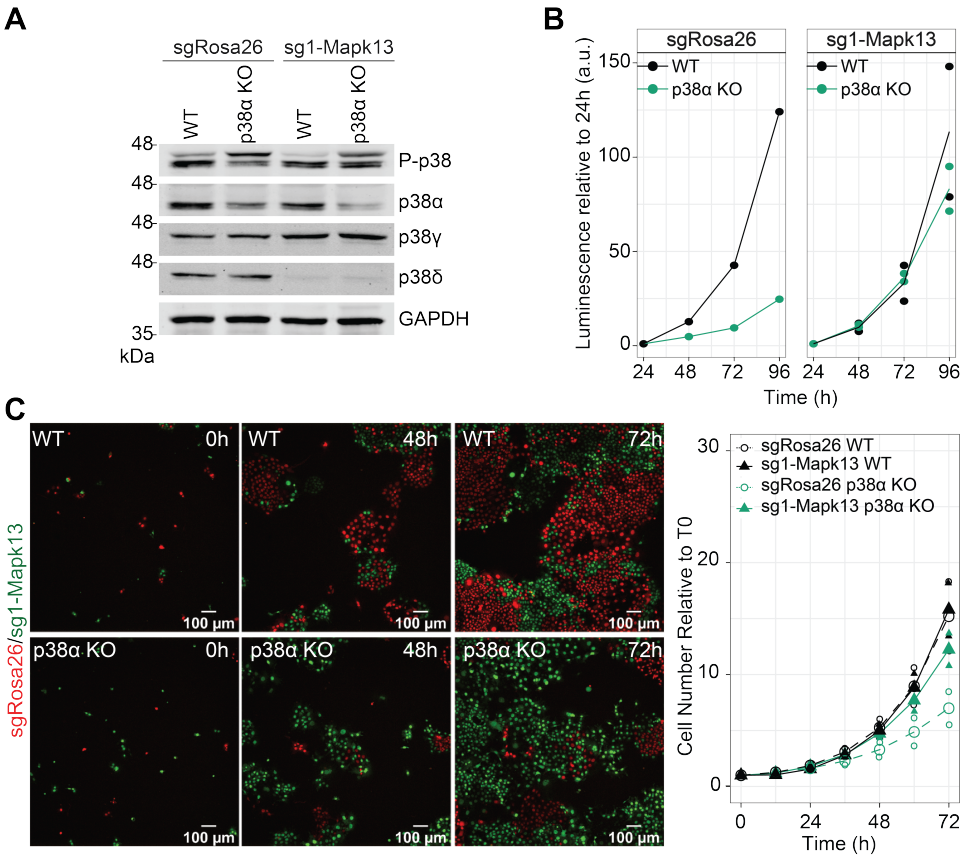

Figure 31. Loss of p38δ increases the viability of p38α KO cells. (A) Western blot analysis of cells transduced with sgRNAs targeting *Mapk13* (sg1-Mapk13) or the Rosa26 locus (sgRosa26) as control. After selection for 48 h with 3 μg/ml puromycin, cells were treated for 48 h with 100 nM 4-hydroxytamoxifen (4-OHT) to induce p38α KO or left untreated as WT. **(B)** The viability of cells transduced with sg1-Mapk13 or sgRosa26 was measured by RealTime-Glo (RTG) assay. Cells were transduced and treated as in (A), and replated in media supplemented with the RTG reagents. Cell metabolic activity was followed by daily measurement of luminescence levels. Plots show the luminescence levels relative to the signal detected after 24 h. Lines connect means of two technical replicates. **(C)** Representative images (left) and quantification (right) of the time-lapse imaging of sg1-Mapk13-GFP cells (green) mixed 1:1 with sgRosa26-mCherry cells (red). Cells were transduced with the indicated sgRNAs, selected for 48 h with puromycin and then treated for 48 h with 4-OHT (p38α KO) or left untreated (WT), then both p38α KO and WT cells with *Mapk13* targeting and control sgRNAs were mixed 1:1, plated and 24 h later were imaged every 12 h over 72 h. The number of nuclei in each channel was quantified for each time point and normalised to the cell count detected at the first imaging time point (T0). Lines and larger symbols indicate mean values of two technical replicates (small symbols).

In addition to the colony formation assay, the viability of p38α KO cells transduced with sg1-Mapk13 was increased in comparison to the p38α KO alone (**Figure 31B**). As an orthogonal approach, we imaged the mixed population of control-mCherry and sg1-Mapk13 GFP expressing cells that are either WT or p38α KO over 72 h. Again we observed that the p38α and p38δ double KO cells were dividing at a similar rate to the WT cells while the p38α KO cell proliferation was impaired (**Figure 31C**).

As the above experiments were performed with a single sgRNA for each target, we repeated the colony formation assays using two additional p38δ targeting sgRNAs in order to exclude off-target effects. These assays showed that p38α KO cells transduced with two different Mapk13-targeting sgRNAs had increased viability (**Figure 32A**). Western blot analysis confirmed that both sgRNAs downregulated the p38δ protein levels (**Figure 32B**).

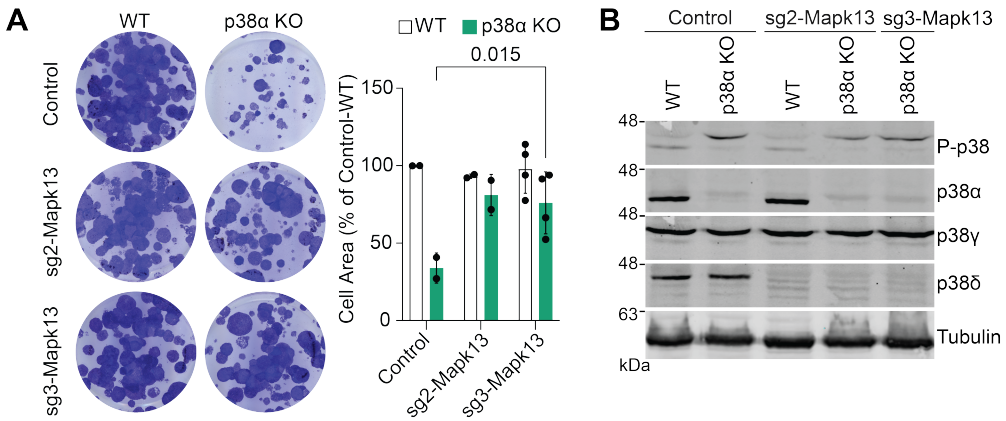

Figure 32. The effect of p38δ depletion in p38α KO cells is recapitulated with two additional sgRNAs. (A) BBL358-Cas9 cells were transduced with two independent sgRNAs targeting p38δ (sg2-Mapk13 and sg3-Mapk13) or the Rosa26 locus (sgRosa26) as control. Cells were infected, selected for 48 h with 3 μg/ml puromycin, and then treated for 48 h with 100 nM 4-hydroxytamoxifen (4-OHT), to induce p38α KO. Both WT and p38α KO cells were plated at low density and 7 days later were stained with crystal violet. Representative images (left) and quantification (right) showing the mean cell area normalised to control WT sample. Points indicate biological replicates. Statistical significance was determined with two-way ANOVA Tukey's multiple comparisons test. **(B)** Targeting p38δ with sg2-Mapk13 and sg3-Mapk13 downregulates total p38δ protein levels. Western blot analysis using the indicated antibodies in cells transduced as in (A).

Interestingly, the analysis of mRNA levels upon p38α downregulation showed a modest but consistent increase in the *Mapk13* mRNA encoding p38δ. We also observed increased levels of the MKK6 (*Map2k6*) mRNA as expected, but no changes were detected in the case of p38γ (*Mapk12*) and MKK3 (*Map2k3*) (**Figure 33**).

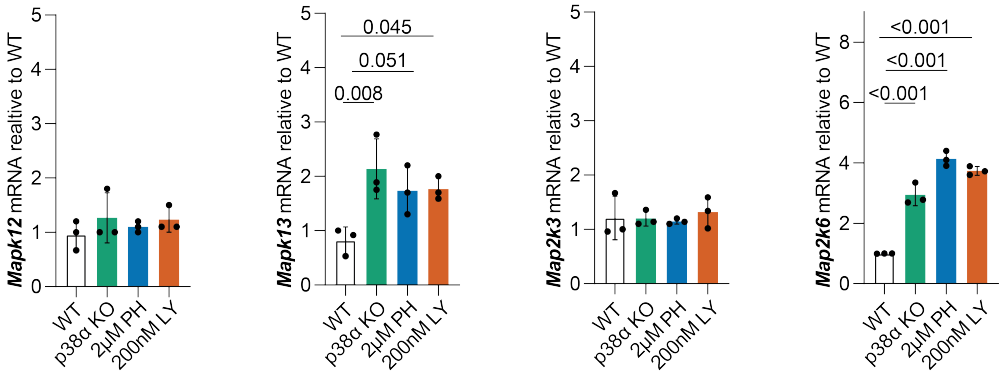

Figure 33. Increased p38δ mRNA levels upon p38α downregulation. The mRNA levels were measured by qRT-PCR in BBL358 cells treated for 48 h with 100 nM 4-hydroxytamoxifen (to induce p38α KO), and the p38α inhibitors 2 μM PH-797804 (PH) or 200 nM LY2228820 (LY), or left untreated as control (WT). *Gapdh* and *Hprt* were used as endogenous controls. Bar plots show mRNA levels of the indicated targets normalised to the WT samples ± SD. Dots indicate biological replicates. Statistical significance was determined using one-way ANOVA and Dunnett's multiple comparisons test.

Although the enrichment of p38δ (*Mapk13*) in the CRISPR screen analysis was modest compared to the values of some other enriched candidates, experimental validation demonstrated the increased viability of p38α KO cells upon p38δ depletion, strongly suggesting the interplay between these two p38 MAPKs in our cancer cell model.

Inhibiting p38α potentiates the effect of a TAK1 inhibitor

Downregulation of the upstream p38α activator TAK1 (*Map3k7*) was predicted to have a deleterious effect in the p38α KO sample, we therefore used the TAK1 inhibitor 5Z-7-oxozeaenol to test this (Ninomiya-Tsuji et al., 2003). MTT assays revealed decreased cell viability upon combination of TAK1 and p38α inhibition. Indeed, we observed a consistent decrease in the IC50 when cells were treated with 5Z-7-oxozeaenol together with a p38α inhibitor (**Figure 34A,B**). To test if this was due to decreased cell survival, we measured cell death levels after 72 h of treatment, and observed neither an effect of the TAK1 inhibitor on the cell death levels, nor a change upon combination with p38α inhibitors (**Figure 34C**). Overall, these preliminary data indicates that TAK1 inhibition sensitizes cells to the loss of p38α.

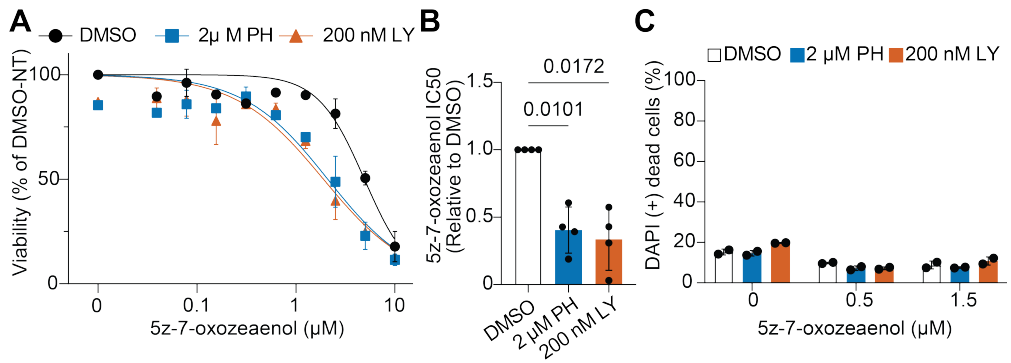

Figure 34. TAK1 inhibition sensitizes cells to p38α inhibition. (A) Combined inhibition of p38α and TAK1 decreases BBL358 cancer cell viability. Representative dose-response curve of an MTT assay performed after 72 h of treatment with increasing doses of the TAK1 inhibitor 5z-7-oxozeanol in combination with the p38α inhibitors 2 μM PH-797804 (PH) and 200 nM LY2228820 (LY), or with DMSO as control. Data represent means ± SD of the measured viability normalised to DMSO non-treated (DMSO-NT) sample. **(B)** The p38α inhibition decreases 5z-7-oxozeanol IC50 values. Barplots show mean IC50 values normalised to DMSO ± SD from 4 independent MTT experiments performed after 72 h of treatment. Statistical significance was determined using one-way ANOVA Dunnett multiple comparison test. **(C)** Inhibiting both p38α and TAK1 has no effect on cell death levels. Cells were plated and treated the following day with the indicated doses of 5z-7-oxozeaenol in combination with 2 μM PH or 200 nM LY for 72 h, then collected and stained with DAPI. Plot shows mean percentage of DAPI+ dead cells in the two technical replicates of the indicated samples.

Investigating hits predicted to synergize with the p38α KO

The effect that we have observed with both Zcchc14 as well as p38δ depletion was robust, as depleting either of them was able to rescue the decreased viability of the p38α KO cells, going in line with the CRISPR screen analysis. However, even though the effect of mTOR, mitochondrial translation or TAK1 inhibition on the p38α KO cells does corroborate the observations derived from the CRISPR screen, we also consistently observed an unexpected effect on the growth of the WT cells. Our analysis aimed to select targets whose downregulation had a deleterious effect exclusively in the p38α KO cells, and this was not confirmed by the results obtained so far.

Targeting the top 10 depleted hits

To further explore how reliable was the identification of hits whose sgRNAs were depleted in the p38α KO cells according to our screen, we decided to analyse the effect of targeting the top 10 underrepresented hits (**Figure 35A**). Preliminary experiments were performed by imaging cells transduced with targeting sgRNAs expressing GFP and control cells transduced with the sgRosa26-mCherry construct. The cells were transduced, selected and treated with 4-OHT to induce p38α depletion or left untreated as WT. Cells were then mixed 1:1 and tracked by time-lapse imaging. The cell number measured at the end of the experiment relative to the first imaging point indicated that some of the sgRNAs tested seem to impair the viability of WT cells (sgLmx1a, sgAfm, sgHc, sgIgf2bp2, sgCuedc2), and although we could observe reduced growth of the p38α KO cells transduced with sgLmx1a, sgAfm and sgCcnb2, the effect was not very consistent with the results obtained in the CRISPR screen analysis (**Figure 35B**).

Albeit a bit preliminary, the lack of a clear effect together with the results observed with previous underrepresented targets that were tested, made us question the reliability of the analysis of targets depleted specifically in the p38α KO cells.

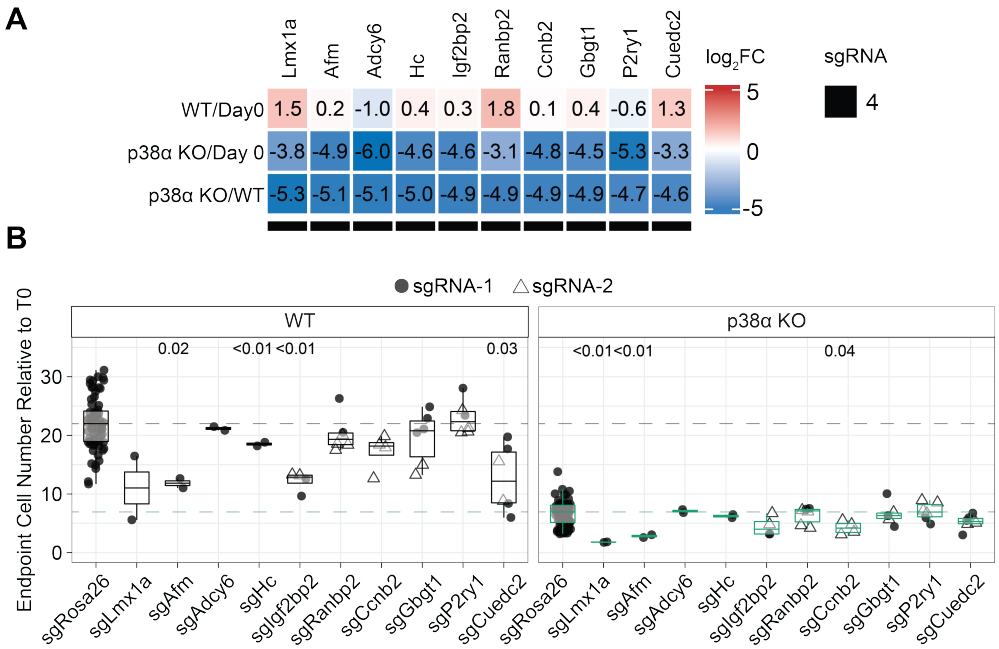

Figure 35. Targeting the top 10 depleted hits does not show a clear phenotype. **(A)** Heatmap showing top 10 targets with sgRNAs depleted (blue) in p38α KO compared to the WT cells. Targets were sorted based on the KO vs WT log_2FC values and the top 10 depleted targets were plotted. Numbers in the heatmap represent the log2FC of the target comparing WT to Day 0 (WT/Day 0), p38α KO to Day 0 (p38α KO/Day0) or p38α KO to WT samples. The sgRNA legend indicates the number of sgRNAs (out of 4) with the same phenotype. **(B)** Targeting the top 10 depleted hits shows variable effect. Quantification of the time-lapse imaging of BBL358-Cas9 cells transduced with the indicated sgRNAs cloned in the GFP expressing vector mixed 1:1 with the sgRosa26-mCherry expressing cells. Cells were transduced with targeting or control sgRNAs, selected for 48 h with puromycin and treated for 48 h with 4-hydroxitamoxifen (p38α KO) or left untreated (WT), then both p38α KO and WT cells with targeting or control sgRNAs were mixed 1:1, plated and 24 h later were imaged every 12 h for 72 h. Plot shows the cell numbers relative to the first imaging time point (T0). Points represent counts from individual wells, and the shape indicates distinct sgRNAs targeting the same gene. Statistical significance was determined with multiple t-test followed by Benjamini-Hochberg p-value adjustment.

Substantial enrichment of sgRNAs targeting *Trp53*

In order to understand the discrepancy between the CRISPR screen analysis and the experimental results obtained, we decided to go back to the data and look at the raw values. We first looked at the raw sgRNA counts for control non-targeting sgRNAs in our library, which are expected to have no effect on the viability of the cells and should be evenly distributed relative to the total

number of reads obtained. Comparison of $\log_2$ raw counts (with pseudo count 1 used to avoid computing $\log_2$ value of zero) showed a substantial decrease of control sgRNA counts in the p38α KO cells compared both to the Day 0 and to WT cells (**Figure 36A**). A possible source of this would be a decreased number of total reads obtained in the p38α KO sample, however this was not the case as the total number and percentage of mapped reads obtained were similar across all three samples (see **Figure 17A**), hence we excluded this as a possible cause.

To investigate this further, we plotted the distribution of targeting sgRNA raw counts, categorising the targets as essential (detrimental to the viability of most cancer cells when depleted) or non-essential, based on the mouse homologues of the pan-cancer list of essential genes (Dempster et al., 2021). This analysis showed that, while in all of the samples the counts for sgRNAs targeting essential genes were lower as expected, distribution of the counts of non-essential genes was greatly skewed towards the lower end in the p38α KO sample, similar to the control sgRNA distribution that we observed previously (**Figure 36B**). The overall lower representation of both control and non-essential gene targeting sgRNAs could be a consequence of the increased enrichment of a particular subset of reads. Indeed, we found an enrichment of the sgRNAs targeting Trp53 (all four sgRNAs present in the library) and Cdkn2a (2 out of 4 sgRNAs) in both WT and p38α KO samples. Strikingly, 30% of the total WT counts and over 50% of the p38α KO counts belonged to these 6 sgRNAs (**Figure 36C**).

Trp53 is a known tumour suppressor gene whose loss of function increases the proliferation of certain cancer cell lines, so it was not surprising to see that sgRNAs targeting *Trp53* were enriched. However, the fact that over half of the reads in the p38α KO cells belong to these sgRNAs complicates the interpretation of the underrepresented sgRNAs. As *Trp53* KO cells were likely proliferating faster than the rest of the cells in the p38α KO pool, it is possible that over the two weeks of passaging the sample was biased, as we kept enriching for the sgRNAs targeting these genes while losing other less fit cells, which proliferate slower than the *Trp53* KO cells, without being necessarily detrimental to the viability of p38α KO cells. The observed

decrease in the counts of non-targeting sgRNAs goes in line with this idea as these guides should have a neutral effect on cell proliferation, yet their levels are decreased in the p38α KO sample (shown in **Figure 36A**).

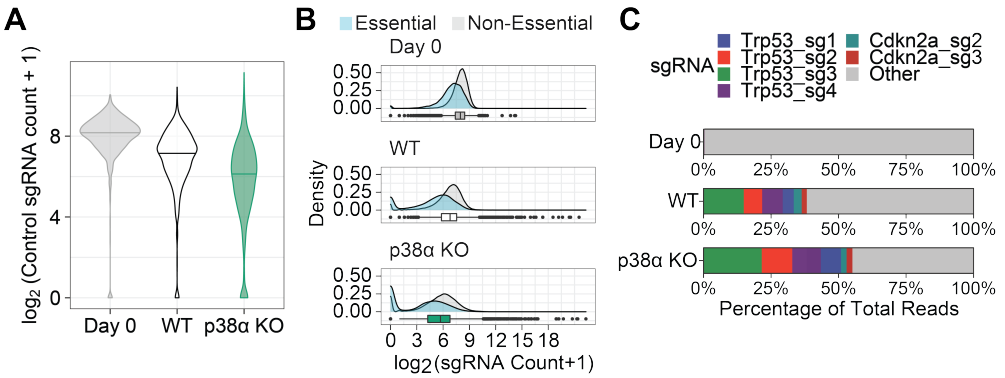

Figure 36. sgRNAs targeting Trp53 and Cdkn2a are overrepresented in the samples of Day 14. (A) Decreased levels of non-targeting control sgRNAs detected in the p38α KO sample. Plot shows distribution of log2 transformed raw counts of control sgRNAs with pseudo count 1 detected in each sample. **(B)** Skewed distribution of targeting sgRNAs in the p38α KO sample. Density plots show the distribution of sgRNAs targeting essential genes (blue) based on mouse orthologs of genes defined as essential in Dempster et al., 2021. **(C)** The sgRNAs targeting Trp53 represent half of the detected reads in the p38α KO sample. The plot shows the percentage of total reads belonging to sgRNAs indicated in the plot legend.

Analysis of samples at earlier time point avoids the p53 bias

Throughout the CRISPR screen we collected additional samples at different time points, and hypothesised that analysing the samples collected at Day 7 might mitigate the massive enrichment of *Trp53* and *Cdkn2a* targeting sgRNAs observed at Day 14, and perhaps allow us to identify hits specifically depleted in p38α KO cells with a higher confidence.

We extracted the DNA from WT and p38α KO cells collected at Day 7 and then sequenced the PCR amplified sgRNAs. For technical reasons, the machine used for sequencing the initial samples was not available, hence we included the same Day 0 library that was previously sequenced with the Day 14 samples, in order to account for any technical differences. We mapped the reads obtained with the MAGeCK algorithm (Li et al., 2014; Wang et al., 2019), reanalysing the previously obtained Day 14 reads in parallel to be able to directly compare them.

In Day 7 analysis, we obtained a much higher number of total reads and over 80% of the reads were successfully mapped to an sgRNA, compared to around 60% of mapped reads in the Day 14 samples (**Figure 37A**). Moreover, the Gini index as well as the percentage of non-detected sgRNAs was substantially lower in the Day 7 samples, while the replicate of the Day 0 sample looked consistent with the previous sequencing batch (**Figure 37B,C**).

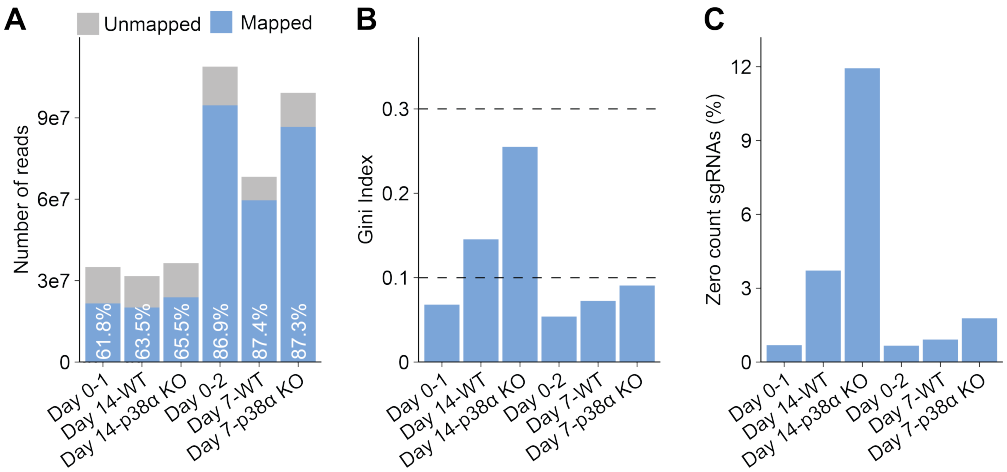

Figure 37. Quality control of Day 7 sample sequencing. (A) Higher percentage of reads and mapped sequences detected in Day 7 samples. Bar plots show the total number of reads (grey) and the percentage of mapped reads (blue) obtained for the indicated samples. Day 0-2 sample is a technical replicate of Day 0-1 previously sequenced together with the Day 14 samples. **(B)** Day 7 samples show lower sgRNA distribution unevenness. Bar plot shows the Gini index for the indicated samples. **(C)** Decreased number of sgRNAs with zero reads detected in the Day 7 samples. Bar plot shows the percentage of all the sgRNAs present in the library not detected (zero counts) for the indicated samples.

We first looked again at the distribution of raw counts of non-targeting sgRNAs. This time we could see that the control sgRNA counts were relatively uniform across Day 0 and Day 7 WT and p38α KO samples, with a slight drop of the counts in the WT sample which corresponds to a lower number of total reads obtained (**Figure 38A**). The distribution of targeting sgRNAs showed a clear peak for counts of sgRNAs targeting non-essential genes, and a higher median read count (**Figure 38B**). In the same line, the percentage of total reads corresponding to *Trp53* or *Cdkn2a* targeting

sgRNAs was much lower compared to the Day 14 samples, although they were still the most enriched sgRNAs (**Figure 38C**).

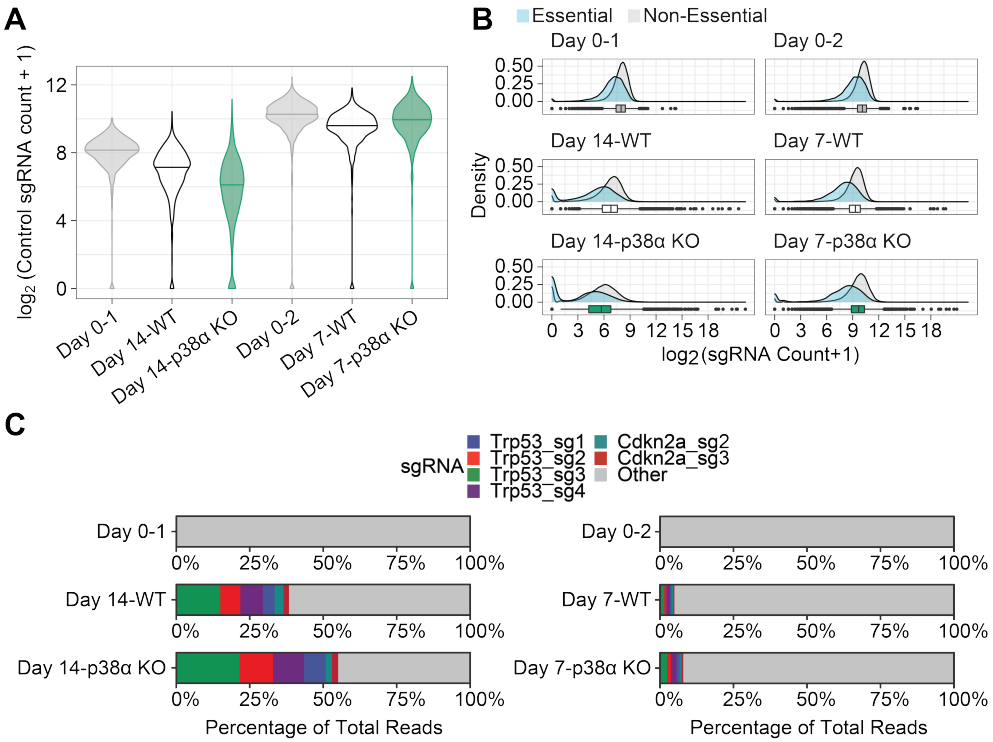

Figure 38. The sgRNA count distribution in Day 7 samples. (A) Day 7 samples show more uniform control sgRNA count distribution. Plot shows the log_2 transformed raw counts of non-targeting sgRNAs with pseudo count 1. **(B)** More regular distribution of sgRNAs targeting non-essential genes in day 7 samples in comparison to the Day 14 samples. Density of log_2 transformed raw counts of sgRNAs targeting essential (blue), mouse orthologs of genes defined in Dempster et al., 2021, or non-essential (grey) shows clear peaks in the Day 7 samples for the non-essential targets. Boxplots show the counts of all targeting sgRNAs for the indicated samples. **(C)** The percentage of total reads belonging to Trp53 and Cdkn2a sgRNAs is decreased in the Day 7 samples. Plot shows Trp53 and Cdkn2a targeting sgRNAs enriched in all of the indicated samples as a percentage of the total reads.

To compare the distribution of the reads across all the samples, we obtained normalised counts using MAGeCK algorithm specifying control non-targeting sgRNAs as normalisation method. This approach resulted in relatively even distribution of the control sgRNAs across samples (**Figure 39A**). Principal component analysis (PCA) of the normalised counts showed high proximity of the two Day 0 samples, indicating low technical variability between the two sequencing batches. A separation between WT and p38α KO samples was observed at both time points. Of note, the majority of the variation stems from the Day 14 p38α KO sample (**Figure 39B**).

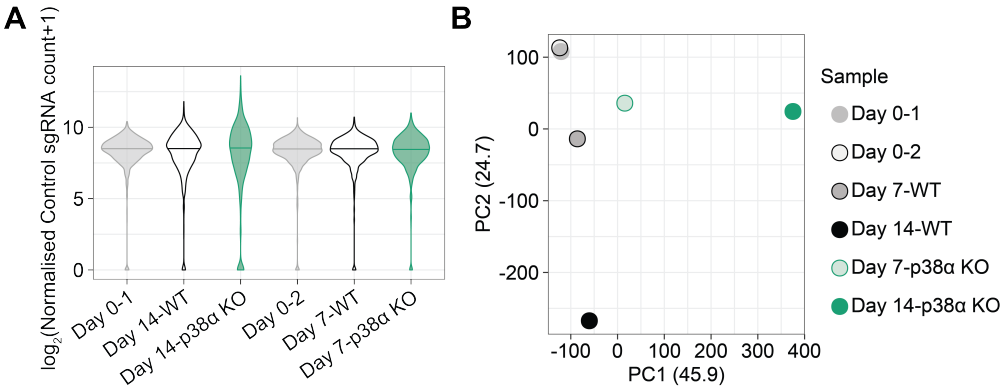

Figure 39. High variability between WT and p38α KO samples. (A) MAGeCK normalisation to control sgRNAs. Plot shows distribution of control non-targeting sgRNAs after performing raw counts normalisation to control sgRNAs. **(B)** Principal component analysis shows low variability between Day 0 samples. PC plots of $\log_2$ counts of the indicated samples normalised to control sgRNAs.

Next, we calculated $\log_2$FC comparing WT to Day 0, p38α KO to Day 0 and p38α KO to WT samples and applied custom group categorisation based on the target phenotype. We first filtered out the sgRNAs with raw count lower than 50 in either of the Day 0 samples, and considered only targets with all 4 sgRNAs detected for further analysis. Next, we calculated average $\log_2$FC across the 4 sgRNAs comparing WT to Day 0, KO to Day 0 and KO to WT samples and applied custom group categorisation based on the target phenotype. For assessing the number of sgRNAs that follow the same trend as the gene level analysis, we defined every individual sgRNA with $\log_2$FC higher than 1 or lower than -1 as enriched or depleted respectively. Every target with 2 or more sgRNAs out of four with the same trend as the gene level analysis and $\log_2$FC lower than -1.5 or higher than 1.5 was considered as depleted or enriched, respectively.

This analysis showed a much lower number of targets enriched or depleted in the p38α KO cells at Day 7, compared to the Day 14 samples (**Figure 40A,B**). Interestingly, the only target enriched that met the thresholds we have established in the Day 7 p38α KO sample was Zcchc14. Gene set enrichment analysis of all targets enriched or depleted in the p38α KO sample showed processes related to RNA polymerase II, mRNA splicing and DNA replication as significantly enriched terms in targets whose loss is

expected to impair the viability of p38α KO cells in both Day 7 and Day 14 samples (**Figure 40C,D**).

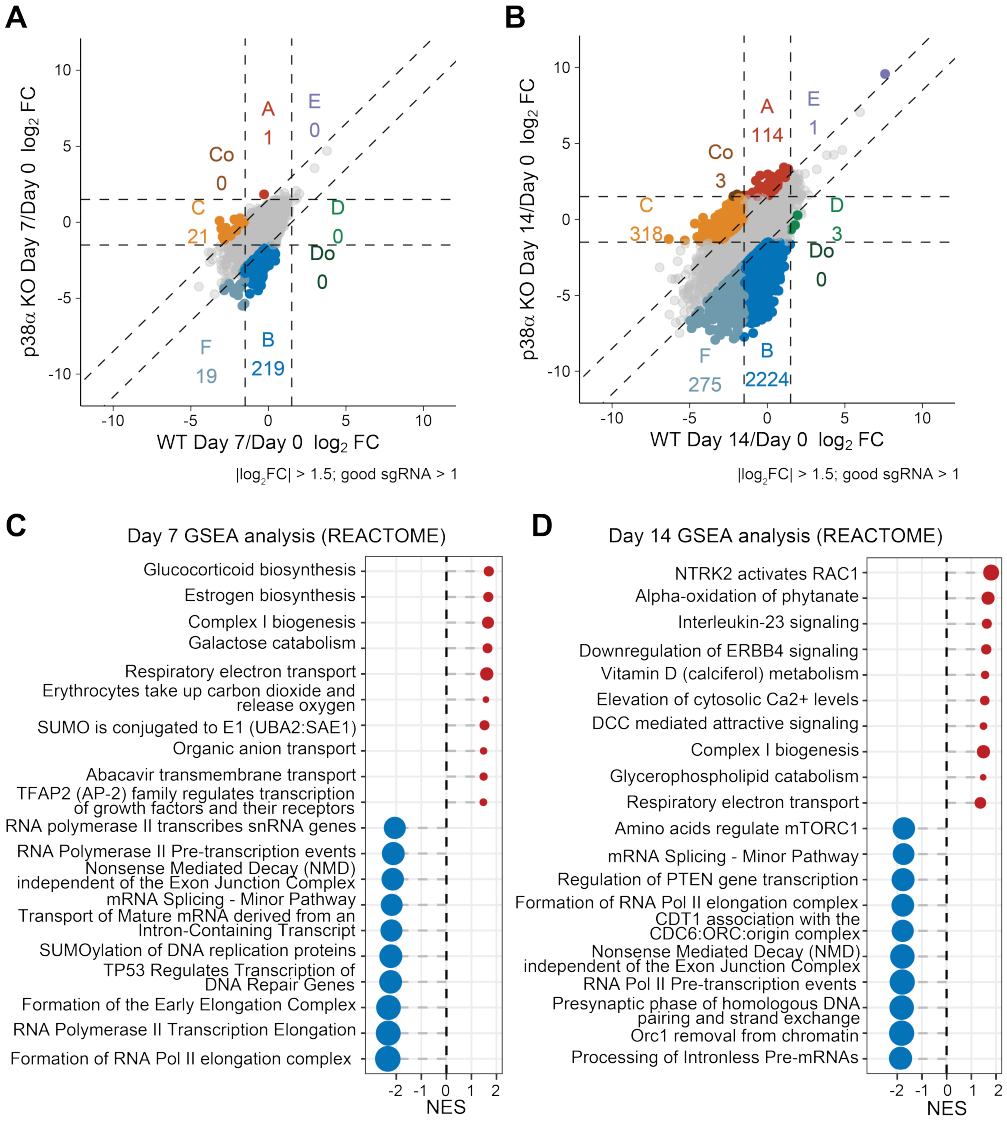

Figure 40. Analysis Day 7 samples and comparison with Day 14 samples. (A, B) Scatter plot of Day 7 **(A)** and Day 14 **(B)** analysis of sgRNAs detected as enriched (groups A and C) or depleted (groups B and F) in the p38α KO cells compared to the WT cells. Threshold of absolute log_2FC higher than 1.5 was used to define target as enriched or depleted. Only targets with 2 or more sgRNAs with the same trend were taken into account. **(C, D)** GSEA analysis of differentially enriched targets in the samples of Day 7 **(C)** and Day 14 **(D)**. Plots show the top 10 terms enriched in overrepresented targets (shown in red) or in depleted targets (shown in blue). The x axis indicates the normalised enrichment score (NES). Analysis was done with all genes ranked based on p38α KO/WT log_2FC. Only terms with p-value < 0.05 were taken into account.

To define a list of targets most likely to be essential only in the p38α KO cells, we compared the hits categorized as group B (genes whose depletion is detrimental in the p38α KO cells but not in WT cells) in either Day 7 or Day 14 samples to select targets that were consistently depleted at both time points (**Figure 41A**). This analysis retrieved 72 genes that were categorised as Group B in both Day 7 and Day 14 samples (**Appendix Table 2**), and the GSEA of these genes identified DNA repair, Cell cycle and rRNA modifications in the nucleus as processes whose impairment is expected to synergise with the loss of p38α (**Figure 41B**). On the other hand, we also identified 47 genes that were categorised as group B in the Day 7 sample and group F in the Day 14 sample. These genes were related mainly to protein translation processes, suggesting that loss of p38α accelerates the deleterious effect of impairing protein translation (**Figure 41C**). In summary, this analysis provides a new list of putative targets whose downregulation should synergise with loss of p38α in an acute manner. Further experiments will be performed to confirm these observations.

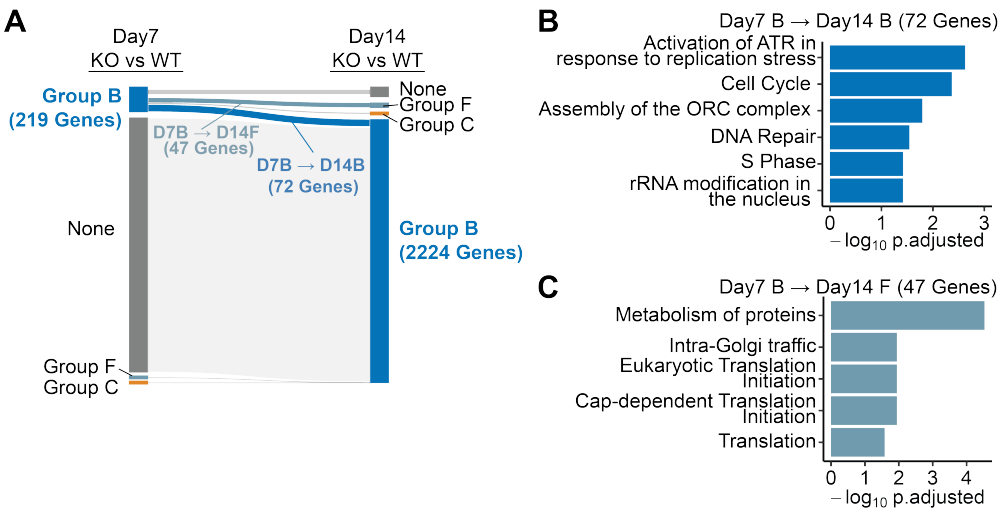

Figure 41. Comparison of the hits depleted in Day 7 and Day 14 samples. (A) Overlap between targets detected as depleted in Day 7 (left) and Day 14 (right) samples. Around 50% of the genes categorised as group B at Day 7 are also depleted in the Day 14 sample, either in the group B (72 genes) or in the group F (47 genes). The majority of the Day 14 genes categorised as group B are not depleted in the Day 7 samples based on this analysis. **(B)** Gene set enrichment analysis of 72 genes detected as group B in both Day 7 and Day 14 samples. List of genes was queried using Enrichr platform (Xie et al., 2021) and the Reactome database. **(C)** Gene set enrichment analysis of 42 genes detected as group B in Day 7 and group F in the Day 14 samples. List of genes was queried using Enrichr platform and the Reactome database.

Exploring p38α dependency by mining the public datasets

Our analysis of the CRISPR screen resulted in several interesting observations, but it remains unclear whether they can be extrapolated to other systems. In an effort to establish additional models of cancer cell dependency on p38α, we took advantage of the publicly available datasets describing diverse molecular characteristics of cancer cells.

Identifying cancer cell lines dependent on p38α

The recent rise of publicly available data aiming to establish cancer cell dependency maps, such as Project score (Sanger) and DepMap (Broad) represents an abundant source of information that could be beneficial for exploring the differences of a wide range of cancer cell line models. We decided to focus on datasets available in the DepMap database.

First, we wanted to identify additional cancer cell lines dependent on p38α. To this end, we used the Chronos Gene effect and Chronos Dependency Probability datasets, which provide a comprehensive analysis of the effect of targeting individual genes across 1086 different cancer cell lines based on genome-wide CRISPR/Cas9 screens. To find potential p38α dependent cancer cells, we selected all the cell lines that had a *MAPK14* Dependency probability (probability that a gene of interest is essential in a given cancer cell line) higher than 0.5, a threshold suggested by the DepMap consortium (Dempster et al., 2021). This approach identified 75 cancer cell lines, in which loss of p38α should impair viability (*Mapk14* Dep) (**Figure 42A, Appendix Table 3**). Examining the primary disease origin of these cell lines suggests that no particular cancer type is abundant in *MAPK14* Dep cell lines (**Figure 42B**). The same was observed when looking at the primary or metastatic origin of the analysed cell lines (**Figure 42C**).

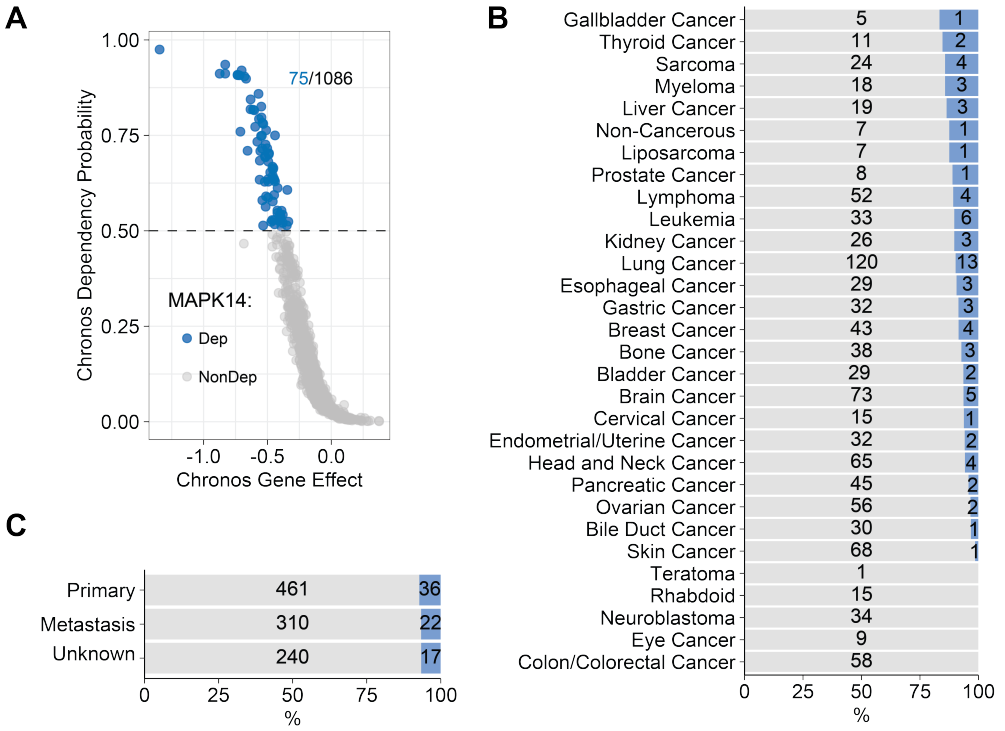

Figure 42. Identification of human cancer cell lines that are dependent on p38α. **(A)** Mining the DepMap dataset identifies 75 cancer cell lines predicted to be dependent on p38α. Plot shows the effect of p38α (*MAPK14*) depletion based on the CRISPR screens performed in 1086 different established cancer cell lines, with negative values indicating negative effect on cell viability (x axis, Chronos Gene Effect) and y axis indicating dependency probability (Dempster et al., 2021). All cell lines with dependency probability higher than 0.5 were selected as dependent. **(B)** No particular cancer type is enriched in p38α dependent cancer cell lines. The bar plot show the percentage (x axis) of p38α dependent cell lines for each of the indicated primary diseases (y axis). Absolute number of cell lines in each category is indicated in the bars. **(C)** No difference in p38α dependent cell lines based on the metastatic or primary tumour origin of the cancer cell lines. The bar plots show the percentage (x axis) of p38α dependent cell lines among models originating from primary, metastatic or unknown sites (y axis). The absolute number of cell lines in each category is indicated in the bars.

Before proceeding with further analysis of the datasets available, we decided to test if the proliferation of cell lines predicted to be dependent on p38α was affected upon p38α inhibition. From the list of 75 *MAPK14* Dep cell lines (**Figure 43A**), we selected two cell lines that were available in the lab, the pancreatic cancer cell line MIA PaCa-2 and the T cell lymphoblastic lymphoma cell line SUP-T1. Cell viability measured with an MTT assay showed decreased viability of both tested cell lines after 72 h of p38α inhibition (**Figure 43B,C**).

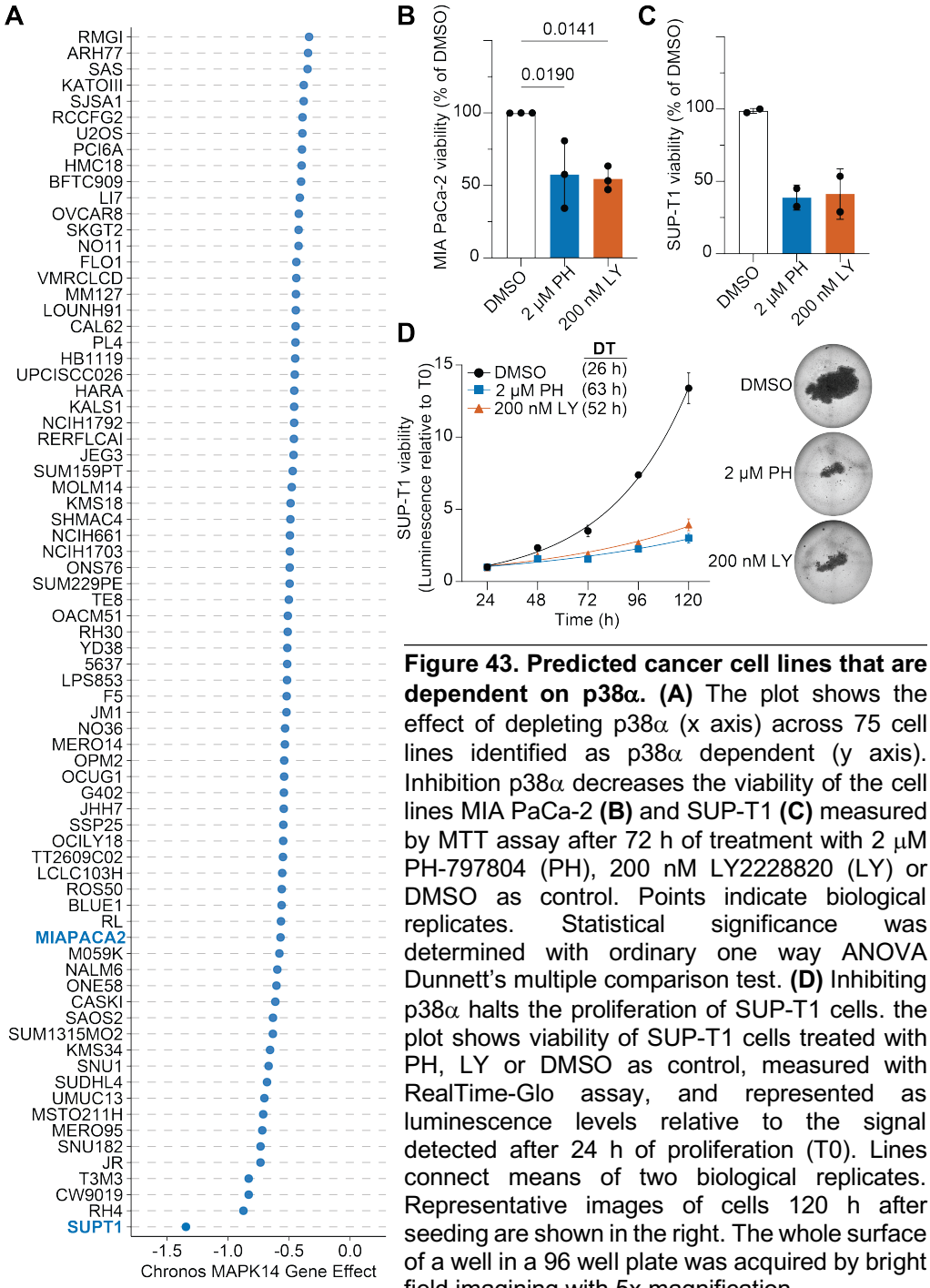

Figure 43. Predicted cancer cell lines that are dependent on p38α. (A) The plot shows the effect of depleting p38α (x axis) across 75 cell lines identified as p38α dependent (y axis). Inhibition p38α decreases the viability of the cell lines MIA PaCa-2 **(B)** and SUP-T1 **(C)** measured by MTT assay after 72 h of treatment with 2 μM PH-797804 (PH), 200 nM LY2228820 (LY) or DMSO as control. Points indicate biological replicates. Statistical significance was determined with ordinary one way ANOVA Dunnett's multiple comparison test. **(D)** Inhibiting p38α halts the proliferation of SUP-T1 cells. the plot shows viability of SUP-T1 cells treated with PH, LY or DMSO as control, measured with RealTime-Glo assay, and represented as luminescence levels relative to the signal detected after 24 h of proliferation (T0). Lines connect means of two biological replicates. Representative images of cells 120 h after seeding are shown in the right. The whole surface of a well in a 96 well plate was acquired by bright field imagining with 5x magnification.

As SUP-T1 was the top *MAPK14* Dep cell line based on the analysis, we performed an additional experiment tracking the viability of the cells treated with p38α inhibitors over time using the RealTime-Glo assay. This approach showed an almost complete halt in the viability of p38α inhibited cells over 5 days, which could also be observed by bright field microscopy (**Figure 43D**). Motivated by the experimental validation of our *in silico* analysis, we decided to take a deeper look in the datasets available.

We first asked if the *MAPK14* Dep cell lines have common CRISPR dependencies, as perhaps there is a specific set of genes whose loss is more deleterious in p38α dependent cells. To achieve this, we looked at the correlation between Chronos Gene effect scores of *MAPK14* and Chronos Gene Effect scores of all the other genes in the dataset across the 1086 cancer cell lines (**Appendix Table 4**). Interestingly, this analysis retrieved MEKK4 (*MAP3K4*) and MKK3 (*MAP2K3*) as two targets whose dependency had the highest correlation with p38α dependency (**Figure 44A**). To understand if the same cell lines are dependent on both proteins, we plotted the correlation of MEKK4 and MKK3 effects and observed a positive

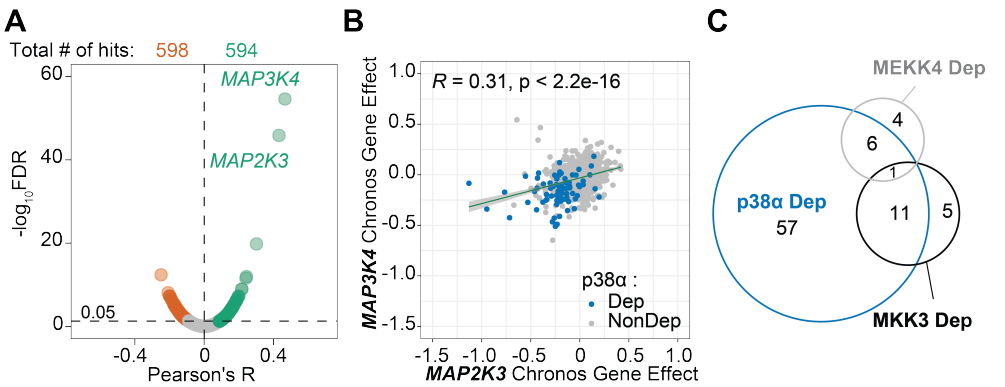

Figure 44. *MAP3K4* and *MAP2K3* are common co-dependencies of the p38α dependent cancer cell lines. (A) Plot showing correlation analysis of p38α (*MAPK14*) Chronos Gene effect and all other genes with available data in Chronos gene effect dataset. Pearson correlation was computed across all gene pairs and p values adjusted with Benjamini & Hohcberg. Y axis shows -log$_{10}$FDR. Genes selected as significantly correlated had p-adjusted value lower than 0.05 and correlation coefficient higher than 0.1 (green dots, positive correlation) or lower than -0.1 (orange dots). The two top correlated targets (*MAP3K4* and *MAP2K3*) are indicated in the plot. **(B)** Correlation between *MAP2K3* gene effect (x axis) and *MAP3K4* gene effect (y axis). Blue dots indicate p38α Dep cells. **(C)** Overlap between MEKK4 (*MAP3K4*), MKK3 (*MAP2K3)* and p38α (*MAPK14*) dependent cell lines. Cell lines were categorised as dependent based on the Chronos probability higher than 0.5 for the indicated genes.

correlation, although their effect was more modest compared to the loss of p38α (**Figure 44B**).

Overlapping cell lines predicted to be dependent on each of these kinases based on the Chronos dependency probability (threshold 0.5) showed that the majority of MEKK4 and MKK3 dependent cell lines were also dependent on p38α, while only one cell line was dependent on all three kinases (**Figure 44C**). This suggests that the context of cancer cell dependency on p38α differs between cell lines also dependent on MEKK4 or MKK3. Furthermore, the predicted deleterious effect of targeting MKK3, but not MEKK4, in our BBL358 CRISPR/Cas9 screen (**Figure 29**) would support this.

As p38α is the most ubiquitously expressed p38 MAPK family member, we next looked at the mRNA levels of the four p38 MAPKs across all the cancer cell lines with available expression data. As expected, p38α (*MAPK14*) was expressed robustly across all the queried cell lines. Interestingly, we could observe a bimodal distribution of p38δ (*MAPK13*), with a clear distinction of cell lines expressing low or high levels of this family member (**Figure 45A**). We next classified the cell lines into *MAPK14* Dep and NonDep (non-dependent) groups and looked for differences in the p38 MAPK expression across these groups. To our surprise, we could observe that the majority of the *MAPK14* Dep cells expressed lower levels of p38δ (*MAPK13*), and a similar trend was observed for p38β (*MAPK11*) (**Figure 45B**).

The observed negative effect of the p38α inhibitors on the proliferation of the cell lines predicted to be dependent on this kinase looks promising. Furthermore, the CRISPR screen that we have performed in the isogenic WT and p38α KO cells provides us with a unique set of targets that might functionally interplay with p38α activity. However, it seems that understanding what drives p38α dependency is not straightforward. It is possible that a number of distinct mechanisms render cancer cell sensitive to the downregulation of this kinase. Altogether, this analysis provides us with a new approach to further investigate the contexts of cancer cell dependency on p38α MAPK.

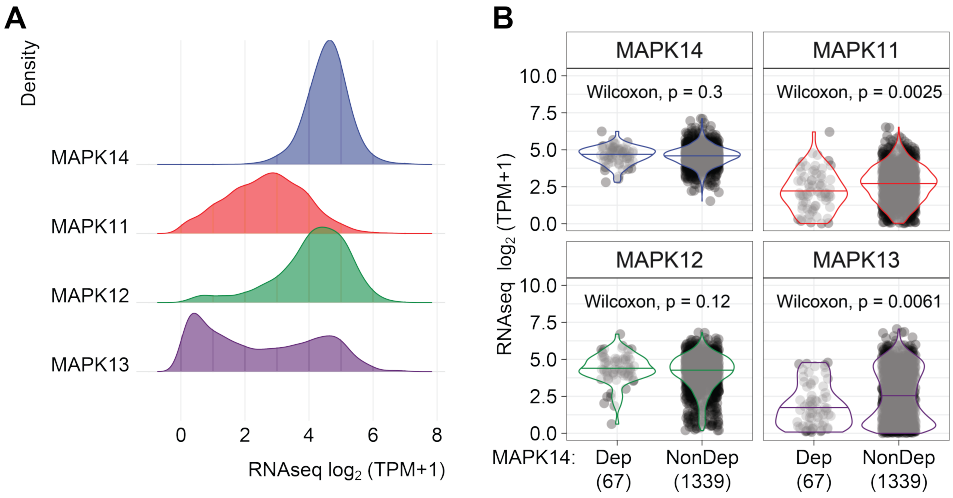

Figure 45. Landscape of mRNA expression patterns of the different p38 MAPK family members across cancer cell lines. (A) The plot shows the distribution of mRNA levels for p38α (*MAPK14*), p38β (*MAPK11*), p38γ (*MAPK12*), and p38δ (*MAPK13*) across 1406 cancer cell lines with available data in the CCLE expression dataset. **(B)** Comparison of the expression levels of different p38 MAPK family members in p38α dependent (Dep) and non-dependent (NonDep) cancer cell lines. The mRNA levels are shown as $\log_2$ transformed transcript per million (TPM) counts with pseudocount 1.

Discussion

In an effort to better understand the context of cancer cell dependency on p38α MAPK and to identify potential synergisms between this pathway and others, we have taken advantage of the genome-wide CRISPR/Cas9 screening technology. This allowed us to investigate the role of p38α in cancer cells in an unbiased manner. As the model, we selected a breast cancer cell line that is known to show reduced viability upon p38α downregulation. This approach allowed us to identify potential mediators of the p38α depletion effects in our model, and we found that targeting the RNA binding protein Zcchc14 or p38δ rescues the viability of p38α KO cells, making them interesting targets for follow-up studies. We have also identified targets that further sensitize the cancer cells to loss of p38α, and showed that interfering with mTOR signalling or mitochondrial translation enhances the deleterious effect of p38α downregulation. Finally, we have leveraged the use of publicly available datasets for the identification of additional cancer cell lines that are dependent on p38α signalling, as well as further exploring their molecular characteristics.

We have identified Zcchc14 as the top target for sgRNAs that are enriched in the p38α KO cells. We confirmed that downregulating Zcchc14 rescues the decreased p38α KO cell viability to the levels close to the control WT cells. The human homologue of Zcchc14 has been identified in two recent genome-wide CRISPR screens as an important host factor during viral infection (Hyrina et al., 2019; Kulsuptrakul et al., 2021). ZCCHC14 can bind to the stem loop of the viral RNA and recruits noncanonical poly(A) polymerases Papd7 and Papd5 (TENT4A and TENT4B), which are capable of incorporating non-Adenine residues, mainly Guanosine, in a process called mixed tailing. For instance, it has been reported that the addition of G to the poly(A) tail leads to increased mRNA stability as it prevents deadenylation by the CCR4-NOT complex (Lim et al., 2018). This is especially interesting in the case of hepatitis B virus and human cytomegalovirus, where the ZCCHC14-TENT4A/B complex is responsible for stabilising viral mRNA precisely through mixed tailing (Kim et al., 2020). However, in the case of hepatitis A, it seems that this complex has a polyadenylation independent role, and can instead modulate directly the translation of viral mRNAs

(Kulsuptrakul et al., 2021), which goes in line with a study in *Caenorhabditis elegans* where loss of gls-1, a ZCCHC14 homologue, leads to decreased polysome formation without impacting poly(A) tail length (Nousch et al., 2014). As very little is known overall on the interactome of Zcchc14, it will be interesting to discern whether its downregulating in our system impacts protein translation or perhaps modulates the poly(A) tail length and composition. It is worth mentioning that a recent study reports that CRISPR/Cas9 downregulation of ZCCHC14 boosts the proliferation of the human non-small cell lung cancer cell lines A549 and H1299, and that this increased proliferation is prevented by treating the cells with the general p38 MAPK inhibitor BIRB769 (Shi et al., 2021). This study suggests that in the absence of ZCCHC14, p38 MAPK signalling might enhance the proliferation of the cancer cells, which is not consistent with the phenotype that we have observed in our model using CRISPR/Cas9 mediated Zcchc14 depletion. One possibility could be that the cell lines used in that study have a completely different molecular milieu compared to our cell line. However, the link to the p38 MAPK pathway was explored using only the BIRB769 inhibitor, suggesting the possibility that what drives the increased proliferation in A549 and H1299 cells is not p38α, but a different p38 family member. Overall, there seems to be an unexpected functional link between p38α and the understudied RNA binding protein Zcchc14, making it an interesting candidate to explore further.

Surprisingly, we have also identified p38δ as a potential mediator of the reduced viability induced upon p38α depletion, as loss of p38δ rendered the cancer cells less sensitive to p38α downregulation. It is tempting to speculate that p38α negatively regulates p38δ, and that the absence of p38α leads to p38δ activation, which in turn mediates some of the detrimental effects of p38α loss. The increase of the p38δ mRNA levels upon p38α downregulation would go in line with this idea, however we have not observed a clear difference in total p38δ protein levels between the WT and p38α KO cells. Negative regulation of p38δ by p38α has been previously reported in the adipose tissue (Matesanz et al., 2018), and it will be important to understand how this is occurring in breast cancer model. So far, we have not observed any effect of p38γ downregulation in the viability of p38α KO

cells, which is somewhat unexpected since p38γ and p38δ are often described to perform similar functions (Cuenda & Sanz-Ezquerro, 2017). As we have not confirmed that sgRNAs targeting p38γ lead to a reduction of the p38γ levels in the experiments performed, we cannot exclude the possibility that that the lack of phenotype is due to the inefficiency of the sgRNA used. Altogether, it will be interesting to explore if this interplay also occurs in other cancer models, perhaps being something common to the p38α dependent cancer cell lines, as well as to understand the extent to which p38δ activity could be generally toxic for the cancer cells or if it depends on the absence of p38α.

Regarding targets that sensitize the cancer cells to p38α downregulation, we have observed that mTOR inhibition potentiates the cytostatic effect of p38α inhibition. The results suggest that our breast cancer model is probably sensitive to both mTORC1 and mTORC2 disruption, and that targeting either of these two complexes increases the effect of p38α depletion or inhibition. This suggests that perhaps a specific branch downstream of mTOR signalling and not a particular complex interacts with p38α signalling. The interplay of the p38α and mTOR pathways is poorly understood. The mTOR pathway is an important regulator of metabolic processes that can also control cell growth, protein translation and autophagy among others (Liu & Sabatini, 2020). The first report of p38α mediated activation of mTOR was described in *Drosophila Melanogaster*, where p38 activating stresses led to mTORC1 activation (Cully et al., 2010). This study was followed by a similar observation in murine cardiomyocytes, MEFs and human cancer cell lines where p38α mediated mTOR activation in response to oxidative stress (Hernández et al., 2011). The MK2 protein kinase, a substrate of p38α, seems to be a potential convergence node of these two pathways, as it has been reported that mTOR regulates translation of the MK2 mRNA through 4EBP-1 in fibroblasts undergoing oncogene-induced senescence (Herranz et al., 2015). In this model, the inhibition of mTOR consistently decreased the MK2 protein levels without affecting p38α. Taking this into account, it is tempting to speculate that mTOR inhibition shifts the output of p38α activation by limiting the availability of the MK2 protein, a target and interactor of p38α that is known to mediate many p38α functions such as inflammation, post-

transcriptional regulation, or actin filament remodelling (Ronkina & Gaestel, 2022).

On the other side, there are several studies describing the interaction of the mTOR pathway with other p38 MAPK family members. In cardiomyocytes, hyperactivation of p38γ and p38δ leads to cardiac hypertrophy by targeting DEPTOR, a negative regulator of mTOR, for degradation, thus resulting in mTOR pathway activation (González-Terán et al., 2016). More recently, the loss of MKK6 has been shown to increase the activation of the MKK3-p38γ/δ axis resulting in increased mTOR activity and protein translation levels (Romero-Becerra et al., 2022). In response to amino acids, p38δ can phosphorylate p62 through the binding of the MKK3 and p62 PB1 domains. This in turn facilitates the ubiquitination and activation of mTOR, leading to cell growth and proliferation (Linares et al., 2015). However, the implications of the crosstalk between these two major signalling pathways remain to be understood. Our results suggest that disruption of either mTORC1 or mTORC2 complexes is detrimental for the cancer cell viability. Hence, further experiments should focus on particular branches of the mTOR pathway to further dissect this interplay, for instance by targeting the mTORC2 downstream kinase SGK1.

We have also obtained promising preliminary data showing that mitochondrial translation inhibition potentiates the effect of p38α inhibition. Curiously, similar to p38α, the importance of mitochondrial translation for cancer cell survival seems to be context dependent (Hart et al., 2015). In the last years, it has become clear that some cancer cells increase the activity of the mitochondrial translation machinery in order to meet their energetic needs, making mitochondrial translation a promising target for cancer treatment (Criscuolo et al., 2021). While some reports indicate a potential role for p38α in mitochondrial biogenesis (Ning et al., 2019; Zhang et al., 2017), to our knowledge there are no reports directly implicating p38α in the regulation of mitochondrial translation. It will be important to test if p38α downregulation affects this process. In addition, it will be interesting to assess the effect of combined p38α downregulation and treatment with compounds described to impair mitochondrial translation, such as tigecycline

or doxycycline. Nonetheless, even if p38α does not directly regulate this process, it seems to have an important role in supporting the cancer cell viability when mitochondrial translation is impaired

The validation of sgRNAs exclusively downregulated in the p38α KO cells, and whose targets are expected to cooperate with p38α to maintain cancer cell viability was somewhat disappointing. Unexpectedly, downregulation of the targets analysed also had a substantial negative effect on the viability of WT cells. This could be due to the different timings of the validation experiments and the CRISPR screen. It is also possible that depleting these hits or impairing the corresponding processes is detrimental to WT cell viability, but for unforeseen reasons, such as the effect of the surrounding clones or the potential adaptation of the cells, we were not able to detect this effect in the Day 14 samples. An interesting possibility is that the WT cells are able to recover from the loss of these genes upon several additional passages, but this adaptation is prevented upon p38α downregulation. If this were the case, analysis of the Day 14 samples could be providing us with targets that when depleted require p38α to circumvent their loss of function.

Of note, the Day 14 samples undergo 10 days of antibiotic selection and 2 more weeks of passaging. At the time of setting up the experiment, most of the studies published applied longer antibiotic selection periods in order to wean out the sgRNAs that target essential genes. This is supported by a clear separation of distributions of sgRNAs targeting essential and non-essential genes in our Day 0 sample. Many of the screens reported were also analysed after 2 weeks of passaging. Furthermore, the integrated analysis of several screens performed at the Broad and the Sanger institutes suggested that differences in the length of the CRISPR screen are not a major source of discrepancies for the data acquired (Dempster et al., 2019; Pacini et al., 2021). Nevertheless, the particularly high proliferation rate of the cell line that we used could be a potential source of bias. The doubling time of our cell line is approximately 14 h, hence at Day 14 of the CRISPR screen, these cells have undergone around 40 cell doublings since the introduction of the CRISPR library. This could explain the massive enrichment of *Trp53* and *Cdkn2a* targeting sgRNAs at Day 14 in both WT and p38α KO samples.

Importantly, these sgRNAs were also the ones with the highest counts in the Day 0 sample, however they cumulatively represented less than 1% of the total reads, thus not affecting the overall sgRNA distribution of the whole library. At Day 14, over half of the reads in the p38α KO cells belong to these overrepresented sgRNAs. Having this in mind, it is likely that many of the sgRNAs that were depleted in the p38α KO cells might be lost due to the lower proliferative fitness compared to the p53 KO pool of cells, and not due to the potentiation of the p38α KO effect. The higher overrepresentation of the p53 targeting sgRNAs in the p38α KO cells would suggest that deleting p53 can partially overcome the effect of the p38α downregulation. However, another possibility is that the effect of p53 disruption is similar in both p38α KO and WT cells, but due to the lower overall proliferation upon p38α deletion, the relative increase in the proliferation of p53 KO cells is more pronounced. Testing the effect of p38α downregulation in WT and p53 KO cells should clarify this point. An unforeseen benefit of this massive overrepresentation of a few sgRNAs is that the analysis of the Day 14 samples is very robust for detecting enriched targets, as these cells had to match the increased proliferation of p53 KO pools in order to persist within the whole population. On the other hand, the conditions should be optimised in order to identify with higher confidence targets that synergise with p38α downregulation. To circumvent this problem, we took advantage of the samples collected at an earlier time point, Day 7 of the screen.

Surprisingly, the new round of sequencing retrieved a much higher number of mapped reads. The most intuitive reason would be differences in the processing of the samples as DNA extraction and sgRNA amplification were performed independently. However the analysis of the Day 0 sample library previously sequenced in the first run also retrieved a much higher percentage of mapped reads, suggesting that this is not the case. Another explanation could be the increased accuracy of the reads obtained due to the higher sequence diversity in the earlier time point samples. During standard Illumina sequencing, only the first four positions in the reads are used to distinguish different clusters on the flowcell (a channel for adsorbing mobile DNA fragments), which is a key step in the sequencing analysis. Therefore, low sequence diversity results in higher error rate of the read sequences obtained

(Mitra et al., 2015). As the majority of the reads in the Day 14 samples were coming from the *Trp53* and *Cdkn2a* targeting sgRNAs, this could be the source of technical difficulties resulting in a large number of erroneously sequenced reads. Based on the analysis of the Day 7 samples, we have retrieved a list of common targets depleted at both time points, providing us with a more accurate list of genes that should have a deleterious effect in the p38α KO cells.

One of the main technical pitfalls of our study is the lack of confirmation of the target downregulation at the protein level upon CRISPR/Cas9 mediated deletion. Moreover, we have avoided the use of single cell clones to generate the target KO cells. While single cell clones facilitate the detection of target downregulation, they come at a cost of subclonal heterogeneity that we wanted to steer clear of (Kuiken et al., 2022).

Importantly, this entire study has been developed using as a model a cancer cell line strongly dependent on p38α activity, which is not a universal characteristic of cancer cells. Hence, we wanted to find novel models of cancer cell dependency on p38α that would allow us to extend our observations. To this end, we have taken advantage of the publicly available databases and identified a list of cancer cell lines that are predicted to be p38α dependent. We confirmed the detrimental effect of p38α inhibitors on the viability of two putative p38α dependent cancer cell lines, SUP-T1 and MIA PaCA-2, supporting the validity of the analysis performed. Moreover, the upstream activators of p38α MEKK4 (*MAP3K4*) and MKK3 (*MAP2K3*) were detected as common genetic dependencies in some of the p38α dependent cancer cell lines. Curiously, there is little overlap between MEKK4-p38α and MKK3-p38α co-dependent cell lines. The most intuitive possibility is that several mechanisms may render cancer cells dependent on p38α signalling, and the general analysis performed in this thesis is not sufficient to discriminate among them. In this line, the CRISPR screen analysis suggests that MKK3 downregulation has a negative effect on the viability of WT cells, which is rescued in the p38α KO cells, while loss of MEKK4 seems to boost their proliferation. It is interesting to speculate that there is a subset of cancer cell lines in which the MKK3-p38α axis is

somewhat deregulated. Another interesting observation is the lower expression of p38β and p38δ mRNAs in the subset of cancer cell lines that depend on p38α, however at the moment this is a descriptive observation, which does not provide us with mechanistic insight. An additional consideration is that publicly available databases such as DepMap are not static, but continuously updated and revised. As an example, the latest release of DepMap at the time of writing this discussion is the 22Q4, in which 80 out of 1078 cancer cell lines are identified as p38α dependent in comparison to the 75/1086 reported in this study. Hence, in the new data release, additional cell lines have been characterised as p38α dependent, and some of the cell lines removed completely from the dataset due to mischaracterisation. While this might seem a nuisance at first glance, because it requires repeating the analysis with every major data update, it is reassuring to know that this data is continuously updated ensuring its high quality and reliability. It will be important to explore all the information available in these databases in more detail, and directly compare it to the molecular characterisation of our p38α dependent BBL358 cancer cell line. Overall, the new models identified, as well as further querying of the available datasets, should help us to further disentangle the molecular cues that underlie the cancer cell line addiction on p38α signalling.

In summary, we have identified Zcchc14 and p38δ as putative mediators of the deleterious effects of p38α KO in cancer cells. We also provide evidence supporting that downregulation of mitochondrial translation or mTOR signalling can potentiate the effect of p38α inhibitors. It remains to be seen to which extent these observations can be extrapolated to other cancer models, and if the increasing molecular characterization of different cancer cell types can provide us with reliable molecular clues to improve our understanding of the cellular context that drives p38α dependency.

Conclusions

- Depletion of the RNA-binding protein Zcchc14 improves the viability of p38α KO cancer cells

- Targeting p38δ enhances the survival of p38α KO cancer cells

- Inhibition of mTOR signalling sensitizes cancer cells to p38α inhibition

- Inhibition of mitochondrial translation further impairs the viability of p38α KO cancer cells

- Database analyses allowes the identification of new p38α-dependent cancer cell models and potential co-dependencies

Appendix

Appendix Table 1 | Top 50 hits at Day 14 based on the DESeq2 Analysis.
DS2 – DESeq2 analysis; sgRNA – number of sgRNAs with the same trend

Symbol	DS2-D14 KO/WT	DS2-D14 sgRNA	D7 WT/Day0	D14 WT/Day0	D7 KO/WT	D7 sgRNA	D14 KO/WT	D14 sgRNA
Zcchc14	5.32	4	-0.28	0.03	2.11	4	2.93	4
Lmx1a	-5.31	4	0.24	0.72	-1.44	2	-5.41	3
Afm	-5.08	4	-0.95	0.04	-0.89	2	-6.38	3
Adcy6	-5.06	4	-0.37	-0.92	-0.56	1	-6.57	4
Hc	-5.01	4	-0.10	0.07	-0.70	1	-5.44	4
Frmd7	4.98	4	0.30	-0.46	0.65	1	3.35	4
Igf2bp2	-4.94	4	-0.88	-0.37	-0.58	1	-6.23	4
Ranbp2	-4.89	4	0.15	0.78	-1.01	2	-3.70	4
Ccnb2	-4.88	4	-0.27	0.01	-1.03	1	-6.42	4
Gbgt1	-4.87	4	-0.10	0.00	-2.05	2	-6.20	3
P2ry1	-4.68	4	-0.33	-0.72	0.03	0	-6.04	4
Adprhl2	4.66	3	0.18	-1.45	-0.27	1	2.94	4
Cuedc2	-4.61	4	0.20	0.33	-1.04	2	-4.46	4
Carm1	-4.60	4	0.27	0.73	-0.89	3	-3.49	3
Zdhhc12	4.58	3	-0.51	-1.85	0.23	1	3.24	3
Skap2	-4.49	4	-0.24	0.27	-0.36	0	-3.82	4
Chat	-4.49	4	0.38	-0.28	-0.38	0	-5.65	3
Dcun1d5	-4.46	3	-0.13	0.15	-0.25	0	-4.89	3
Dus1l	-4.44	4	-0.21	-0.63	-0.29	0	-6.02	3
Mdm1	-4.43	4	-0.35	0.09	-0.87	1	-3.99	3
Gps1	-4.40	4	2.87	3.30	-2.17	1	-7.00	2
1700122O11Rik	4.40	3	-0.34	-1.16	0.19	1	2.42	3
Vmn1r23	-4.39	4	-0.18	-0.20	-0.19	0	-5.87	4
Gpr179	4.35	4	0.16	-0.35	0.42	2	2.43	4
Hps5	-4.35	4	-0.44	-1.02	-0.26	1	-5.82	4
Tacc1	4.33	3	-0.83	-1.17	1.43	2	2.73	4

Symbol	DS2-D14 KO/WT	DS2-D14 sgRNA	D7 WT/Day0	D14 WT/Day0	D7 KO/WT	D7 sgRNA	D14 KO/WT	D14 sgRNA
Il10	-4.33	4	-0.06	0.46	-0.13	0	-3.43	3
Ap2a2	-4.32	4	-0.31	0.00	0.28	1	-5.02	3
Myo3b	-4.28	4	0.44	0.11	-0.37	0	-4.56	3
Defb38	-4.27	4	0.30	0.67	-1.15	1	-3.62	3
Dcp2	-4.27	4	-0.73	-0.61	-0.56	1	-5.71	4
Dram2	-4.26	4	0.01	0.47	-0.43	0	-4.33	3
Usp53	-4.26	4	0.05	0.80	-0.28	1	-3.29	3
Srrd	-4.24	4	-0.84	-0.02	-1.62	1	-5.94	3
A430078G23Rik	4.20	3	-0.26	-2.61	0.48	2	3.55	4
Btbd1	4.20	4	-0.36	-0.57	0.58	1	1.78	3
Topors	4.20	4	0.38	0.26	0.96	2	2.58	4
Sdccag8	-4.20	3	-0.31	0.34	-0.73	1	-4.58	3
Olfr1084	-4.20	4	0.41	0.84	-0.45	0	-5.88	2
Myl6	-4.18	4	0.62	1.78	-0.43	0	-2.16	4
2610028H24Rik	-4.15	4	-0.01	0.52	-0.17	1	-3.78	3
Suv39h1	4.15	3	-0.50	-1.19	0.48	1	2.48	3
Guf1	-4.15	4	0.04	0.22	-0.58	1	-3.63	3
Dhx30	4.14	3	0.00	-1.32	0.60	0	2.61	3
Olfr1465	-4.13	4	-0.57	-0.18	-1.27	2	-4.83	3
Il25	-4.12	4	-0.34	0.28	0.04	1	-3.26	4
Olfr776	-4.12	4	-0.46	-0.05	-2.53	3	-4.38	3
Lrrc24	-4.11	4	-0.38	0.58	-0.18	0	-4.53	3
Mag	-4.11	4	-0.26	0.51	-0.22	0	-5.19	3
Bub3	-4.11	4	0.12	0.50	-0.46	0	-6.83	3

Appendix Table 2 | Overlap between the Day 7 and Day 14 analyses (72 genes)

DS2 – DESeq2 analysis; sgRNA – number of sgRNAs with the same trend

Symbol	DS2-D14 KO/WT	DS2-D14 sgRNA	D7 WT/Day 0	D14 WT/Day 0	D7 KO/WT	D7 sgRNA	D14 KO/WT	D14 sgRNA
Atp6v1c1	-2.50	4	-0.59	-0.06	-3.32	2	-4.23	3
Noc4l	-3.52	4	-0.84	-0.06	-3.17	3	-5.10	4
Mup1	-2.04	3	-0.36	-1.20	-3.12	2	-4.22	3
Smc2	-2.84	3	0.43	-1.34	-2.97	3	-4.20	3
Lce1g	-2.25	3	0.03	-1.02	-2.84	3	-3.09	2
Sympk	-3.27	4	-0.43	0.02	-2.78	4	-4.56	3
Nuf2	-2.11	4	-0.57	-0.19	-2.77	2	-3.40	3
Rhox4f	-1.57	3	0.04	-0.54	-2.72	2	-2.60	2
Cbx5	-1.24	3	-0.37	-0.81	-2.62	2	-2.35	2
Trp53i13	-2.41	3	-0.02	-0.52	-2.61	4	-3.35	2
Chordc1	-1.62	4	-0.94	-1.41	-2.58	2	-4.32	3
Klhdc10	-2.10	4	0.14	-0.28	-2.58	2	-1.99	2
Usf2	-2.83	4	-0.58	0.33	-2.56	3	-4.16	2
Olfr776	-4.12	4	-0.46	-0.05	-2.53	3	-4.38	3
1110008L16Rik	-0.59	3	-0.42	-1.48	-2.52	2	-2.18	2
Atr	-3.50	4	-0.21	0.04	-2.51	2	-2.80	2
Mrpl44	-2.40	4	-0.34	-0.98	-2.43	3	-3.64	2
Tmprss3	-0.69	3	0.41	0.01	-2.42	2	-1.70	2
Pigs	-0.82	3	0.19	-0.07	-2.41	2	-2.89	2
Top2b	-0.69	2	-0.67	-0.97	-2.37	3	-2.47	2
Dido1	-2.02	4	-0.65	-0.81	-2.36	2	-3.50	3
Hsd17b13	-1.41	4	0.11	-0.04	-2.36	2	-1.82	2
Vmn1r119	-1.57	4	-0.16	-0.23	-2.35	2	-2.48	3
Orc2	-2.83	3	-0.78	-1.14	-2.33	3	-2.97	2
Fen1	-2.36	4	-1.11	-0.95	-2.32	3	-4.13	3
Tssc1	-2.03	4	-0.40	-0.70	-2.32	3	-2.36	2

Symbol	DS2-D14 KO/WT	DS2-D14 sgRNA	D7 WT/Day 0	D14 WT/Day 0	D7 KO/WT	D7 sgRNA	D14 KO/WT	D14 sgRNA
Fip1l1	-0.80	3	-0.13	-0.01	-2.28	2	-2.97	2
Sprr2a2	-2.50	4	0.28	0.12	-2.23	2	-2.68	2
Wdr3	-3.03	4	-0.40	-0.92	-2.21	3	-5.04	4
Aars	-3.17	3	-0.51	-1.33	-2.20	3	-4.12	3
Aamp	-2.84	4	-0.90	-0.27	-2.15	3	-3.90	4
Vmn1r148	-3.56	3	-0.07	-0.31	-2.13	2	-4.82	3
Hist1h3f	-2.22	4	-0.70	-0.05	-2.08	2	-2.60	2
Gbgt1	-4.87	4	-0.10	0.00	-2.05	2	-6.20	3
Rab3gap1	-2.31	3	-0.50	-0.44	-2.04	2	-3.45	2
Znhit6	-1.53	3	-0.08	-0.74	-2.02	2	-2.53	2
Gnb1l	-2.91	4	-1.23	-0.54	-2.01	2	-4.76	3
Coq6	-1.01	4	-1.26	-1.25	-1.96	2	-1.97	3
Fabp5	-1.60	3	-0.71	-0.81	-1.95	2	-1.86	2
Zfp942	-2.45	4	-0.36	0.15	-1.95	2	-3.78	2
Atp6v0e	-3.40	4	-0.03	0.05	-1.94	2	-5.11	3
Tceal6	-1.56	4	-0.31	-0.32	-1.94	3	-2.05	3
Caml	-2.41	4	-0.14	-0.04	-1.94	2	-2.26	2
Lsm3	-2.88	4	-0.41	-0.40	-1.94	2	-4.16	3
Nfkb2	-3.87	4	0.06	0.24	-1.88	2	-5.78	3
Mrpl28	-3.24	4	-0.90	-0.79	-1.88	2	-4.07	4
Pdap1	-2.21	4	-0.18	-0.43	-1.88	3	-2.96	3
Vmn1r91	-2.74	4	0.10	-0.40	-1.87	2	-3.27	4
Mnat1	-1.82	4	0.01	-0.93	-1.87	2	-3.00	2
Dctn6	-2.63	4	-1.02	-1.42	-1.85	2	-4.00	3
Orc6	-3.15	3	-0.13	-0.85	-1.85	3	-4.29	3
Olfr490	-2.17	4	-0.34	-0.29	-1.82	2	-2.62	2
Cops2	-2.92	4	-0.68	-0.29	-1.77	2	-5.20	3
Slc33a1	-2.16	4	-0.11	-0.54	-1.76	2	-2.42	3
Snrnp40	-0.72	2	-0.47	-0.35	-1.75	2	-2.67	2

Symbol	DS2-D14 KO/WT	DS2-D14 sgRNA	D7 WT/Day 0	D14 WT/Day 0	D7 KO/WT	D7 sgRNA	D14 KO/WT	D14 sgRNA
Zfp35	-0.67	3	-0.86	-1.40	-1.74	2	-1.84	2
Tead2	-2.27	3	0.19	0.07	-1.74	2	-3.39	3
Smc6	-1.84	4	-0.85	-0.16	-1.72	2	-1.57	3
Srp68	-3.01	3	-0.33	-1.13	-1.70	2	-3.08	2
Skp1a	-2.72	4	-1.16	-0.27	-1.70	2	-5.17	3
Ddx26b	-2.87	4	-0.61	-0.40	-1.69	2	-3.78	3
Nop16	-0.94	4	-0.83	-0.76	-1.63	3	-2.15	2
Olfr825	-1.39	3	-0.28	-0.75	-1.63	3	-2.01	2
Gm15386	-2.15	3	-0.54	-0.37	-1.61	2	-2.42	3
Eed	-0.51	3	-0.55	-1.24	-1.61	2	-2.32	2
Fdps	-3.31	4	-0.76	-1.23	-1.61	2	-5.43	3
Cramp1l	-2.02	4	-0.63	-1.18	-1.60	2	-2.66	3
Jmjd1c	-1.21	2	-1.29	-1.35	-1.58	2	-2.39	2
Nhp2	-1.94	3	-0.65	-0.91	-1.56	2	-3.46	3
Wbp5	-2.82	4	-0.48	-1.01	-1.55	2	-3.63	3
Hus1	-1.77	4	-0.62	-0.91	-1.53	4	-4.06	3
Kpna2	-4.05	4	-0.96	0.03	-1.51	3	-5.67	4

Appendix Table 3 | The p38α dependent cancer cell lines

DepMap ID	Cell Line	MAPK14 Chronos GeneEffect	MAPK14 Chronos Prob	Primary disease	Cellosaurus NCIt_disease
ACH-000953	SUP-T1	-1.35	0.97	Leukemia	Childhood T lymphoblastic lymphoma
ACH-001050	CW9019	-0.83	0.94	Sarcoma	Alveolar rhabdomyosarcoma
ACH-001407	UM-UC-13	-0.70	0.92	Bladder Cancer	Bladder carcinoma
ACH-002021	T3M-3	-0.83	0.91	Endometrial/Uterine Cancer	Gestational choriocarcinoma
ACH-001765	Rh4	-0.87	0.91	Sarcoma	Alveolar rhabdomyosarcoma
ACH-001096	JR	-0.73	0.91	Sarcoma	Alveolar rhabdomyosarcoma
ACH-000483	SNU-182	-0.73	0.91	Liver Cancer	Adult hepatocellular carcinoma
ACH-001562	Mero-95	-0.72	0.91	Lung Cancer	Pleural epithelioid mesothelioma
ACH-000365	SU-DHL-4	-0.68	0.90	Lymphoma	Diffuse large B-cell lymphoma germinal center B-cell type
ACH-000932	SNU-1	-0.67	0.90	Gastric Cancer	Gastric adenocarcinoma
ACH-000601	MIA PaCa-2	-0.57	0.86	Pancreatic Cancer	Pancreatic ductal adenocarcinoma
ACH-000410	Saos-2	-0.63	0.84	Bone Cancer	Osteosarcoma
ACH-001616	OCI-LY18	-0.55	0.83	Lymphoma	Diffuse large B-cell lymphoma
ACH-001389	SUM-1315MO2	-0.63	0.82	Breast Cancer	Invasive breast carcinoma of no special type
ACH-001336	Ca Ski	-0.61	0.82	Cervical Cancer	Human papillomavirus-related cervical squamous cell carcinoma
ACH-001992	ONE58	-0.60	0.82	Lung Cancer	Pleural epithelioid mesothelioma
ACH-001858	SSP-25	-0.55	0.80	Bile Duct Cancer	Intrahepatic cholangiocarcinoma

DepMap ID	Cell Line	MAPK14 Chronos GeneEffect	MAPK14 Chronos Prob	Primary disease	Cellosaurus NCIt_disease
ACH-000371	RL	-0.57	0.79	Lymphoma	Diffuse large B-cell lymphoma
ACH-000024	OPM-2	-0.54	0.78	Myeloma	Plasma cell myeloma
ACH-001977	NO36	-0.53	0.78	Lung Cancer	Pleural malignant mesothelioma
ACH-000938	NALM-6	-0.60	0.77	Leukemia	Adult B acute lymphoblastic leukemia
ACH-001368	OAC-M5.1	-0.51	0.76	Esophageal Cancer	Esophageal adenocarcinoma
ACH-000335	MSTO-211H	-0.71	0.76	Lung Cancer	Pleural biphasic mesothelioma
ACH-001233	VMRC-LCD	-0.44	0.75	Lung Cancer	Lung adenocarcinoma
ACH-000848	JHH-7	-0.54	0.75	Liver Cancer	Adult hepatocellular carcinoma
ACH-000716	TT2609-C02	-0.55	0.75	Thyroid Cancer	Thyroid gland follicular carcinoma
ACH-000152	M059K	-0.58	0.73	Brain Cancer	Glioblastoma
ACH-000905	5637	-0.52	0.73	Bladder Cancer	Bladder carcinoma
ACH-000452	TE-8	-0.50	0.72	Esophageal Cancer	Esophageal squamous cell carcinoma
ACH-000375	G-402	-0.54	0.72	Kidney Cancer	Kidney neoplasm
ACH-000541	KMS-34	-0.66	0.71	Myeloma	Plasma cell myeloma
ACH-000627	LCLC-103H	-0.56	0.71	Lung Cancer	Lung large cell carcinoma
ACH-000658	KMS-18	-0.49	0.70	Myeloma	Plasma cell myeloma
ACH-001648	Shmac 4	-0.49	0.70	Prostate Cancer	Prostate carcinoma
ACH-001067	F5	-0.52	0.70	Brain Cancer	Meningioma
ACH-001802	LPS853	-0.52	0.69	Liposarcoma	Dedifferentiated liposarcoma
ACH-001639	ROS-50	-0.56	0.68	Leukemia	Diffuse large B-cell lymphoma

DepMap ID	Cell Line	MAPK14 Chronos GeneEffect	MAPK14 Chronos Prob	Primary disease	Cellosaurus NCIt_disease
ACH-000747	NCI-H1703	-0.49	0.68	Lung Cancer	Lung squamous cell carcinoma
ACH-000261	RERF-LC-AI	-0.46	0.67	Lung Cancer	Lung squamous cell carcinoma
ACH-001690	UPCI-SCC-026	-0.45	0.66	Head and Neck Cancer	Oral cavity squamous cell carcinoma
ACH-000843	HARA	-0.46	0.66	Lung Cancer	Lung squamous cell carcinoma
ACH-001574	MOLM-14	-0.48	0.65	Leukemia	Adult acute myeloid leukemia
ACH-000231	KALS-1	-0.46	0.64	Brain Cancer	Glioblastoma
ACH-001736	HB1119	-0.45	0.64	Leukemia	B acute lymphoblastic leukemia
ACH-001394	SUM-229PE	-0.50	0.64	Breast Cancer	Breast carcinoma
ACH-001450	BLUE-1	-0.56	0.63	Lymphoma	Burkitt lymphoma
ACH-000174	CAL-62	-0.45	0.63	Thyroid Cancer	Thyroid gland anaplastic carcinoma
ACH-001500	FLO-1	-0.44	0.63	Esophageal Cancer	Barrett adenocarcinoma
ACH-000853	NCI-H661	-0.49	0.63	Lung Cancer	Lung large cell carcinoma
ACH-000151	JM1	-0.52	0.63	Leukemia	B acute lymphoblastic leukemia
ACH-000696	OVCAR-8	-0.42	0.61	Ovarian Cancer	High grade ovarian serous adenocarcinoma
ACH-002210	ARH-77	-0.34	0.61	Blood	
ACH-002186	PL4	-0.45	0.59	Pancreatic Cancer	Pancreatic ductal adenocarcinoma
ACH-000833	RH-30	-0.51	0.59	Sarcoma	Alveolar rhabdomyosarcoma
ACH-000776	ONS-76	-0.49	0.59	Brain Cancer	Medulloblastoma
ACH-001619	OCUG-1	-0.54	0.58	Gallbladder Cancer	Gallbladder carcinoma
ACH-000496	NCI-H1792	-0.46	0.58	Lung Cancer	Lung adenocarcinoma

DepMap ID	Cell Line	MAPK14 Chronos GeneEffect	MAPK14 Chronos Prob	Primary disease	Cellosaurus NCIt_disease
ACH-000762	YD-38	-0.51	0.56	Head and Neck Cancer	Gingival squamous cell carcinoma
ACH-001606	no.11	-0.42	0.55	Brain Cancer	Glioblastoma
ACH-002189	RCC-FG2	-0.39	0.55	Kidney Cancer	Clear cell renal cell carcinoma
ACH-001653	SK-GT-2	-0.42	0.55	Gastric Cancer	Gastric fundus carcinoma
ACH-000792	BFTC-909	-0.40	0.54	Kidney Cancer	Renal pelvis urothelial carcinoma
ACH-000793	KATO III	-0.38	0.54	Gastric Cancer	Down syndrome
ACH-000721	HMC-1-8	-0.40	0.54	Breast Cancer	Breast carcinoma
ACH-002298	PCI-6A	-0.39	0.53	Head and Neck Cancer	Tonsillar squamous cell carcinoma
ACH-000176	LOU-NH91	-0.44	0.53	Lung Cancer	Lung squamous cell carcinoma
ACH-001530	JEG-3	-0.46	0.53	Endometrial/Uterine Cancer	Gestational choriocarcinoma
ACH-000471	Li-7	-0.41	0.53	Liver Cancer	Adult hepatocellular carcinoma
ACH-000719	RMG-I	-0.34	0.52	Ovarian Cancer	Ovarian clear cell adenocarcinoma
ACH-001391	SUM-159PT	-0.47	0.52	Breast Cancer	Breast pleomorphic carcinoma
ACH-000748	SJSA-1	-0.38	0.52	Bone Cancer	Osteosarcoma
ACH-001563	MM127	-0.44	0.52	Skin Cancer	Amelanotic melanoma
ACH-002029	SAS	-0.35	0.51	Head and Neck Cancer	Tongue squamous cell carcinoma
ACH-001555	Mero-14	-0.53	0.51	Lung Cancer	Pleural epithelioid mesothelioma
ACH-000364	U-2 OS	-0.39	0.51	Bone Cancer	Osteosarcoma

Appendix Table 4 | Top 20 p38α co-dependencies in cancer cells

Gene	p_adj	Pearson's R
MAP3K4	2.59E-55	0.465691
MAP2K3	1.43E-46	0.431632
GADD45B	1.52E-20	0.30182
MIDEAS	1.05E-12	0.244499
CCNC	2.42E-12	0.240912
MLST8	1.04E-09	0.217129
TCF3	1.04E-09	0.217067
MED23	4.81E-08	0.199943
DYRK1A	5.04E-08	0.198613
AFF1	8.66E-08	0.195592
DCPS	1.03E-07	0.194536
MED24	4.14E-07	0.187721
MED13	4.30E-07	0.187139
UBE2J1	4.30E-07	0.186672
CD19	4.30E-07	0.186666
MED16	8.23E-07	0.183412
MRE11	8.43E-07	0.183103
IRF2	1.73E-06	0.179468
PWP2	5.83E-06	0.172185
DNTTIP1	5.83E-06	0.17199

References

Adams, R. H., Porras, A., Alonso, G., Jones, M., Vintersten, K., Panelli, S., Valladares, A., Perez, L., Klein, R., & Nebreda, A. R. (2000). Essential role of p38alpha MAP kinase in placental but not embryonic cardiovascular development. *Molecular Cell*, *6*(1), 109–116.

Alonso, G., Ambrosino, C., Jones, M., & Nebreda, A. R. (2000). Differential activation of p38 mitogen-activated protein kinase isoforms depending on signal strength. *The Journal of Biological Chemistry*, *275*(51), 40641–40648. https://doi.org/10.1074/jbc.M007835200

Alves, S., Castro, L., Fernandes, M. S., Francisco, R., Castro, P., Priault, M., Chaves, S. R., Moyer, M. P., Oliveira, C., Seruca, R., Côrte-Real, M., Sousa, M. J., & Preto, A. (2015). Colorectal cancer-related mutant KRAS alleles function as positive regulators of autophagy. *Oncotarget*, *6*(31), 30787–30802. https://doi.org/10.18632/oncotarget.5021

Ambrosino, C., Mace, G., Galban, S., Fritsch, C., Vintersten, K., Black, E., Gorospe, M., & Nebreda, A. R. (2003). Negative Feedback Regulation of MKK6 mRNA Stability by p38α Mitogen-Activated Protein Kinase. *Molecular and Cellular Biology*, *23*(1), 370–381. https://doi.org/10.1128/MCB.23.1.370-381.2003

Aviv, T., Lin, Z., Lau, S., Rendl, L. M., Sicheri, F., & Smibert, C. A. (2003). The RNA-binding SAM domain of Smaug defines a new family of post-transcriptional regulators. *Nature Structural & Molecular Biology*, *10*(8), Article 8. https://doi.org/10.1038/nsb956

Baker, S. J., Fearon, E. R., Nigro, J. M., Hamilton, S. R., Preisinger, A. C., Jessup, J. M., vanTuinen, P., Ledbetter, D. H., Barker, D. F., Nakamura, Y., White, R., & Vogelstein, B. (1989). Chromosome 17 deletions and p53 gene mutations in colorectal carcinomas. *Science (New York, N.Y.)*, *244*(4901), 217–221. https://doi.org/10.1126/science.2649981

Barrangou, R., Fremaux, C., Deveau, H., Richards, M., Boyaval, P., Moineau, S., Romero, D. A., & Horvath, P. (2007). CRISPR provides acquired resistance against viruses in prokaryotes. *Science (New York, N.Y.)*, *315*(5819), 1709–1712. https://doi.org/10.1126/science.1138140

Barretina, J., Caponigro, G., Stransky, N., Venkatesan, K., Margolin, A. A., Kim, S., Wilson, C. J., Lehár, J., Kryukov, G. V., Sonkin, D., Reddy, A., Liu, M., Murray, L., Berger, M. F., Monahan, J. E., Morais, P., Meltzer, J., Korejwa, A., Jané-Valbuena, J., … Garraway, L. A. (2012). The Cancer Cell Line Encyclopedia enables predictive modelling of anticancer

drug sensitivity. *Nature*, *483*(7391), 603–607. https://doi.org/10.1038/nature11003

Batlle, R., Andrés, E., Gonzalez, L., Llonch, E., Igea, A., Gutierrez-Prat, N., Berenguer-Llergo, A., & Nebreda, A. R. (2019). Regulation of tumor angiogenesis and mesenchymal-endothelial transition by p38α through TGF-β and JNK signaling. *Nature Communications*, *10*(1), 3071. https://doi.org/10.1038/s41467-019-10946-y

Beardmore, V. A., Hinton, H. J., Eftychi, C., Apostolaki, M., Armaka, M., Darragh, J., McIlrath, J., Carr, J. M., Armit, L. J., Clacher, C., Malone, L., Kollias, G., & Arthur, J. S. C. (2005). Generation and Characterization of p38β (MAPK11) Gene-Targeted Mice. *Molecular and Cellular Biology*, *25*(23), 10454–10464. https://doi.org/10.1128/MCB.25.23.10454-10464.2005

Behan, F. M., Iorio, F., Picco, G., Gonçalves, E., Beaver, C. M., Migliardi, G., Santos, R., Rao, Y., Sassi, F., Pinnelli, M., Ansari, R., Harper, S., Jackson, D. A., McRae, R., Pooley, R., Wilkinson, P., van der Meer, D., Dow, D., Buser-Doepner, C., … Garnett, M. J. (2019). Prioritization of cancer therapeutic targets using CRISPR-Cas9 screens. *Nature*, *568*(7753), 511–516. https://doi.org/10.1038/s41586-019-1103-9

Bister, K., & Duesberg, P. H. (1979). Structure and specific sequences of avian erythroblastosis virus RNA: Evidence for multiple classes of transforming genes among avian tumor viruses. *Proceedings of the National Academy of Sciences of the United States of America*, *76*(10), 5023–5027. https://doi.org/10.1073/pnas.76.10.5023

Bloem, L. J., Pickard, T. R., Acton, S., Donoghue, M., Beavis, R. C., Knierman, M. D., & Wang, X. (2001). Tissue distribution and functional expression of a cDNA encoding a novel mixed lineage kinase. *Journal of Molecular and Cellular Cardiology*, *33*(9), 1739–1750. https://doi.org/10.1006/jmcc.2001.1437

Bondeson, D. P., Paolella, B. R., Asfaw, A., Rothberg, M. V., Skipper, T. A., Langan, C., Mesa, G., Gonzalez, A., Surface, L. E., Ito, K., Kazachkova, M., Colgan, W. N., Warren, A., Dempster, J. M., Krill-Burger, J. M., Ericsson, M., Tang, A. A., Fung, I., Chambers, E. S., … Golub, T. R. (2022). Phosphate dysregulation via the XPR1–KIDINS220 protein complex is a therapeutic vulnerability in ovarian cancer. *Nature Cancer*, *3*(6), Article 6. https://doi.org/10.1038/s43018-022-00360-7

Bonnet, S., Archer, S. L., Allalunis-Turner, J., Haromy, A., Beaulieu, C., Thompson, R., Lee, C. T., Lopaschuk, G. D., Puttagunta, L., Bonnet, S., Harry, G., Hashimoto, K., Porter, C. J., Andrade, M. A., Thebaud, B., &

Michelakis, E. D. (2007). A mitochondria-K+ channel axis is suppressed in cancer and its normalization promotes apoptosis and inhibits cancer growth. *Cancer Cell*, *11*(1), 37–51. https://doi.org/10.1016/j.ccr.2006.10.020

Boutros, M., & Ahringer, J. (2008). The art and design of genetic screens: RNA interference. *Nature Reviews. Genetics*, *9*(7), 554–566. https://doi.org/10.1038/nrg2364

Bragado, P., Armesilla, A., Silva, A., & Porras, A. (2007). Apoptosis by cisplatin requires p53 mediated p38alpha MAPK activation through ROS generation. *Apoptosis: An International Journal on Programmed Cell Death*, *12*(9), 1733–1742. https://doi.org/10.1007/s10495-007-0082-8

Brancho, D., Tanaka, N., Jaeschke, A., Ventura, J.-J., Kelkar, N., Tanaka, Y., Kyuuma, M., Takeshita, T., Flavell, R. A., & Davis, R. J. (2003). Mechanism of p38 MAP kinase activation in vivo. *Genes & Development*, *17*(16), 1969–1978. https://doi.org/10.1101/gad.1107303

Brichkina, A., Nguyen, N. T., Baskar, R., Wee, S., Gunaratne, J., Robinson, R. C., & Bulavin, D. V. (2016). Proline isomerisation as a novel regulatory mechanism for p38MAPK activation and functions. *Cell Death and Differentiation*, *23*(10), 1592–1601. https://doi.org/10.1038/cdd.2016.45

Bridges, C. B. (1922). The Origin of Variations in Sexual and Sex-Limited Characters. *The American Naturalist*, *56*(642), 51–63. https://doi.org/10.1086/279847

Bryant, H. E., Schultz, N., Thomas, H. D., Parker, K. M., Flower, D., Lopez, E., Kyle, S., Meuth, M., Curtin, N. J., & Helleday, T. (2005). Specific killing of BRCA2-deficient tumours with inhibitors of poly(ADP-ribose) polymerase. *Nature*, *434*(7035), Article 7035. https://doi.org/10.1038/nature03443

Bulavin, D. V., Demidov, O. N., Saito, S., Kauraniemi, P., Phillips, C., Amundson, S. A., Ambrosino, C., Sauter, G., Nebreda, A. R., Anderson, C. W., Kallioniemi, A., Fornace, A. J., & Appella, E. (2002). Amplification of PPM1D in human tumors abrogates p53 tumor-suppressor activity. *Nature Genetics*, *31*(2), 210–215. https://doi.org/10.1038/ng894

Bulavin, D. V., Phillips, C., Nannenga, B., Timofeev, O., Donehower, L. A., Anderson, C. W., Appella, E., & Fornace, A. J. (2004). Inactivation of the Wip1 phosphatase inhibits mammary tumorigenesis through

p38 MAPK-mediated activation of the p16(Ink4a)-p19(Arf) pathway. *Nature Genetics*, *36*(4), 343–350. https://doi.org/10.1038/ng1317

Campaner, S., & Amati, B. (2012). Two sides of the Myc-induced DNA damage response: From tumor suppression to tumor maintenance. *Cell Division*, *7*(1), 6. https://doi.org/10.1186/1747-1028-7-6

Campbell, R. M., Anderson, B. D., Brooks, N. A., Brooks, H. B., Chan, E. M., De Dios, A., Gilmour, R., Graff, J. R., Jambrina, E., Mader, M., McCann, D., Na, S., Parsons, S. H., Pratt, S. E., Shih, C., Stancato, L. F., Starling, J. J., Tate, C., Velasco, J. A., … Ye, X. S. (2014). Characterization of LY2228820 dimesylate, a potent and selective inhibitor of p38 MAPK with antitumor activity. *Molecular Cancer Therapeutics*, *13*(2), 364–374. https://doi.org/10.1158/1535-7163.MCT-13-0513

Cancer Genome Atlas Research Network, Weinstein, J. N., Collisson, E. A., Mills, G. B., Shaw, K. R. M., Ozenberger, B. A., Ellrott, K., Shmulevich, I., Sander, C., & Stuart, J. M. (2013). The Cancer Genome Atlas Pan-Cancer analysis project. *Nature Genetics*, *45*(10), 1113–1120. https://doi.org/10.1038/ng.2764

Cánovas, B., Igea, A., Sartori, A. A., Gomis, R. R., Paull, T. T., Isoda, M., Pérez-Montoyo, H., Serra, V., González-Suárez, E., Stracker, T. H., & Nebreda, A. R. (2018). Targeting p38α Increases DNA Damage, Chromosome Instability, and the Anti-tumoral Response to Taxanes in Breast Cancer Cells. *Cancer Cell*, *33*(6), 1094-1110.e8. https://doi.org/10.1016/j.ccell.2018.04.010

Canovas, B., & Nebreda, A. R. (2021). Diversity and versatility of p38 kinase signalling in health and disease. *Nature Reviews Molecular Cell Biology*, *22*(5), Article 5. https://doi.org/10.1038/s41580-020-00322-w

Casanovas, O., Miró, F., Estanyol, J. M., Itarte, E., Agell, N., & Bachs, O. (2000). Osmotic stress regulates the stability of cyclin D1 in a p38SAPK2-dependent manner. *The Journal of Biological Chemistry*, *275*(45), 35091–35097. https://doi.org/10.1074/jbc.M006324200

Chan, E. M., Shibue, T., McFarland, J. M., Gaeta, B., Ghandi, M., Dumont, N., Gonzalez, A., McPartlan, J. S., Li, T., Zhang, Y., Bin Liu, J., Lazaro, J.-B., Gu, P., Piett, C. G., Apffel, A., Ali, S. O., Deasy, R., Keskula, P., Ng, R. W. S., … Bass, A. J. (2019). WRN helicase is a synthetic lethal target in microsatellite unstable cancers. *Nature*, *568*(7753), 551–556. https://doi.org/10.1038/s41586-019-1102-x

Chang, L., Ruiz, P., Ito, T., & Sellers, W. R. (2021). Targeting pan-essential genes in cancer: Challenges and opportunities. *Cancer Cell*, *39*(4), 466–479. https://doi.org/10.1016/j.ccell.2020.12.008

Chapman, P. B., Hauschild, A., Robert, C., Haanen, J. B., Ascierto, P., Larkin, J., Dummer, R., Garbe, C., Testori, A., Maio, M., Hogg, D., Lorigan, P., Lebbe, C., Jouary, T., Schadendorf, D., Ribas, A., O'Day, S. J., Sosman, J. A., Kirkwood, J. M., … BRIM-3 Study Group. (2011). Improved survival with vemurafenib in melanoma with BRAF V600E mutation. *The New England Journal of Medicine*, *364*(26), 2507–2516. https://doi.org/10.1056/NEJMoa1103782

Chen, L., Mayer, J. A., Krisko, T. I., Speers, C. W., Wang, T., Hilsenbeck, S. G., & Brown, P. H. (2009). Inhibition of the p38 kinase suppresses the proliferation of human ER-negative breast cancer cells. *Cancer Research*, *69*(23), 8853–8861. https://doi.org/10.1158/0008-5472.CAN-09-1636

Chen, Z., Hutchison, M., & Cobb, M. H. (1999). Isolation of the Protein Kinase TAO2 and Identification of Its Mitogen-activated Protein Kinase/Extracellular Signal-regulated Kinase Kinase Binding Domain*. *Journal of Biological Chemistry*, *274*(40), 28803–28807. https://doi.org/10.1074/jbc.274.40.28803

Cheung, P. C. F., Campbell, D. G., Nebreda, A. R., & Cohen, P. (2003). Feedback control of the protein kinase TAK1 by SAPK2a/p38alpha. *The EMBO Journal*, *22*(21), 5793–5805. https://doi.org/10.1093/emboj/cdg552

Chiacchiera, F., Grossi, V., Cappellari, M., Peserico, A., Simonatto, M., Germani, A., Russo, S., Moyer, M. P., Resta, N., Murzilli, S., & Simone, C. (2012). Blocking p38/ERK crosstalk affects colorectal cancer growth by inducing apoptosis in vitro and in preclinical mouse models. *Cancer Letters*, *324*(1), 98–108. https://doi.org/10.1016/j.canlet.2012.05.006

Chiacchiera, F., Matrone, A., Ferrari, E., Ingravallo, G., Lo Sasso, G., Murzilli, S., Petruzzelli, M., Salvatore, L., Moschetta, A., & Simone, C. (2009). P38α blockade inhibits colorectal cancer growth in vivo by inducing a switch from HIF1α- to FoxO-dependent transcription. *Cell Death & Differentiation*, *16*(9), Article 9. https://doi.org/10.1038/cdd.2009.36

Cho, S. W., Kim, S., Kim, J. M., & Kim, J.-S. (2013). Targeted genome engineering in human cells with the Cas9 RNA-guided endonuclease. *Nature Biotechnology*, *31*(3), 230–232. https://doi.org/10.1038/nbt.2507

Comes, F., Matrone, A., Lastella, P., Nico, B., Susca, F. C., Bagnulo, R., Ingravallo, G., Modica, S., Lo Sasso, G., Moschetta, A., Guanti, G., & Simone, C. (2007). A novel cell type-specific role of p38α in the control of autophagy and cell death in colorectal cancer cells. *Cell*

Death & Differentiation, *14*(4), Article 4. https://doi.org/10.1038/sj.cdd.4402076

Cong, L., Ran, F. A., Cox, D., Lin, S., Barretto, R., Habib, N., Hsu, P. D., Wu, X., Jiang, W., Marraffini, L. A., & Zhang, F. (2013). Multiplex genome engineering using CRISPR/Cas systems. *Science (New York, N.Y.)*, *339*(6121), 819–823. https://doi.org/10.1126/science.1231143

Corsello, S. M., Nagari, R. T., Spangler, R. D., Rossen, J., Kocak, M., Bryan, J. G., Humeidi, R., Peck, D., Wu, X., Tang, A. A., Wang, V. M., Bender, S. A., Lemire, E., Narayan, R., Montgomery, P., Ben-David, U., Garvie, C. W., Chen, Y., Rees, M. G., … Golub, T. R. (2020). Discovering the anticancer potential of non-oncology drugs by systematic viability profiling. *Nature Cancer*, *1*(2), Article 2. https://doi.org/10.1038/s43018-019-0018-6

Coulombe, P., & Meloche, S. (2007). Atypical mitogen-activated protein kinases: Structure, regulation and functions. *Biochimica et Biophysica Acta (BBA) - Molecular Cell Research*, *1773*(8), 1376–1387. https://doi.org/10.1016/j.bbamcr.2006.11.001

Cowley, G. S., Weir, B. A., Vazquez, F., Tamayo, P., Scott, J. A., Rusin, S., East-Seletsky, A., Ali, L. D., Gerath, W. F., Pantel, S. E., Lizotte, P. H., Jiang, G., Hsiao, J., Tsherniak, A., Dwinell, E., Aoyama, S., Okamoto, M., Harrington, W., Gelfand, E., … Hahn, W. C. (2014). Parallel genome-scale loss of function screens in 216 cancer cell lines for the identification of context-specific genetic dependencies. *Scientific Data*, *1*(1), Article 1. https://doi.org/10.1038/sdata.2014.35

Criscuolo, D., Avolio, R., Matassa, D. S., & Esposito, F. (2021). Targeting Mitochondrial Protein Expression as a Future Approach for Cancer Therapy. *Frontiers in Oncology*, *11*. https://www.frontiersin.org/articles/10.3389/fonc.2021.797265

Cuadrado, A., & Nebreda, A. R. (2010). Mechanisms and functions of p38 MAPK signalling. *The Biochemical Journal*, *429*(3), 403–417. https://doi.org/10.1042/BJ20100323

Cuenda, A., Cohen, P., Buée-Scherrer, V., & Goedert, M. (1997). Activation of stress-activated protein kinase-3 (SAPK3) by cytokines and cellular stresses is mediated via SAPKK3 (MKK6); comparison of the specificities of SAPK3 and SAPK2 (RK/p38). *The EMBO Journal*, *16*(2), 295–305. https://doi.org/10.1093/emboj/16.2.295

Cuenda, A., & Sanz-Ezquerro, J. J. (2017). p38γ and p38δ: From Spectators to Key Physiological Players. *Trends in Biochemical Sciences*, *42*(6), 431–442. https://doi.org/10.1016/j.tibs.2017.02.008

Cully, M., Genevet, A., Warne, P., Treins, C., Liu, T., Bastien, J., Baum, B., Tapon, N., Leevers, S. J., & Downward, J. (2010). A Role for p38 Stress-Activated Protein Kinase in Regulation of Cell Growth via TORC1. *Molecular and Cellular Biology*, *30*(2), 481–495. https://doi.org/10.1128/MCB.00688-09

Dai, C., Whitesell, L., Rogers, A. B., & Lindquist, S. (2007). Heat Shock Factor 1 Is a Powerful Multifaceted Modifier of Carcinogenesis. *Cell*, *130*(6), 1005–1018. https://doi.org/10.1016/j.cell.2007.07.020

Daley, G. Q., Van Etten, R. A., & Baltimore, D. (1990). Induction of Chronic Myelogenous Leukemia in Mice by the P210bcr/abl Gene of the Philadelphia Chromosome. *Science*, *247*(4944), 824–830. https://doi.org/10.1126/science.2406902

D'Andrea, A. D., & Grompe, M. (2003). The Fanconi anaemia/BRCA pathway. *Nature Reviews. Cancer*, *3*(1), 23–34. https://doi.org/10.1038/nrc970

de Nadal, E., & Posas, F. (2022). The HOG pathway and the regulation of osmoadaptive responses in yeast. *FEMS Yeast Research*, *22*(1), foac013. https://doi.org/10.1093/femsyr/foac013

del Barco Barrantes, I., Coya, J. M., Maina, F., Arthur, J. S. C., & Nebreda, A. R. (2011). Genetic analysis of specific and redundant roles for p38α and p38β MAPKs during mouse development. *Proceedings of the National Academy of Sciences of the United States of America*, *108*(31), 12764–12769. https://doi.org/10.1073/pnas.1015013108

Dempster, J. M., Boyle, I., Vazquez, F., Root, D. E., Boehm, J. S., Hahn, W. C., Tsherniak, A., & McFarland, J. M. (2021). Chronos: A cell population dynamics model of CRISPR experiments that improves inference of gene fitness effects. *Genome Biology*, *22*(1), 343. https://doi.org/10.1186/s13059-021-02540-7

Dempster, J. M., Pacini, C., Pantel, S., Behan, F. M., Green, T., Krill-Burger, J., Beaver, C. M., Younger, S. T., Zhivich, V., Najgebauer, H., Allen, F., Gonçalves, E., Shepherd, R., Doench, J. G., Yusa, K., Vazquez, F., Parts, L., Boehm, J. S., Golub, T. R., … Iorio, F. (2019). Agreement between two large pan-cancer CRISPR-Cas9 gene dependency data sets. *Nature Communications*, *10*(1), 5817. https://doi.org/10.1038/s41467-019-13805-y

Dérijard, B., Raingeaud, J., Barrett, T., Wu, I.-H., Han, J., Ulevitch, R. J., & Davis, R. J. (1995). Independent Human MAP-Kinase Signal Transduction Pathways Defined by MEK and MKK Isoforms. *Science*, *267*(5198), 682–685. https://doi.org/10.1126/science.7839144

Dickinson, S. E., Olson, E. R., Zhang, J., Cooper, S. J., Melton, T., Criswell, P. J., Casanova, A., Dong, Z., Hu, C., Saboda, K., Jacobs, E. T., Alberts, D. S., & Bowden, G. T. (2011). P38 MAP kinase plays a functional role in UVB-induced mouse skin carcinogenesis. *Molecular Carcinogenesis*, *50*(6), 469–478. https://doi.org/10.1002/mc.20734

Dobzhansky, Th. (1946). Genetics of Natural Populations. Xiii. Recombination and Variability in Populations of Drosophila Pseudoobscura. *Genetics*, *31*(3), 269–290.

Doench, J. G. (2018). Am I ready for CRISPR? A user's guide to genetic screens. *Nature Reviews Genetics*, *19*(2), Article 2. https://doi.org/10.1038/nrg.2017.97

Doench, J. G., Fusi, N., Sullender, M., Hegde, M., Vaimberg, E. W., Donovan, K. F., Smith, I., Tothova, Z., Wilen, C., Orchard, R., Virgin, H. W., Listgarten, J., & Root, D. E. (2016). Optimized sgRNA design to maximize activity and minimize off-target effects of CRISPR-Cas9. *Nature Biotechnology*, *34*(2), 184–191. https://doi.org/10.1038/nbt.3437

Doench, J. G., Hartenian, E., Graham, D. B., Tothova, Z., Hegde, M., Smith, I., Sullender, M., Ebert, B. L., Xavier, R. J., & Root, D. E. (2014). Rational design of highly active sgRNAs for CRISPR-Cas9-mediated gene inactivation. *Nature Biotechnology*, *32*(12), 1262–1267. https://doi.org/10.1038/nbt.3026

Dolado, I., Swat, A., Ajenjo, N., Vita, G. D., Cuadrado, A., & Nebreda, A. R. (2007). P38α MAP Kinase as a Sensor of Reactive Oxygen Species in Tumorigenesis. *Cancer Cell*, *11*(2), 191–205. https://doi.org/10.1016/j.ccr.2006.12.013

Donzelli, M., & Draetta, G. F. (2003). Regulating mammalian checkpoints through Cdc25 inactivation. *EMBO Reports*, *4*(7), 671–677. https://doi.org/10.1038/sj.embor.embor887

Dowell, J., Minna, J. D., & Kirkpatrick, P. (2005). Erlotinib hydrochloride. *Nature Reviews Drug Discovery*, *4*(1), Article 1. https://doi.org/10.1038/nrd1612

Druker, B. J., Talpaz, M., Resta, D. J., Peng, B., Buchdunger, E., Ford, J. M., Lydon, N. B., Kantarjian, H., Capdeville, R., Ohno-Jones, S., & Sawyers, C. L. (2001). Efficacy and Safety of a Specific Inhibitor of the BCR-ABL Tyrosine Kinase in Chronic Myeloid Leukemia. *New England Journal of Medicine*, *344*(14), 1031–1037. https://doi.org/10.1056/NEJM200104053441401

Druker, B. J., Tamura, S., Buchdunger, E., Ohno, S., Segal, G. M., Fanning, S., Zimmermann, J., & Lydon, N. B. (1996). Effects of a selective inhibitor

of the Abl tyrosine kinase on the growth of Bcr-Abl positive cells. *Nature Medicine*, *2*(5), 561–566. https://doi.org/10.1038/nm0596-561

Duesberg, P. H., Bister, K., & Vogt, P. K. (1977). The RNA of avian acute leukemia virus MC29. *Proceedings of the National Academy of Sciences of the United States of America*, *74*(10), 4320–4324. https://doi.org/10.1073/pnas.74.10.4320

Duesberg, P. H., & Vogt, P. K. (1970). Differences between the ribonucleic acids of transforming and nontransforming avian tumor viruses. *Proceedings of the National Academy of Sciences of the United States of America*, *67*(4), 1673–1680. https://doi.org/10.1073/pnas.67.4.1673

Efron, B., & Tibshirani, R. (2007). On testing the significance of sets of genes. *The Annals of Applied Statistics*, *1*(1), 107–129. https://doi.org/10.1214/07-AOAS101

Enslen, H., Raingeaud, J., & Davis, R. J. (1998). Selective activation of p38 mitogen-activated protein (MAP) kinase isoforms by the MAP kinase kinases MKK3 and MKK6. *The Journal of Biological Chemistry*, *273*(3), 1741–1748. https://doi.org/10.1074/jbc.273.3.1741

Farmer, H., McCabe, N., Lord, C. J., Tutt, A. N. J., Johnson, D. A., Richardson, T. B., Santarosa, M., Dillon, K. J., Hickson, I., Knights, C., Martin, N. M. B., Jackson, S. P., Smith, G. C. M., & Ashworth, A. (2005). Targeting the DNA repair defect in BRCA mutant cells as a therapeutic strategy. *Nature*, *434*(7035), Article 7035. https://doi.org/10.1038/nature03445

Ferrari, G., Terushkin, V., Wolff, M. J., Zhang, X., Valacca, C., Poggio, P., Pintucci, G., & Mignatti, P. (2012). TGF-β1 Induces Endothelial Cell Apoptosis by Shifting VEGF Activation of p38MAPK from the Prosurvival p38β to Proapoptotic p38α. *Molecular Cancer Research*, *10*(5), 605–614. https://doi.org/10.1158/1541-7786.MCR-11-0507

Freshney, N. W., Rawlinson, L., Guesdon, F., Jones, E., Cowley, S., Hsuan, J., & Saklatvala, J. (1994). Interleukin-1 activates a novel protein kinase cascade that results in the phosphorylation of Hsp27. *Cell*, *78*(6), 1039–1049. https://doi.org/10.1016/0092-8674(94)90278-x

Friedrich, G., & Soriano, P. (1991). Promoter traps in embryonic stem cells: A genetic screen to identify and mutate developmental genes in mice. *Genes & Development*, *5*(9), 1513–1523. https://doi.org/10.1101/gad.5.9.1513

Gad, H., Koolmeister, T., Jemth, A.-S., Eshtad, S., Jacques, S. A., Ström, C. E., Svensson, L. M., Schultz, N., Lundbäck, T., Einarsdottir, B. O., Saleh,

A., Göktürk, C., Baranczewski, P., Svensson, R., Berntsson, R. P.-A., Gustafsson, R., Strömberg, K., Sanjiv, K., Jacques-Cordonnier, M.-C., … Helleday, T. (2014). MTH1 inhibition eradicates cancer by preventing sanitation of the dNTP pool. *Nature*, *508*(7495), 215–221. https://doi.org/10.1038/nature13181

Gallo, D., Young, J. T. F., Fourtounis, J., Martino, G., Álvarez-Quilón, A., Bernier, C., Duffy, N. M., Papp, R., Roulston, A., Stocco, R., Szychowski, J., Veloso, A., Alam, H., Baruah, P. S., Fortin, A. B., Bowlan, J., Chaudhary, N., Desjardins, J., Dietrich, E., … Durocher, D. (2022). CCNE1 amplification is synthetic lethal with PKMYT1 kinase inhibition. *Nature*, *604*(7907), 749–756. https://doi.org/10.1038/s41586-022-04638-9

Gao, Z., Xu, J., Fan, Y., Qi, Y., Wang, S., Zhao, S., Guo, X., Xue, H., Deng, L., Zhao, R., Sun, C., Zhang, P., & Li, G. (2022). PDIA3P1 promotes Temozolomide resistance in glioblastoma by inhibiting C/EBPβ degradation to facilitate proneural-to-mesenchymal transition. *Journal of Experimental & Clinical Cancer Research*, *41*(1), 223. https://doi.org/10.1186/s13046-022-02431-0

Ge, B., Gram, H., Di Padova, F., Huang, B., New, L., Ulevitch, R. J., Luo, Y., & Han, J. (2002). MAPKK-independent activation of p38alpha mediated by TAB1-dependent autophosphorylation of p38alpha. *Science (New York, N.Y.)*, *295*(5558), 1291–1294. https://doi.org/10.1126/science.1067289

Ghandi, M., Huang, F. W., Jané-Valbuena, J., Kryukov, G. V., Lo, C. C., McDonald, E. R., Barretina, J., Gelfand, E. T., Bielski, C. M., Li, H., Hu, K., Andreev-Drakhlin, A. Y., Kim, J., Hess, J. M., Haas, B. J., Aguet, F., Weir, B. A., Rothberg, M. V., Paolella, B. R., … Sellers, W. R. (2019). Next-generation characterization of the Cancer Cell Line Encyclopedia. *Nature*, *569*(7757), 503–508. https://doi.org/10.1038/s41586-019-1186-3

Giardino Torchia, M. L., Dutta, D., Mittelstadt, P. R., Guha, J., Gaida, M. M., Fish, K., Barr, V. A., Akpan, I. O., Samelson, L. E., Tagad, H. D., Debnath, S., Miller Jenkins, L. M., Appella, E., & Ashwell, J. D. (2018). Intensity and duration of TCR signaling is limited by p38 phosphorylation of ZAP-70T293 and destabilization of the signalosome. *Proceedings of the National Academy of Sciences of the United States of America*, *115*(9), 2174–2179. https://doi.org/10.1073/pnas.1713301115

Goedert, M., Cuenda, A., Craxton, M., Jakes, R., & Cohen, P. (1997). Activation of the novel stress-activated protein kinase SAPK4 by

cytokines and cellular stresses is mediated by SKK3 (MKK6); comparison of its substrate specificity with that of other SAP kinases. *The EMBO Journal*, *16*(12), 3563–3571. https://doi.org/10.1093/emboj/16.12.3563

Goloudina, A., Yamaguchi, H., Chervyakova, D. B., Appella, E., Fornace, A. J., & Bulavin, D. V. (2003). Regulation of human Cdc25A stability by Serine 75 phosphorylation is not sufficient to activate a S phase checkpoint. *Cell Cycle (Georgetown, Tex.)*, *2*(5), 473–478.

González-Terán, B., López, J. A., Rodríguez, E., Leiva, L., Martínez-Martínez, S., Bernal, J. A., Jiménez-Borreguero, L. J., Redondo, J. M., Vazquez, J., & Sabio, G. (2016). P38γ and δ promote heart hypertrophy by targeting the mTOR-inhibitory protein DEPTOR for degradation. *Nature Communications*, *7*(1), Article 1. https://doi.org/10.1038/ncomms10477

Grimm, D., Streetz, K. L., Jopling, C. L., Storm, T. A., Pandey, K., Davis, C. R., Marion, P., Salazar, F., & Kay, M. A. (2006). Fatality in mice due to oversaturation of cellular microRNA/short hairpin RNA pathways. *Nature*, *441*(7092), Article 7092. https://doi.org/10.1038/nature04791

Guay, J., Lambert, H., Gingras-Breton, G., Lavoie, J. N., Huot, J., & Landry, J. (1997). Regulation of actin filament dynamics by p38 map kinase-mediated phosphorylation of heat shock protein 27. *Journal of Cell Science*, *110 (Pt 3)*, 357–368. https://doi.org/10.1242/jcs.110.3.357

Gupta, J., del Barco Barrantes, I., Igea, A., Sakellariou, S., Pateras, I. S., Gorgoulis, V. G., & Nebreda, A. R. (2014). Dual function of p38α MAPK in colon cancer: Suppression of colitis-associated tumor initiation but requirement for cancer cell survival. *Cancer Cell*, *25*(4), 484–500. https://doi.org/10.1016/j.ccr.2014.02.019

Han, J., Lee, J.-D., Bibbs, L., & Ulevitch, R. J. (1994). A MAP Kinase Targeted by Endotoxin and Hyperosmolarity in Mammalian Cells. *Science*, *265*(5173), 808–811. https://doi.org/10.1126/science.7914033

Han, J., Lee, J.-D., Jiang, Y., Li, Z., Feng, L., & Ulevitch, R. J. (1996). Characterization of the Structure and Function of a Novel MAP Kinase Kinase (MKK6) (∗). *Journal of Biological Chemistry*, *271*(6), 2886–2891. https://doi.org/10.1074/jbc.271.6.2886

Han, J., Wu, J., & Silke, J. (2020). An overview of mammalian p38 mitogen-activated protein kinases, central regulators of cell stress and receptor signaling. *F1000Research*, *9*, F1000 Faculty Rev-653. https://doi.org/10.12688/f1000research.22092.1

Hanahan, D. (2022). Hallmarks of Cancer: New Dimensions. *Cancer Discovery*, *12*(1), 31–46. https://doi.org/10.1158/2159-8290.CD-21-1059

Hanahan, D., & Weinberg, R. A. (2000). The Hallmarks of Cancer. *Cell*, *100*(1), 57–70. https://doi.org/10.1016/S0092-8674(00)81683-9

Hanahan, D., & Weinberg, R. A. (2011). Hallmarks of Cancer: The Next Generation. *Cell*, *144*(5), 646–674. https://doi.org/10.1016/j.cell.2011.02.013

Harris, H., Miller, O. J., Klein, G., Worst, P., & Tachibana, T. (1969). Suppression of malignancy by cell fusion. *Nature*, *223*(5204), 363–368. https://doi.org/10.1038/223363a0

Hart, T., Brown, K. R., Sircoulomb, F., Rottapel, R., & Moffat, J. (2014). Measuring error rates in genomic perturbation screens: Gold standards for human functional genomics. *Molecular Systems Biology*, *10*, 733. https://doi.org/10.15252/msb.20145216

Hart, T., Chandrashekhar, M., Aregger, M., Steinhart, Z., Brown, K. R., MacLeod, G., Mis, M., Zimmermann, M., Fradet-Turcotte, A., Sun, S., Mero, P., Dirks, P., Sidhu, S., Roth, F. P., Rissland, O. S., Durocher, D., Angers, S., & Moffat, J. (2015). High-Resolution CRISPR Screens Reveal Fitness Genes and Genotype-Specific Cancer Liabilities. *Cell*, *163*(6), 1515–1526. https://doi.org/10.1016/j.cell.2015.11.015

Hartwell, L. H., Szankasi, P., Roberts, C. J., Murray, A. W., & Friend, S. H. (1997). Integrating Genetic Approaches into the Discovery of Anticancer Drugs. *Science*, *278*(5340), 1064–1068. https://doi.org/10.1126/science.278.5340.1064

He, D., Zhao, X., Chen, X., Fang, Y., Singh, S., Talele, T. T., Qiu, H., Liang, Y., Wang, X., Zhang, G., Chen, Z., & Fu, L. (2013). BIRB796, the Inhibitor of p38 Mitogen-Activated Protein Kinase, Enhances the Efficacy of Chemotherapeutic Agents in ABCB1 Overexpression Cells. *PLOS ONE*, *8*(1), e54181. https://doi.org/10.1371/journal.pone.0054181

He, X., Arrotta, N., Radhakrishnan, D., Wang, Y., Romigh, T., & Eng, C. (2013). Cowden syndrome-related mutations in PTEN associate with enhanced proteasome activity. *Cancer Research*, *73*(10), 3029–3040. https://doi.org/10.1158/0008-5472.CAN-12-3811

Heitman, J., Movva, N. R., & Hall, M. N. (1991). Targets for cell cycle arrest by the immunosuppressant rapamycin in yeast. *Science (New York, N.Y.)*, *253*(5022), 905–909. https://doi.org/10.1126/science.1715094

Hernández, G., Lal, H., Fidalgo, M., Guerrero, A., Zalvide, J., Force, T., & Pombo, C. M. (2011). A novel cardioprotective p38-MAPK/mTOR

pathway. *Experimental Cell Research*, *317*(20), 2938–2949. https://doi.org/10.1016/j.yexcr.2011.09.011

Herranz, N., Gallage, S., Mellone, M., Wuestefeld, T., Klotz, S., Hanley, C. J., Raguz, S., Acosta, J. C., Innes, A. J., Banito, A., Georgilis, A., Montoya, A., Wolter, K., Dharmalingam, G., Faull, P., Carroll, T., Martínez-Barbera, J. P., Cutillas, P., Reisinger, F., … Gil, J. (2015). MTOR regulates MAPKAPK2 translation to control the senescence-associated secretory phenotype. *Nature Cell Biology*, *17*(9), Article 9. https://doi.org/10.1038/ncb3225

Hirose, Y., Katayama, M., Stokoe, D., Haas-Kogan, D. A., Berger, M. S., & Pieper, R. O. (2003). The p38 mitogen-activated protein kinase pathway links the DNA mismatch repair system to the G2 checkpoint and to resistance to chemotherapeutic DNA-methylating agents. *Molecular and Cellular Biology*, *23*(22), 8306–8315. https://doi.org/10.1128/MCB.23.22.8306-8315.2003

Hope, H. R., Anderson, G. D., Burnette, B. L., Compton, R. P., Devraj, R. V., Hirsch, J. L., Keith, R. H., Li, X., Mbalaviele, G., Messing, D. M., Saabye, M. J., Schindler, J. F., Selness, S. R., Stillwell, L. I., Webb, E. G., Zhang, J., & Monahan, J. B. (2009). Anti-inflammatory properties of a novel N-phenyl pyridinone inhibitor of p38 mitogen-activated protein kinase: Preclinical-to-clinical translation. *The Journal of Pharmacology and Experimental Therapeutics*, *331*(3), 882–895. https://doi.org/10.1124/jpet.109.158329

Hu, P., Nebreda, A. R., Hanenberg, H., Kinnebrew, G. H., Ivan, M., Yoder, M. C., Filippi, M.-D., Broxmeyer, H. E., & Kapur, R. (2018). P38α/JNK signaling restrains erythropoiesis by suppressing Ezh2-mediated epigenetic silencing of Bim. *Nature Communications*, *9*(1), 3518. https://doi.org/10.1038/s41467-018-05955-2

Hui, L., Bakiri, L., Mairhorfer, A., Schweifer, N., Haslinger, C., Kenner, L., Komnenovic, V., Scheuch, H., Beug, H., & Wagner, E. F. (2007). P38alpha suppresses normal and cancer cell proliferation by antagonizing the JNK-c-Jun pathway. *Nature Genetics*, *39*(6), 741–749. https://doi.org/10.1038/ng2033

Hutchison, M., Berman, K. S., & Cobb, M. H. (1998). Isolation of TAO1, a protein kinase that activates MEKs in stress-activated protein kinase cascades. *The Journal of Biological Chemistry*, *273*(44), 28625–28632. https://doi.org/10.1074/jbc.273.44.28625

Hyrina, A., Jones, C., Chen, D., Clarkson, S., Cochran, N., Feucht, P., Hoffman, G., Lindeman, A., Russ, C., Sigoillot, F., Tsang, T., Uehara, K., Xie, L., Ganem, D., & Holdorf, M. (2019). A Genome-wide CRISPR Screen

Identifies ZCCHC14 as a Host Factor Required for Hepatitis B Surface Antigen Production. *Cell Reports*, *29*(10), 2970-2978.e6. https://doi.org/10.1016/j.celrep.2019.10.113

Ichijo, H., Nishida, E., Irie, K., ten Dijke, P., Saitoh, M., Moriguchi, T., Takagi, M., Matsumoto, K., Miyazono, K., & Gotoh, Y. (1997). Induction of apoptosis by ASK1, a mammalian MAPKKK that activates SAPK/JNK and p38 signaling pathways. *Science (New York, N.Y.)*, *275*(5296), 90–94. https://doi.org/10.1126/science.275.5296.90

Jandhyala, D. M., Ahluwalia, A., Obrig, T., & Thorpe, C. M. (2008). ZAK: A MAP3Kinase that transduces Shiga toxin- and ricin-induced proinflammatory cytokine expression. *Cellular Microbiology*, *10*(7), 1468–1477. https://doi.org/10.1111/j.1462-5822.2008.01139.x

Jeong, H.-J., Lee, S.-J., Lee, H.-J., Kim, H.-B., Anh Vuong, T., Cho, H., Bae, G.-U., & Kang, J.-S. (2020). Prmt7 promotes myoblast differentiation via methylation of p38MAPK on arginine residue 70. *Cell Death and Differentiation*, *27*(2), 573–586. https://doi.org/10.1038/s41418-019-0373-y

Jiang, Y., Chen, C., Li, Z., Guo, W., Gegner, J. A., Lin, S., & Han, J. (1996). Characterization of the structure and function of a new mitogen-activated protein kinase (p38beta). *The Journal of Biological Chemistry*, *271*(30), 17920–17926. https://doi.org/10.1074/jbc.271.30.17920

Jinek, M., Chylinski, K., Fonfara, I., Hauer, M., Doudna, J. A., & Charpentier, E. (2012). A Programmable Dual-RNA–Guided DNA Endonuclease in Adaptive Bacterial Immunity. *Science*, *337*(6096), 816–821. https://doi.org/10.1126/science.1225829

Jinek, M., East, A., Cheng, A., Lin, S., Ma, E., & Doudna, J. (2013). RNA-programmed genome editing in human cells. *ELife*, *2*, e00471. https://doi.org/10.7554/eLife.00471

Jochum, W., Passegué, E., & Wagner, E. F. (2001). AP-1 in mouse development and tumorigenesis. *Oncogene*, *20*(19), 2401–2412. https://doi.org/10.1038/sj.onc.1204389

Jolly, C., & Morimoto, R. I. (2000). Role of the heat shock response and molecular chaperones in oncogenesis and cell death. *Journal of the National Cancer Institute*, *92*(19), 1564–1572. https://doi.org/10.1093/jnci/92.19.1564

Khan, A. A., Betel, D., Miller, M. L., Sander, C., Leslie, C. S., & Marks, D. S. (2009). Transfection of small RNAs globally perturbs gene regulation by endogenous microRNAs. *Nature Biotechnology*, *27*(6), 549–555. https://doi.org/10.1038/nbt.1543

Kim, D., Lee, Y.-S., Jung, S.-J., Yeo, J., Seo, J. J., Lee, Y.-Y., Lim, J., Chang, H., Song, J., Yang, J., Kim, J.-S., Jung, G., Ahn, K., & Kim, V. N. (2020). Viral hijacking of the TENT4-ZCCHC14 complex protects viral RNAs via mixed tailing. *Nature Structural & Molecular Biology*, *27*(6), 581–588. https://doi.org/10.1038/s41594-020-0427-3

Kim, G.-Y., Mercer, S. E., Ewton, D. Z., Yan, Z., Jin, K., & Friedman, E. (2002). The stress-activated protein kinases p38 alpha and JNK1 stabilize p21(Cip1) by phosphorylation. *The Journal of Biological Chemistry*, *277*(33), 29792–29802. https://doi.org/10.1074/jbc.M201299200

King, C. R., Kraus, M. H., & Aaronson, S. A. (1985). Amplification of a novel v-erbB-related gene in a human mammary carcinoma. *Science (New York, N.Y.)*, *229*(4717), 974–976. https://doi.org/10.1126/science.2992089

Knudson, A. G. (1971). Mutation and Cancer: Statistical Study of Retinoblastoma. *Proceedings of the National Academy of Sciences*, *68*(4), 820–823. https://doi.org/10.1073/pnas.68.4.820

Kryukov, G. V., Wilson, F. H., Ruth, J. R., Paulk, J., Tsherniak, A., Marlow, S. E., Vazquez, F., Weir, B. A., Fitzgerald, M. E., Tanaka, M., Bielski, C. M., Scott, J. M., Dennis, C., Cowley, G. S., Boehm, J. S., Root, D. E., Golub, T. R., Clish, C. B., Bradner, J. E., … Garraway, L. A. (2016). MTAP deletion confers enhanced dependency on the PRMT5 arginine methyltransferase in cancer cells. *Science*, *351*(6278), 1214–1218. https://doi.org/10.1126/science.aad5214

Kuiken, H. J., Dhakal, S., Selfors, L. M., Friend, C. M., Zhang, T., Callari, M., Schackmann, R. C. J., Gray, G. K., Crowdis, J., Bhang, H. C., Baslan, T., Stegmeier, F., Gygi, S. P., Caldas, C., & Brugge, J. S. (2022). Clonal populations of a human TNBC model display significant functional heterogeneity and divergent growth dynamics in distinct contexts. *Oncogene*, *41*(1), Article 1. https://doi.org/10.1038/s41388-021-02075-y

Kulsuptrakul, J., Wang, R., Meyers, N. L., Ott, M., & Puschnik, A. S. (2021). A genome-wide CRISPR screen identifies UFMylation and TRAMP-like complexes as host factors required for hepatitis A virus infection. *Cell Reports*, *34*(11), 108859. https://doi.org/10.1016/j.celrep.2021.108859

Kuma, Y., Sabio, G., Bain, J., Shpiro, N., Márquez, R., & Cuenda, A. (2005). BIRB796 Inhibits All p38 MAPK Isoforms in Vitro and in Vivo*. *Journal of Biological Chemistry*, *280*(20), 19472–19479. https://doi.org/10.1074/jbc.M414221200

Kwak, E. L., Bang, Y.-J., Camidge, D. R., Shaw, A. T., Solomon, B., Maki, R. G., Ou, S.-H. I., Dezube, B. J., Jänne, P. A., Costa, D. B., Varella-Garcia, M., Kim, W.-H., Lynch, T. J., Fidias, P., Stubbs, H., Engelman, J. A., Sequist, L. V., Tan, W., Gandhi, L., … Iafrate, A. J. (2010). Anaplastic lymphoma kinase inhibition in non-small-cell lung cancer. *The New England Journal of Medicine*, *363*(18), 1693–1703. https://doi.org/10.1056/NEJMoa1006448

Lai, M. M., Duesberg, P. H., Horst, J., & Vogt, P. K. (1973). Avian tumor virus RNA: A comparison of three sarcoma viruses and their transformation-defective derivatives by oligonucleotide fingerprinting and DNA-RNA hybridization. *Proceedings of the National Academy of Sciences of the United States of America*, *70*(8), 2266–2270. https://doi.org/10.1073/pnas.70.8.2266

Laken, S. J., Petersen, G. M., Gruber, S. B., Oddoux, C., Ostrer, H., Giardiello, F. M., Hamilton, S. R., Hampel, H., Markowitz, A., Klimstra, D., Jhanwar, S., Winawer, S., Offit, K., Luce, M. C., Kinzler, K. W., & Vogelstein, B. (1997). Familial colorectal cancer in Ashkenazim due to a hypermutable tract in APC. *Nature Genetics*, *17*(1), 79–83. https://doi.org/10.1038/ng0997-79

Lamming, D. W., Ye, L., Katajisto, P., Goncalves, M. D., Saitoh, M., Stevens, D. M., Davis, J. G., Salmon, A. B., Richardson, A., Ahima, R. S., Guertin, D. A., Sabatini, D. M., & Baur, J. A. (2012). Rapamycin-induced insulin resistance is mediated by mTORC2 loss and uncoupled from longevity. *Science (New York, N.Y.)*, *335*(6076), 1638–1643. https://doi.org/10.1126/science.1215135

Langmead, B., Trapnell, C., Pop, M., & Salzberg, S. L. (2009). Ultrafast and memory-efficient alignment of short DNA sequences to the human genome. *Genome Biology*, *10*(3), R25. https://doi.org/10.1186/gb-2009-10-3-r25

Lavoie, H., Gagnon, J., & Therrien, M. (2020). ERK signalling: A master regulator of cell behaviour, life and fate. *Nature Reviews Molecular Cell Biology*, *21*(10), Article 10. https://doi.org/10.1038/s41580-020-0255-7

Lavoie, J. N., L'Allemain, G., Brunet, A., Müller, R., & Pouysségur, J. (1996). Cyclin D1 Expression Is Regulated Positively by the p42/p44MAPK and Negatively by the p38/HOGMAPK Pathway*. *Journal of Biological Chemistry*, *271*(34), 20608–20616. https://doi.org/10.1074/jbc.271.34.20608

Lechner, C., Zahalka, M. A., Giot, J. F., Møller, N. P., & Ullrich, A. (1996). ERK6, a mitogen-activated protein kinase involved in C2C12

myoblast differentiation. *Proceedings of the National Academy of Sciences*, *93*(9), 4355–4359. https://doi.org/10.1073/pnas.93.9.4355

Lee, J. C., Laydon, J. T., McDonnell, P. C., Gallagher, T. F., Kumar, S., Green, D., McNulty, D., Blumenthal, M. J., Keys, J. R., Land vatter, S. W., Strickler, J. E., McLaughlin, M. M., Siemens, I. R., Fisher, S. M., Livi, G. P., White, J. R., Adams, J. L., & Young, P. R. (1994). A protein kinase involved in the regulation of inflammatory cytokine biosynthesis. *Nature*, *372*(6508), Article 6508. https://doi.org/10.1038/372739a0

Leelahavanichkul, K., Amornphimoltham, P., Molinolo, A. A., Basile, J. R., Koontongkaew, S., & Gutkind, J. S. (2014). A role for p38 MAPK in head and neck cancer cell growth and tumor-induced angiogenesis and lymphangiogenesis. *Molecular Oncology*, *8*(1), 105–118. https://doi.org/10.1016/j.molonc.2013.10.003

Lemaire, M., Froment, C., Boutros, R., Mondesert, O., Nebreda, A. R., Monsarrat, B., & Ducommun, B. (2006). CDC25B phosphorylation by p38 and MK-2. *Cell Cycle (Georgetown, Tex.)*, *5*(15), 1649–1653. https://doi.org/10.4161/cc.5.15.3006

Lepore Signorile, M., Grossi, V., Di Franco, S., Forte, G., Disciglio, V., Fasano, C., Sanese, P., De Marco, K., Susca, F. C., Mangiapane, L. R., Nicotra, A., Di Carlo, G., Dituri, F., Giannelli, G., Ingravallo, G., Canettieri, G., Stassi, G., & Simone, C. (2021). Pharmacological targeting of the novel β-catenin chromatin-associated kinase p38α in colorectal cancer stem cell tumorspheres and organoids. *Cell Death & Disease*, *12*(4), Article 4. https://doi.org/10.1038/s41419-021-03572-4

Levy, J. M. M., Towers, C. G., & Thorburn, A. (2017). Targeting autophagy in cancer. *Nature Reviews Cancer*, *17*(9), Article 9. https://doi.org/10.1038/nrc.2017.53

Li, J., Yen, C., Liaw, D., Podsypanina, K., Bose, S., Wang, S. I., Puc, J., Miliaresis, C., Rodgers, L., McCombie, R., Bigner, S. H., Giovanella, B. C., Ittmann, M., Tycko, B., Hibshoosh, H., Wigler, M. H., & Parsons, R. (1997). PTEN, a putative protein tyrosine phosphatase gene mutated in human brain, breast, and prostate cancer. *Science (New York, N.Y.)*, *275*(5308), 1943–1947. https://doi.org/10.1126/science.275.5308.1943

Li, W., Xu, H., Xiao, T., Cong, L., Love, M. I., Zhang, F., Irizarry, R. A., Liu, J. S., Brown, M., & Liu, X. S. (2014). MAGeCK enables robust identification of essential genes from genome-scale CRISPR/Cas9 knockout screens. *Genome Biology*, *15*(12), 554. https://doi.org/10.1186/s13059-014-0554-4

Li, Z., Jiang, Y., Ulevitch, R. J., & Han, J. (1996). The primary structure of p38 gamma: A new member of p38 group of MAP kinases. *Biochemical and Biophysical Research Communications*, *228*(2), 334–340. https://doi.org/10.1006/bbrc.1996.1662

Lim, J., Kim, D., Lee, Y.-S., Ha, M., Lee, M., Yeo, J., Chang, H., Song, J., Ahn, K., & Kim, V. N. (2018). Mixed tailing by TENT4A and TENT4B shields mRNA from rapid deadenylation. *Science (New York, N.Y.)*, *361*(6403), 701–704. https://doi.org/10.1126/science.aam5794

Lin, A., Giuliano, C. J., Palladino, A., John, K. M., Abramowicz, C., Yuan, M. L., Sausville, E. L., Lukow, D. A., Liu, L., Chait, A. R., Galluzzo, Z. C., Tucker, C., & Sheltzer, J. M. (2019). Off-target toxicity is a common mechanism of action of cancer drugs undergoing clinical trials. *Science Translational Medicine*, *11*(509), eaaw8412. https://doi.org/10.1126/scitranslmed.aaw8412

Lin, A., Minden, A., Martinetto, H., Claret, F.-X., Lange-Carter, C., Mercurio, F., Johnson, G. L., & Karin, M. (1995). Identification of a Dual Specificity Kinase That Activates the Jun Kinases and p38-Mpk2. *Science*, *268*(5208), 286–290. https://doi.org/10.1126/science.7716521

Lin, J., Lee, D., Choi, Y., & Lee, S. Y. (2015). The scaffold protein RACK1 mediates the RANKL-dependent activation of p38 MAPK in osteoclast precursors. *Science Signaling*, *8*(379), ra54. https://doi.org/10.1126/scisignal.2005867

Linares, J. F., Duran, A., Reina-Campos, M., Aza-Blanc, P., Campos, A., Moscat, J., & Diaz-Meco, M. T. (2015). Amino Acid Activation of mTORC1 by a PB1-Domain-Driven Kinase Complex Cascade. *Cell Reports*, *12*(8), 1339–1352. https://doi.org/10.1016/j.celrep.2015.07.045

Liu, K., Yu, D., Cho, Y.-Y., Bode, A. M., Ma, W., Yao, K., Li, S., Li, J., Bowden, G. T., Dong, Z., & Dong, Z. (2013). Sunlight UV-induced skin cancer relies upon activation of the p38α signaling pathway. *Cancer Research*, *73*(7), 2181–2188. https://doi.org/10.1158/0008-5472.CAN-12-3408

Liu, M.-Y., Hua, W.-K., Chen, C.-J., & Lin, W.-J. (2020). The MKK-Dependent Phosphorylation of p38α Is Augmented by Arginine Methylation on Arg49/Arg149 during Erythroid Differentiation. *International Journal of Molecular Sciences*, *21*(10), Article 10. https://doi.org/10.3390/ijms21103546

Lord, C. J., & Ashworth, A. (2017). PARP inhibitors: Synthetic lethality in the clinic. *Science*, *355*(6330), 1152–1158. https://doi.org/10.1126/science.aam7344

Love, M. I., Huber, W., & Anders, S. (2014). Moderated estimation of fold change and dispersion for RNA-seq data with DESeq2. *Genome Biology*, *15*(12), 550. https://doi.org/10.1186/s13059-014-0550-8

Luo, J., Emanuele, M. J., Li, D., Creighton, C. J., Schlabach, M. R., Westbrook, T. F., Wong, K.-K., & Elledge, S. J. (2009). A genome-wide RNAi screen identifies multiple synthetic lethal interactions with the Ras oncogene. *Cell*, *137*(5), 835–848. https://doi.org/10.1016/j.cell.2009.05.006

Maia, V., Sanz, M., Gutierrez-Berzal, J., de Luis, A., Gutierrez-Uzquiza, A., Porras, A., & Guerrero, C. (2009). C3G silencing enhances STI-571-induced apoptosis in CML cells through p38 MAPK activation, but it antagonizes STI-571 inhibitory effect on survival. *Cellular Signalling*, *21*(7), 1229–1235. https://doi.org/10.1016/j.cellsig.2009.03.015

Mali, P., Yang, L., Esvelt, K. M., Aach, J., Guell, M., DiCarlo, J. E., Norville, J. E., & Church, G. M. (2013). RNA-guided human genome engineering via Cas9. *Science (New York, N.Y.)*, *339*(6121), 823–826. https://doi.org/10.1126/science.1232033

Manke, I. A., Nguyen, A., Lim, D., Stewart, M. Q., Elia, A. E. H., & Yaffe, M. B. (2005). MAPKAP kinase-2 is a cell cycle checkpoint kinase that regulates the G2/M transition and S phase progression in response to UV irradiation. *Molecular Cell*, *17*(1), 37–48. https://doi.org/10.1016/j.molcel.2004.11.021

Marcotte, R., Brown, K. R., Suarez, F., Sayad, A., Karamboulas, K., Krzyzanowski, P. M., Sircoulomb, F., Medrano, M., Fedyshyn, Y., Koh, J. L. Y., van Dyk, D., Fedyshyn, B., Luhova, M., Brito, G. C., Vizeacoumar, F. J., Vizeacoumar, F. S., Datti, A., Kasimer, D., Buzina, A., … Moffat, J. (2012). Essential gene profiles in breast, pancreatic, and ovarian cancer cells. *Cancer Discovery*, *2*(2), 172–189. https://doi.org/10.1158/2159-8290.CD-11-0224

Martens-de Kemp, S. R., Nagel, R., Stigter-van Walsum, M., van der Meulen, I. H., van Beusechem, V. W., Braakhuis, B. J. M., & Brakenhoff, R. H. (2013). Functional genetic screens identify genes essential for tumor cell survival in head and neck and lung cancer. *Clinical Cancer Research: An Official Journal of the American Association for Cancer Research*, *19*(8), 1994–2003. https://doi.org/10.1158/1078-0432.CCR-12-2539

Martin, M. (2011). Cutadapt removes adapter sequences from high-throughput sequencing reads. *EMBnet.Journal*, *17*(1), Article 1. https://doi.org/10.14806/ej.17.1.200

Martincorena, I. (2019). Somatic mutation and clonal expansions in human tissues. *Genome Medicine*, *11*, 35. https://doi.org/10.1186/s13073-019-0648-4

Martínez-Limón, A., Joaquin, M., Caballero, M., Posas, F., & de Nadal, E. (2020). The p38 Pathway: From Biology to Cancer Therapy. *International Journal of Molecular Sciences*, *21*(6), Article 6. https://doi.org/10.3390/ijms21061913

Matesanz, N., Nikolic, I., Leiva, M., Pulgarín-Alfaro, M., Santamans, A. M., Bernardo, E., Mora, A., Herrera-Melle, L., Rodríguez, E., Beiroa, D., Caballero, A., Martín-García, E., Acín-Pérez, R., Hernández-Cosido, L., Leiva-Vega, L., Torres, J. L., Centeno, F., Nebreda, A. R., Enríquez, J. A., … Sabio, G. (2018). P38α blocks brown adipose tissue thermogenesis through p38δ inhibition. *PLoS Biology*, *16*(7), e2004455. https://doi.org/10.1371/journal.pbio.2004455

McDonald, E. R., de Weck, A., Schlabach, M. R., Billy, E., Mavrakis, K. J., Hoffman, G. R., Belur, D., Castelletti, D., Frias, E., Gampa, K., Golji, J., Kao, I., Li, L., Megel, P., Perkins, T. A., Ramadan, N., Ruddy, D. A., Silver, S. J., Sovath, S., … Sellers, W. R. (2017). Project DRIVE: A Compendium of Cancer Dependencies and Synthetic Lethal Relationships Uncovered by Large-Scale, Deep RNAi Screening. *Cell*, *170*(3), 577-592.e10. https://doi.org/10.1016/j.cell.2017.07.005

Medicherla, S., Reddy, M., Ying, J., Navas, T. A., Li, L., Nguyen, A. N., Kerr, I., Hanjarappa, N., Protter, A. A., & Higgins, L. S. (2008). P38alpha-selective MAP kinase inhibitor reduces tumor growth in mouse xenograft models of multiple myeloma. *Anticancer Research*, *28*(6A), 3827–3833.

Menon, M. B., Kotlyarov, A., & Gaestel, M. (2011). SB202190-Induced Cell Type-Specific Vacuole Formation and Defective Autophagy Do Not Depend on p38 MAP Kinase Inhibition. *PLOS ONE*, *6*(8), e23054. https://doi.org/10.1371/journal.pone.0023054

Mertens, S., Craxton, M., & Goedert, M. (1996). SAP kinase-3, a new member of the family of mammalian stress-activated protein kinases. *FEBS Letters*, *383*(3), 273–276. https://doi.org/10.1016/0014-5793(96)00255-4

Mitra, A., Skrzypczak, M., Ginalski, K., & Rowicka, M. (2015). Strategies for Achieving High Sequencing Accuracy for Low Diversity Samples and

Avoiding Sample Bleeding Using Illumina Platform. *PLoS ONE*, *10*(4), e0120520. https://doi.org/10.1371/journal.pone.0120520

Mittelstadt, P. R., Yamaguchi, H., Appella, E., & Ashwell, J. D. (2009). T Cell Receptor-mediated Activation of p38α by Mono-phosphorylation of the Activation Loop Results in Altered Substrate Specificity. *The Journal of Biological Chemistry*, *284*(23), 15469–15474. https://doi.org/10.1074/jbc.M901004200

Miura, H., Kondo, Y., Matsuda, M., & Aoki, K. (2018). Cell-to-Cell Heterogeneity in p38-Mediated Cross-Inhibition of JNK Causes Stochastic Cell Death. *Cell Reports*, *24*(10), 2658–2668. https://doi.org/10.1016/j.celrep.2018.08.020

Moriguchi, T., Kuroyanagi, N., Yamaguchi, K., Gotoh, Y., Irie, K., Kano, T., Shirakabe, K., Muro, Y., Shibuya, H., Matsumoto, K., Nishida, E., & Hagiwara, M. (1996). A novel kinase cascade mediated by mitogen-activated protein kinase kinase 6 and MKK3. *The Journal of Biological Chemistry*, *271*(23), 13675–13679. https://doi.org/10.1074/jbc.271.23.13675

Mudgett, J. S., Ding, J., Guh-Siesel, L., Chartrain, N. A., Yang, L., Gopal, S., & Shen, M. M. (2000). Essential role for p38alpha mitogen-activated protein kinase in placental angiogenesis. *Proceedings of the National Academy of Sciences of the United States of America*, *97*(19), 10454–10459. https://doi.org/10.1073/pnas.180316397

Mullenders, J., & Bernards, R. (2009). Loss-of-function genetic screens as a tool to improve the diagnosis and treatment of cancer. *Oncogene*, *28*(50), 4409–4420. https://doi.org/10.1038/onc.2009.295

Murga, M., Campaner, S., Lopez-Contreras, A. J., Toledo, L. I., Soria, R., Montaña, M. F., Artista, L. D., Schleker, T., Guerra, C., Garcia, E., Barbacid, M., Hidalgo, M., Amati, B., & Fernandez-Capetillo, O. (2011). Exploiting oncogene-induced replicative stress for the selective killing of Myc-driven tumors. *Nature Structural & Molecular Biology*, *18*(12), 1331–1335. https://doi.org/10.1038/nsmb.2189

Nagel, R., Stigter-van Walsum, M., Buijze, M., van den Berg, J., van der Meulen, I. H., Hodzic, J., Piersma, S. R., Pham, T. V., Jiménez, C. R., van Beusechem, V. W., & Brakenhoff, R. H. (2015). Genome-wide siRNA Screen Identifies the Radiosensitizing Effect of Downregulation of MASTL and FOXM1 in NSCLC. *Molecular Cancer Therapeutics*, *14*(6), 1434–1444. https://doi.org/10.1158/1535-7163.MCT-14-0846

Neggers, J. E., Paolella, B. R., Asfaw, A., Rothberg, M. V., Skipper, T. A., Yang, A., Kalekar, R. L., Krill-Burger, J. M., Dharia, N. V., Kugener, G.,

Kalfon, J., Yuan, C., Dumont, N., Gonzalez, A., Abdusamad, M., Li, Y. Y., Spurr, L. F., Wu, W. W., Durbin, A. D., … Aguirre, A. J. (2020). Synthetic Lethal Interaction between the ESCRT Paralog Enzymes VPS4A and VPS4B in Cancers Harboring Loss of Chromosome 18q or 16q. *Cell Reports*, *33*(11), 108493. https://doi.org/10.1016/j.celrep.2020.108493

Nicke, B., Bastien, J., Khanna, S. J., Warne, P. H., Cowling, V., Cook, S. J., Peters, G., Delpuech, O., Schulze, A., Berns, K., Mullenders, J., Beijersbergen, R. L., Bernards, R., Ganesan, T. S., Downward, J., & Hancock, D. C. (2005). Involvement of MINK, a Ste20 family kinase, in Ras oncogene-induced growth arrest in human ovarian surface epithelial cells. *Molecular Cell*, *20*(5), 673–685. https://doi.org/10.1016/j.molcel.2005.10.038

Nigro, J. M., Baker, S. J., Preisinger, A. C., Jessup, J. M., Hostetter, R., Cleary, K., Bigner, S. H., Davidson, N., Baylin, S., & Devilee, P. (1989). Mutations in the p53 gene occur in diverse human tumour types. *Nature*, *342*(6250), 705–708. https://doi.org/10.1038/342705a0

Ning, X., He, J., Shi, X., Yu, T., & Yang, G. (2019). Wnt3a regulates mitochondrial biogenesis through p38/CREB pathway. *Biochemical and Biophysical Research Communications*, *516*(3), 1019–1025. https://doi.org/10.1016/j.bbrc.2016.05.004

Ninomiya-Tsuji, J., Kajino, T., Ono, K., Ohtomo, T., Matsumoto, M., Shiina, M., Mihara, M., Tsuchiya, M., & Matsumoto, K. (2003). A resorcylic acid lactone, 5Z-7-oxozeaenol, prevents inflammation by inhibiting the catalytic activity of TAK1 MAPK kinase kinase. *The Journal of Biological Chemistry*, *278*(20), 18485–18490. https://doi.org/10.1074/jbc.M207453200

Noordermeer, S. M., Adam, S., Setiaputra, D., Barazas, M., Pettitt, S. J., Ling, A. K., Olivieri, M., Álvarez-Quilón, A., Moatti, N., Zimmermann, M., Annunziato, S., Krastev, D. B., Song, F., Brandsma, I., Frankum, J., Brough, R., Sherker, A., Landry, S., Szilard, R. K., … Durocher, D. (2018). The shieldin complex mediates 53BP1-dependent DNA repair. *Nature*, *560*(7716), Article 7716. https://doi.org/10.1038/s41586-018-0340-7

Nousch, M., Yeroslaviz, A., Habermann, B., & Eckmann, C. R. (2014). The cytoplasmic poly(A) polymerases GLD-2 and GLD-4 promote general gene expression via distinct mechanisms. *Nucleic Acids Research*, *42*(18), 11622–11633. https://doi.org/10.1093/nar/gku838

Nowell, P. C., & Hungerford, D. A. (1961). Chromosome studies in human leukemia. II. Chronic granulocytic leukemia. *Journal of the National Cancer Institute*, *27*, 1013–1035.

Nurgali, K., Jagoe, R. T., & Abalo, R. (2018). Editorial: Adverse Effects of Cancer Chemotherapy: Anything New to Improve Tolerance and Reduce Sequelae? *Frontiers in Pharmacology*, *9*, 245. https://doi.org/10.3389/fphar.2018.00245

Olivieri, M., Cho, T., Álvarez-Quilón, A., Li, K., Schellenberg, M. J., Zimmermann, M., Hustedt, N., Rossi, S. E., Adam, S., Melo, H., Heijink, A. M., Sastre-Moreno, G., Moatti, N., Szilard, R. K., McEwan, A., Ling, A. K., Serrano-Benitez, A., Ubhi, T., Feng, S., … Durocher, D. (2020). A Genetic Map of the Response to DNA Damage in Human Cells. *Cell*, *182*(2), 481-496.e21. https://doi.org/10.1016/j.cell.2020.05.040

Pacini, C., Dempster, J. M., Boyle, I., Gonçalves, E., Najgebauer, H., Karakoc, E., van der Meer, D., Barthorpe, A., Lightfoot, H., Jaaks, P., McFarland, J. M., Garnett, M. J., Tsherniak, A., & Iorio, F. (2021). Integrated cross-study datasets of genetic dependencies in cancer. *Nature Communications*, *12*(1), 1661. https://doi.org/10.1038/s41467-021-21898-7

Parada, L. F., Tabin, C. J., Shih, C., & Weinberg, R. A. (1982). Human EJ bladder carcinoma oncogene is homologue of Harvey sarcoma virus ras gene. *Nature*, *297*(5866), 474–478. https://doi.org/10.1038/297474a0

Pereira, L., Igea, A., Canovas, B., Dolado, I., & Nebreda, A. R. (2013). Inhibition of p38 MAPK sensitizes tumour cells to cisplatin-induced apoptosis mediated by reactive oxygen species and JNK. *EMBO Molecular Medicine*, *5*(11), 1759–1774. https://doi.org/10.1002/emmm.201302732

Phong, M. S., Van Horn, R. D., Li, S., Tucker-Kellogg, G., Surana, U., & Ye, X. S. (2010). P38 mitogen-activated protein kinase promotes cell survival in response to DNA damage but is not required for the G(2) DNA damage checkpoint in human cancer cells. *Molecular and Cellular Biology*, *30*(15), 3816–3826. https://doi.org/10.1128/MCB.00949-09

Pillai, V. B., Sundaresan, N. R., Samant, S. A., Wolfgeher, D., Trivedi, C. M., & Gupta, M. P. (2011). Acetylation of a conserved lysine residue in the ATP binding pocket of p38 augments its kinase activity during hypertrophy of cardiomyocytes. *Molecular and Cellular Biology*, *31*(11), 2349–2363. https://doi.org/10.1128/MCB.01205-10

Pinder, A., Loo, D., Harrington, B., Oakes, V., Hill, M. M., & Gabrielli, B. (2015). JIP4 is a PLK1 binding protein that regulates p38MAPK activity in G2 phase. *Cellular Signalling*, *27*(11), 2296–2303. https://doi.org/10.1016/j.cellsig.2015.08.009

Poveda, A., Floquet, A., Ledermann, J. A., Asher, R., Penson, R. T., Oza, A. M., Korach, J., Huzarski, T., Pignata, S., Friedlander, M., Baldoni, A., Park-Simon, T.-W., Sonke, G. S., Lisyanskaya, A. S., Kim, J.-H., Filho, E. A., Vergote, I., Rowe, P., & Pujade-Lauraine, E. (2020). Final overall survival (OS) results from SOLO2/ENGOT-ov21: A phase III trial assessing maintenance olaparib in patients (pts) with platinum-sensitive, relapsed ovarian cancer and a BRCA mutation. *Journal of Clinical Oncology*, *38*(15_suppl), 6002–6002. https://doi.org/10.1200/JCO.2020.38.15_suppl.6002

Pramanik, R., Qi, X., Borowicz, S., Choubey, D., Schultz, R. M., Han, J., & Chen, G. (2003). p38 Isoforms Have Opposite Effects on AP-1-dependent Transcription through Regulation of c-Jun: THE DETERMINANT ROLE OF THE ISOFORMS IN THE p38 MAPK SIGNAL SPECIFICITY *. *Journal of Biological Chemistry*, *278*(7), 4831–4839. https://doi.org/10.1074/jbc.M207732200

R Core Team. (2008). *R: A Language and Environment for Statistical Computing*. R Foundation for Statistical Computing. https://www.R-project.org/

Raman, M., Earnest, S., Zhang, K., Zhao, Y., & Cobb, M. H. (2007). TAO kinases mediate activation of p38 in response to DNA damage. *The EMBO Journal*, *26*(8), 2005–2014. https://doi.org/10.1038/sj.emboj.7601668

Rasmussen, M. H., Lyskjær, I., Jersie-Christensen, R. R., Tarpgaard, L. S., Primdal-Bengtson, B., Nielsen, M. M., Pedersen, J. S., Hansen, T. P., Hansen, F., Olsen, J. V., Pfeiffer, P., Ørntoft, T. F., & Andersen, C. L. (2016). MiR-625-3p regulates oxaliplatin resistance by targeting MAP2K6-p38 signalling in human colorectal adenocarcinoma cells. *Nature Communications*, *7*, 12436. https://doi.org/10.1038/ncomms12436

Remy, G., Risco, A. M., Iñesta-Vaquera, F. A., González-Terán, B., Sabio, G., Davis, R. J., & Cuenda, A. (2010). Differential activation of p38MAPK isoforms by MKK6 and MKK3. *Cellular Signalling*, *22*(4), 660–667. https://doi.org/10.1016/j.cellsig.2009.11.020

Reyskens, K. M. S. E., & Arthur, J. S. C. (2016). Emerging Roles of the Mitogen and Stress Activated Kinases MSK1 and MSK2. *Frontiers in*

Cell and Developmental Biology, *4*, 56. https://doi.org/10.3389/fcell.2016.00056

Richter, U., Lahtinen, T., Marttinen, P., Myöhänen, M., Greco, D., Cannino, G., Jacobs, H. T., Lietzén, N., Nyman, T. A., & Battersby, B. J. (2013). A mitochondrial ribosomal and RNA decay pathway blocks cell proliferation. *Current Biology: CB*, *23*(6), 535–541. https://doi.org/10.1016/j.cub.2013.02.019

Ricoult, S. J. H., Yecies, J. L., Ben-Sahra, I., & Manning, B. D. (2016). Oncogenic PI3K and K-Ras stimulate de novo lipid synthesis through mTORC1 and SREBP. *Oncogene*, *35*(10), 1250–1260. https://doi.org/10.1038/onc.2015.179

Romero-Becerra, R., Mora, A., Manieri, E., Nikolic, I., Santamans, A. M., Montalvo-Romeral, V., Cruz, F. M., Rodríguez, E., León, M., Leiva-Vega, L., Sanz, L., Bondía, V., Filgueiras-Rama, D., Jiménez-Borreguero, L. J., Jalife, J., Gonzalez-Teran, B., & Sabio, G. (2022). MKK6 deficiency promotes cardiac dysfunction through MKK3-p38γ/δ-mTOR hyperactivation. *ELife*, *11*, e75250. https://doi.org/10.7554/eLife.75250

Ronkina, N., & Gaestel, M. (2022). MAPK-Activated Protein Kinases: Servant or Partner? *Annual Review of Biochemistry*, *91*(1), 505–540. https://doi.org/10.1146/annurev-biochem-081720-114505

Rous, P. (1911). A SARCOMA OF THE FOWL TRANSMISSIBLE BY AN AGENT SEPARABLE FROM THE TUMOR CELLS. *The Journal of Experimental Medicine*, *13*(4), 397–411. https://doi.org/10.1084/jem.13.4.397

Rouse, J., Cohen, P., Trigon, S., Morange, M., Alonso-Llamazares, A., Zamanillo, D., Hunt, T., & Nebreda, A. R. (1994). A novel kinase cascade triggered by stress and heat shock that stimulates MAPKAP kinase-2 and phosphorylation of the small heat shock proteins. *Cell*, *78*(6), 1027–1037. https://doi.org/10.1016/0092-8674(94)90277-1

Rudalska, R., Dauch, D., Longerich, T., McJunkin, K., Wuestefeld, T., Kang, T.-W., Hohmeyer, A., Pesic, M., Leibold, J., von Thun, A., Schirmacher, P., Zuber, J., Weiss, K.-H., Powers, S., Malek, N. P., Eilers, M., Sipos, B., Lowe, S. W., Geffers, R., … Zender, L. (2014). In vivo RNAi screening identifies a mechanism of sorafenib resistance in liver cancer. *Nature Medicine*, *20*(10), 1138–1146. https://doi.org/10.1038/nm.3679

Sabio, G., Arthur, J. S. C., Kuma, Y., Peggie, M., Carr, J., Murray-Tait, V., Centeno, F., Goedert, M., Morrice, N. A., & Cuenda, A. (2005). P38gamma regulates the localisation of SAP97 in the cytoskeleton

by modulating its interaction with GKAP. *The EMBO Journal*, *24*(6), 1134–1145. https://doi.org/10.1038/sj.emboj.7600578

Sahu, R. P., Batra, S., Kandala, P. K., Brown, T. L., & Srivastava, S. K. (2011). The role of K-ras gene mutation in TRAIL-induced apoptosis in pancreatic and lung cancer cell lines. *Cancer Chemotherapy and Pharmacology*, *67*(2), 481–487. https://doi.org/10.1007/s00280-010-1463-1

Salvador, J. M., Mittelstadt, P. R., Guszczynski, T., Copeland, T. D., Yamaguchi, H., Appella, E., Fornace, A. J., & Ashwell, J. D. (2005). Alternative p38 activation pathway mediated by T cell receptor-proximal tyrosine kinases. *Nature Immunology*, *6*(4), 390–395. https://doi.org/10.1038/ni1177

Sanjana, N. E., Shalem, O., & Zhang, F. (2014). Improved vectors and genome-wide libraries for CRISPR screening. *Nature Methods*, *11*(8), 783–784. https://doi.org/10.1038/nmeth.3047

Santos, E., Tronick, S. R., Aaronson, S. A., Pulciani, S., & Barbacid, M. (1982). T24 human bladder carcinoma oncogene is an activated form of the normal human homologue of BALB- and Harvey-MSV transforming genes. *Nature*, *298*(5872), 343–347. https://doi.org/10.1038/298343a0

Sapranauskas, R., Gasiunas, G., Fremaux, C., Barrangou, R., Horvath, P., & Siksnys, V. (2011). The Streptococcus thermophilus CRISPR/Cas system provides immunity in Escherichia coli. *Nucleic Acids Research*, *39*(21), 9275–9282. https://doi.org/10.1093/nar/gkr606

Sarbassov, D. D., Ali, S. M., Sengupta, S., Sheen, J.-H., Hsu, P. P., Bagley, A. F., Markhard, A. L., & Sabatini, D. M. (2006). Prolonged rapamycin treatment inhibits mTORC2 assembly and Akt/PKB. *Molecular Cell*, *22*(2), 159–168. https://doi.org/10.1016/j.molcel.2006.03.029

Satoh, H., Moriguchi, T., Takai, J., Ebina, M., & Yamamoto, M. (2013). Nrf2 prevents initiation but accelerates progression through the Kras signaling pathway during lung carcinogenesis. *Cancer Research*, *73*(13), 4158–4168. https://doi.org/10.1158/0008-5472.CAN-12-4499

Savage, D. G., & Antman, K. H. (2002). Imatinib Mesylate—A New Oral Targeted Therapy. *New England Journal of Medicine*, *346*(9), 683–693. https://doi.org/10.1056/NEJMra013339

Schechter, A. L., Stern, D. F., Vaidyanathan, L., Decker, S. J., Drebin, J. A., Greene, M. I., & Weinberg, R. A. (1984). The neu oncogene: An erb-B-related gene encoding a 185,000-Mr tumour antigen. *Nature*, *312*(5994), Article 5994. https://doi.org/10.1038/312513a0

Schmidt, U., Weigert, M., Broaddus, C., & Myers, G. (2018). Cell Detection with Star-Convex Polygons. In A. F. Frangi, J. A. Schnabel, C. Davatzikos, C. Alberola-López, & G. Fichtinger (Eds.), *Medical Image Computing and Computer Assisted Intervention – MICCAI 2018* (pp. 265–273). Springer International Publishing. https://doi.org/10.1007/978-3-030-00934-2_30

Sehgal, S. N., Baker, H., & Vézina, C. (1975). Rapamycin (AY-22,989), a new antifungal antibiotic. II. Fermentation, isolation and characterization. *The Journal of Antibiotics*, *28*(10), 727–732. https://doi.org/10.7164/antibiotics.28.727

Setton, J., Zinda, M., Riaz, N., Durocher, D., Zimmermann, M., Koehler, M., Reis-Filho, J. S., & Powell, S. N. (2021). Synthetic Lethality in Cancer Therapeutics: The Next Generation. *Cancer Discovery*, *11*(7), 1626–1635. https://doi.org/10.1158/2159-8290.CD-20-1503

Shalem, O., Sanjana, N. E., Hartenian, E., Shi, X., Scott, D. A., Mikkelson, T., Heckl, D., Ebert, B. L., Root, D. E., Doench, J. G., & Zhang, F. (2014). Genome-scale CRISPR-Cas9 knockout screening in human cells. *Science (New York, N.Y.)*, *343*(6166), 84–87. https://doi.org/10.1126/science.1247005

Shi, X., Han, X., Cao, Y., Li, C., & Cao, Y. (2021). ZCCHC14 regulates proliferation and invasion of non-small cell lung cancer through the MAPK-P38 signalling pathway. *Journal of Cellular and Molecular Medicine*, *25*(3), 1406–1414. https://doi.org/10.1111/jcmm.16223

Slamon, D. J., Leyland-Jones, B., Shak, S., Fuchs, H., Paton, V., Bajamonde, A., Fleming, T., Eiermann, W., Wolter, J., Pegram, M., Baselga, J., & Norton, L. (2001). Use of chemotherapy plus a monoclonal antibody against HER2 for metastatic breast cancer that overexpresses HER2. *The New England Journal of Medicine*, *344*(11), 783–792. https://doi.org/10.1056/NEJM200103153441101

Solimini, N. L., Luo, J., & Elledge, S. J. (2007). Non-Oncogene Addiction and the Stress Phenotype of Cancer Cells. *Cell*, *130*(6), 986–988. https://doi.org/10.1016/j.cell.2007.09.007

Soni, S., Anand, P., & Padwad, Y. S. (2019). MAPKAPK2: The master regulator of RNA-binding proteins modulates transcript stability and tumor progression. *Journal of Experimental & Clinical Cancer Research: CR*, *38*(1), 121. https://doi.org/10.1186/s13046-019-1115-1

Stanbridge, E. J. (1976). Suppression of malignancy in human cells. *Nature*, *260*(5546), 17–20. https://doi.org/10.1038/260017a0

Staples, C. J., Owens, D. M., Maier, J. V., Cato, A. C. B., & Keyse, S. M. (2010). Cross-talk between the p38α and JNK MAPK Pathways Mediated by MAP Kinase Phosphatase-1 Determines Cellular Sensitivity to UV Radiation. *The Journal of Biological Chemistry*, *285*(34), 25928–25940. https://doi.org/10.1074/jbc.M110.117911

Stehelin, D., Varmus, H. E., Bishop, J. M., & Vogt, P. K. (1976). DNA related to the transforming gene(s) of avian sarcoma viruses is present in normal avian DNA. *Nature*, *260*(5547), 170–173. https://doi.org/10.1038/260170a0

Sunaga, N., Miura, Y., Tsukagoshi, Y., Kasahara, N., Masuda, T., Sakurai, R., Kaira, K., & Hisada, T. (2019). Dual inhibition of MEK and p38 impairs tumor growth in KRAS-mutated non-small cell lung cancer. *Oncology Letters*, *17*(3), 3569–3575. https://doi.org/10.3892/ol.2019.10009

Swain, S. M., Shastry, M., & Hamilton, E. (2023). Targeting HER2-positive breast cancer: Advances and future directions. *Nature Reviews Drug Discovery*, *22*(2), Article 2. https://doi.org/10.1038/s41573-022-00579-0

Takekawa, M., Adachi, M., Nakahata, A., Nakayama, I., Itoh, F., Tsukuda, H., Taya, Y., & Imai, K. (2000). P53-inducible Wip1 phosphatase mediates a negative feedback regulation of p38 MAPK-p53 signaling in response to UV radiation. *The EMBO Journal*, *19*(23), 6517. https://doi.org/10.1093/emboj/19.23.6517

Tanoue, T., Yamamoto, T., Maeda, R., & Nishida, E. (2001). A Novel MAPK phosphatase MKP-7 acts preferentially on JNK/SAPK and p38 alpha and beta MAPKs. *The Journal of Biological Chemistry*, *276*(28), 26629–26639. https://doi.org/10.1074/jbc.M101981200

Tecleab, A., & Sebti, S. M. (2013). Depletion of K-Ras promotes proteasome degradation of survivin. *Cell Cycle (Georgetown, Tex.)*, *12*(3), 522–532. https://doi.org/10.4161/cc.23407

Tough, I. M., Court Brown, W. M., Baikie, A. G., Buckton, K. E., Harnden, D. G., Jacobs, P. A., King, M. J., & McBRIDE, J. A. (1961). Cytogenetic studies in chronic myeloid leukaemia and acute leukaemia associated with monogolism. *Lancet (London, England)*, *1*(7174), 411–417. https://doi.org/10.1016/s0140-6736(61)90001-0

Trachootham, D., Zhou, Y., Zhang, H., Demizu, Y., Chen, Z., Pelicano, H., Chiao, P. J., Achanta, G., Arlinghaus, R. B., Liu, J., & Huang, P. (2006). Selective killing of oncogenically transformed cells through a ROS-mediated mechanism by beta-phenylethyl isothiocyanate. *Cancer Cell*, *10*(3), 241–252. https://doi.org/10.1016/j.ccr.2006.08.009

Trempolec, N., Dave-Coll, N., & Nebreda, A. R. (2013). SnapShot: P38 MAPK substrates. *Cell*, *152*(4), 924-924.e1. https://doi.org/10.1016/j.cell.2013.01.047

Tront, J. S., Hoffman, B., & Liebermann, D. A. (2006). Gadd45a suppresses Ras-driven mammary tumorigenesis by activation of c-Jun NH2-terminal kinase and p38 stress signaling resulting in apoptosis and senescence. *Cancer Research*, *66*(17), 8448–8454. https://doi.org/10.1158/0008-5472.CAN-06-2013

Tsherniak, A., Vazquez, F., Montgomery, P. G., Weir, B. A., Kryukov, G., Cowley, G. S., Gill, S., Harrington, W. F., Pantel, S., Krill-Burger, J. M., Meyers, R. M., Ali, L., Goodale, A., Lee, Y., Jiang, G., Hsiao, J., Gerath, W. F. J., Howell, S., Merkel, E., … Hahn, W. C. (2017). Defining a Cancer Dependency Map. *Cell*, *170*(3), 564-576.e16. https://doi.org/10.1016/j.cell.2017.06.010

Uhlik, M. T., Abell, A. N., Johnson, N. L., Sun, W., Cuevas, B. D., Lobel-Rice, K. E., Horne, E. A., Dell'Acqua, M. L., & Johnson, G. L. (2003). Rac-MEKK3-MKK3 scaffolding for p38 MAPK activation during hyperosmotic shock. *Nature Cell Biology*, *5*(12), 1104–1110. https://doi.org/10.1038/ncb1071

van Houdt, W. J., de Bruijn, M. T., Emmink, B. L., Raats, D., Hoogwater, F. J. H., Borel Rinkes, I. H. M., & Kranenburg, O. (2010). Oncogenic K-ras activates p38 to maintain colorectal cancer cell proliferation during MEK inhibition. *Cellular Oncology: The Official Journal of the International Society for Cellular Oncology*, *32*(4), 245–257. https://doi.org/10.3233/CLO-2010-0521

van Neerven, S. M., & Vermeulen, L. (2022). Cell competition in development, homeostasis and cancer. *Nature Reviews Molecular Cell Biology*, 1–16. https://doi.org/10.1038/s41580-022-00538-y

Vanderkerken, K., Medicherla, S., Coulton, L., De Raeve, H., Willems, A., Lawson, M., Van Camp, B., Protter, A. A., Higgins, L. S., Menu, E., & Croucher, P. I. (2007). Inhibition of p38α Mitogen-Activated Protein Kinase Prevents the Development of Osteolytic Bone Disease, Reduces Tumor Burden, and Increases Survival in Murine Models of Multiple Myeloma. *Cancer Research*, *67*(10), 4572–4577. https://doi.org/10.1158/0008-5472.CAN-06-4361

Ventura, J. J., Tenbaum, S., Perdiguero, E., Huth, M., Guerra, C., Barbacid, M., Pasparakis, M., & Nebreda, A. R. (2007). P38alpha MAP kinase is essential in lung stem and progenitor cell proliferation and differentiation. *Nature Genetics*, *39*(6), 750–758. https://doi.org/10.1038/ng2037

Vitos-Faleato, J., Real, S. M., Gutierrez-Prat, N., Villanueva, A., Llonch, E., Drosten, M., Barbacid, M., & Nebreda, A. R. (2020). Requirement for epithelial p38α in KRAS-driven lung tumor progression. *Proceedings of the National Academy of Sciences*, *117*(5), 2588–2596. https://doi.org/10.1073/pnas.1921404117

Vogt, P. K. (2012). Retroviral oncogenes: A historical primer. *Nature Reviews Cancer*, *12*(9), Article 9. https://doi.org/10.1038/nrc3320

Vu, V., Verster, A. J., Schertzberg, M., Chuluunbaatar, T., Spensley, M., Pajkic, D., Hart, G. T., Moffat, J., & Fraser, A. G. (2015). Natural Variation in Gene Expression Modulates the Severity of Mutant Phenotypes. *Cell*, *162*(2), 391–402. https://doi.org/10.1016/j.cell.2015.06.037

Wakeman, D., Schneider, J. E., Liu, J., Wandu, W. S., Erwin, C. R., Guo, J., Stappenbeck, T. S., & Warner, B. W. (2012). Deletion of p38-alpha MAPK within the Intestinal Epithelium Promotes Colon Tumorigenesis. *Surgery*, *152*(2), 286–293. https://doi.org/10.1016/j.surg.2012.05.009

Wang, B., Krall, E. B., Aguirre, A. J., Kim, M., Widlund, H. R., Doshi, M. B., Sicinska, E., Sulahian, R., Goodale, A., Cowley, G. S., Piccioni, F., Doench, J. G., Root, D. E., & Hahn, W. C. (2017). ATXN1L, CIC, and ETS Transcription Factors Modulate Sensitivity to MAPK Pathway Inhibition. *Cell Reports*, *18*(6), 1543–1557. https://doi.org/10.1016/j.celrep.2017.01.031

Wang, B., Wang, M., Zhang, W., Xiao, T., Chen, C.-H., Wu, A., Wu, F., Traugh, N., Wang, X., Li, Z., Mei, S., Cui, Y., Shi, S., Lipp, J. J., Hinterndorfer, M., Zuber, J., Brown, M., Li, W., & Liu, X. S. (2019). Integrative analysis of pooled CRISPR genetic screens using MAGeCKFlute. *Nature Protocols*, *14*(3), 756–780. https://doi.org/10.1038/s41596-018-0113-7

Wang, L. H., Duesberg, P., Beemon, K., & Vogt, P. K. (1975). Mapping RNase T1-resistant oligonucleotides of avian tumor virus RNAs: Sarcoma-specific oligonucleotides are near the poly(A) end and oligonucleotides common to sarcoma and transformation-defective viruses are at the poly(A) end. *Journal of Virology*, *16*(4), 1051–1070. https://doi.org/10.1128/JVI.16.4.1051-1070.1975

Wang, L. H., Duesberg, P. H., Kawai, S., & Hanafusa, H. (1976). Location of envelope-specific and sarcoma-specific oligonucleotides on RNA of Schmidt-Ruppin Rous sarcoma virus. *Proceedings of the National Academy of Sciences of the United States of America*, *73*(2), 447–451. https://doi.org/10.1073/pnas.73.2.447

Wang, T., Wei, J. J., Sabatini, D. M., & Lander, E. S. (2014). Genetic screens in human cells using the CRISPR-Cas9 system. *Science (New York, N.Y.)*, *343*(6166), 80–84. https://doi.org/10.1126/science.1246981

Wang, T., Yu, H., Hughes, N. W., Liu, B., Kendirli, A., Klein, K., Chen, W. W., Lander, E. S., & Sabatini, D. M. (2017). Gene Essentiality Profiling Reveals Gene Networks and Synthetic Lethal Interactions with Oncogenic Ras. *Cell*, *168*(5), 890-903.e15. https://doi.org/10.1016/j.cell.2017.01.013

Wang, W., Chen, J. X., Liao, R., Deng, Q., Zhou, J. J., Huang, S., & Sun, P. (2002). Sequential activation of the MEK-extracellular signal-regulated kinase and MKK3/6-p38 mitogen-activated protein kinase pathways mediates oncogenic ras-induced premature senescence. *Molecular and Cellular Biology*, *22*(10), 3389–3403. https://doi.org/10.1128/MCB.22.10.3389-3403.2002

Wang, X., Flynn, A., Waskiewicz, A. J., Webb, B. L., Vries, R. G., Baines, I. A., Cooper, J. A., & Proud, C. G. (1998). The phosphorylation of eukaryotic initiation factor eIF4E in response to phorbol esters, cell stresses, and cytokines is mediated by distinct MAP kinase pathways. *The Journal of Biological Chemistry*, *273*(16), 9373–9377. https://doi.org/10.1074/jbc.273.16.9373

Wang, X., Mader, M. M., Toth, J. E., Yu, X., Jin, N., Campbell, R. M., Smallwood, J. K., Christe, M. E., Chatterjee, A., Goodson, T., Vlahos, C. J., Matter, W. F., & Bloem, L. J. (2005). Complete inhibition of anisomycin and UV radiation but not cytokine induced JNK and p38 activation by an aryl-substituted dihydropyrrolopyrazole quinoline and mixed lineage kinase 7 small interfering RNA. *The Journal of Biological Chemistry*, *280*(19), 19298–19305. https://doi.org/10.1074/jbc.M413059200

Wang, Y., Yu, Y., Pang, Y., Yu, H., Zhang, W., Zhao, X., & Yu, J. (2021). The distinct roles of zinc finger CCHC-type (ZCCHC) superfamily proteins in the regulation of RNA metabolism. *RNA Biology*, *18*(12), 2107–2126. https://doi.org/10.1080/15476286.2021.1909320

Xin, X., Zhou, L., Reyes, C. M., Liu, F., & Dong, L. Q. (2011). APPL1 mediates adiponectin-stimulated p38 MAPK activation by scaffolding the TAK1-MKK3-p38 MAPK pathway. *American Journal of Physiology. Endocrinology and Metabolism*, *300*(1), E103-110. https://doi.org/10.1152/ajpendo.00427.2010

Yamaguchi, K., Shirakabe, K., Shibuya, H., Irie, K., Oishi, I., Ueno, N., Taniguchi, T., Nishida, E., & Matsumoto, K. (1995). Identification of a member of the MAPKKK family as a potential mediator of TGF-beta

signal transduction. *Science (New York, N.Y.)*, *270*(5244), 2008–2011. https://doi.org/10.1126/science.270.5244.2008

Yang, W., Soares, J., Greninger, P., Edelman, E. J., Lightfoot, H., Forbes, S., Bindal, N., Beare, D., Smith, J. A., Thompson, I. R., Ramaswamy, S., Futreal, P. A., Haber, D. A., Stratton, M. R., Benes, C., McDermott, U., & Garnett, M. J. (2013). Genomics of Drug Sensitivity in Cancer (GDSC): A resource for therapeutic biomarker discovery in cancer cells. *Nucleic Acids Research*, *41*(Database issue), D955-961. https://doi.org/10.1093/nar/gks1111

Yu, C., Mannan, A. M., Yvone, G. M., Ross, K. N., Zhang, Y.-L., Marton, M. A., Taylor, B. R., Crenshaw, A., Gould, J. Z., Tamayo, P., Weir, B. A., Tsherniak, A., Wong, B., Garraway, L. A., Shamji, A. F., Palmer, M. A., Foley, M. A., Winckler, W., Schreiber, S. L., … Golub, T. R. (2016). High-throughput identification of genotype-specific cancer vulnerabilities in mixtures of barcoded tumor cell lines. *Nature Biotechnology*, *34*(4), Article 4. https://doi.org/10.1038/nbt.3460

Zhang, T., Ikejima, T., Li, L., Wu, R., Yuan, X., Zhao, J., Wang, Y., & Peng, S. (2017). Impairment of Mitochondrial Biogenesis and Dynamics Involved in Isoniazid-Induced Apoptosis of HepG2 Cells Was Alleviated by p38 MAPK Pathway. *Frontiers in Pharmacology*, *8*, 753. https://doi.org/10.3389/fphar.2017.00753

Zwang, Y., & Yarden, Y. (2006). p38 MAP kinase mediates stress-induced internalization of EGFR: Implications for cancer chemotherapy. *The EMBO Journal*, *25*(18), 4195–4206. https://doi.org/10.1038/sj.emboj.7601297